UNIVERSITY OF SOUTHAMPTON

FACULTY OF ENGINEERING, SCIENCE & MATHEMATICS

SCHOOL OF PHYSICS AND ASTRONOMY

Plastic Scintillation Spectrometry

BY

CHRISTOPHER BURT

THESIS FOR THE DEGREE OF DOCTOR OF PHILOSOPHY

OCTOBER 2009

Abstract

Plastic scintillators provide homeland security organisations with large area, low cost gamma-ray counters at international borders. Currently these detectors cannot distinguish between the sources they detect, leading to high false alarm rates during primary screening. These alarms must be followed up by time consuming secondary screening techniques using spectroscopic detectors.

Here we review current PVT scintillators and present a range of techniques that optimise their characteristics. By combining these optimisations with Symetrica's spectral deconvolution and isotope identification software, PVT detectors were given isotope identification ability. Far from being simple gamma-ray counters, these detectors were used to successfully identify a range of complex isotopes, such as Eu-152, Ra-226 and Th-232. The resulting clarity produced by these detectors was impressive, with a measured full width at half maximum of 5% at 662keV in a deconvovled Cs-137 spectrum. Detector designs are also presented here which allow PVT detectors to identify a full range of isotopes during primary screening, potentially eradicating the need for follow up examinations.

Author's Declaration

I, Christopher Burt declare that this thesis and the work presented here is my own and has been generated by me as a result of my own original research under the guidance of my supervisors Dr Tony Bird and Dr David Ramsden. Sources included other than my own work have been fully referenced and contributions made by others are listed below.

The detector designs presented in Chapter 4 were jointly developed by Christopher Burt and David Ramsden who are the inventors listed in the patent [Ramsden and Burt, 2009] owned by Symetrica Ltd covering such designs.

The software code for operating the scintillator detectors presented here was developed largely by Thomas Meeks and Grant Crossingham with additions made for use with PVT by Christopher Burt. The software code also included use of Symetrica's proprietary software.

Part of this work has been published in [Burt and Ramsden, 2008].

Acknowledgements

I would firstly like to thank my supervisors from both the University of Southampton School of Physics and Astronomy and from Symetrica Ltd. At Symetrica, David Ramsden for his continued support, appraisals, constructive criticism, and a rare combination of intellect and creativity. At the University of Southampton, Tony Bird for his critical contribution, guidance and friendship over the years, his direct resolve and willingness to help at any time.

I would like to thank my family and friends for their help, both before and during my studies. Special thanks to Mum, Dad, my wife Mina and my brother Adam for all their help, support and patience. Thanks to all my relatives who have all contributed in their own way.

Thanks to all the following people who have made my time studying at University enjoyable: Omar, Dan, Simone, Clement, Rob F, Pete, Jake, Josh, Cathy, Peter, Tony, Dave C and Dave B.

I would like to thank the University of Southampton for the use of its facilities. Thanks to Mark Scully and the School of Physics & Astronomy mechanical workshop staff for all their help. Many thanks to the team at Symetrica for their continued help and support. In no particular order: Heddwyn, Brian, Matthew, Grant, Chad, Tom, Mark, Colin and Alex.

Finally I would like to give thanks for the funding provided by the Southampton University SULIS fund and by Symetrica Ltd.

Contents

List of Tables

List of Figures

Chapter 1

Introduction and Overview

1.1 Introduction

On the 11th of September 2001 the United States of America was targeted for series of terrorist attacks. In these attacks four passenger jet airliners were hijacked; two were crashed into the world trade centre, one crashed into the pentagon and the last crashed in a field after passengers and crew attempted to re-take the plane. In response to these attacks NATO issued a statement declaring that the attacks were considered an attack on all of the NATO nations [NATO, 2001] and the United States of America launched a "war on terrorism" for the "elimination of terrorism as a threat to our way of life" [National Commission on Terrorist Attacks Upon the United States, 2004]. This series of events led to the United States of America, along with other countries, reinforcing their counter terrorism legislation and introducing new anti-terrorism technologies. The Department of Homeland Security (DHS) was created by the United States of America to unify their efforts towards counter terrorism. The Department of Homeland Security proposed the creation of the four following divisions[Bush, 2002]:

- Border and Transportation Security;
- Emergency Preparedness and Response;
- Chemical, Biological, Radiological and Nuclear Countermeasures;
- Information Analysis and Infrastructure Protection.

Emphasis was placed on the use of advanced science and technology available to the United States as a key advantage in the war against terrorism. One such area of tech-

nology concerned the possibility of a radiological threat, such as a nuclear bomb or radiological dispersion device being used in a future terrorist attack. The Domestic Nuclear Detection Office (DNDO) was formed as part of the Department of Homeland Security to specifically combat nuclear smuggling in the hope of preventing such an attack. DNDO would work closely with the US Customs and Borders Protection (CBP) with the aim of securing ports of entry all around the United States, whilst facilitating legitimate trade and travel.

The technology employed for this task was large-scale radiation detection devices in the form of radiation portal monitors (RPMs). By October of 2002, customs and borders protection had deployed the first radiation portal monitor at the Ambassador Bridge in Detroit. Today, customs and borders protection has 1,120 radiation portal monitors operational at seaports, land border ports of entry and mail facilities. Additionally, customs and borders protection has deployed over 1,200 Radiation Isotope Identifier Devices (RIID) and over 16,400 Personal Radiation Detectors (PRD). These devices allowed customs and borders protection to inspect 100 percent of all identified high-risk cargo [Winkowski, 2008].

Large scale radiation portal monitors that are in place today consist of large volumes of plastic scintillator inside a portal structure. The plastic scintillator is designed to detect gamma-rays emitted from any passing radioactive sources, sounding an alarm if the radiation measured is significantly above background levels. However, problems have since arisen in the use of such portal monitors as innocent materials such as bananas, cat litter, and various aggregates emit enough naturally occuring radiation to set off the alarms. Given the volume of traffic through customs and borders, the portal operators are dealing with a large number of these innocent alarms each day which must all be investigated. These follow up investigations involve using a hand held gamma-ray spectrometer to identify the source of the radiation and therefore determine if it is innocent or threatening. This procedure causes a large delay in the traffic and has ultimately led to operators reducing the sensitivity of the radiation portal monitors in order to increase traffic flow. Such action however negates the initial reason for having portal monitors in the first place as they are no longer effective in

detecting radiation from any source.

Radiation portal monitors in the form of personnel portals are also used to detect illicit materials, specifically those carried by pedestrians. The threat of a nuclear attack at establishments or events with a large gathering of people such as airports or the Olympic Games is significant, leading to the employment of personnel portals for radiation detection. Personnel portals, like vehicle portals, currently have no inherent identification abilities and are therefore also susceptible to false alarms. The majority of false alarms in personnel portals are triggered by hospital patients who have recently undergone radioiodine therapy. Whilst the extent of this problem is much lower than that of vehicle portals, a plastic scintillator based portal which can distinguish between isotopes at little extra cost than a standard portal would be largely beneficial to the security of events like the Olympic Games.

The study of plastic scintillation detectors used in radiation portal monitors of any variety therefore forms the basis of this thesis, with the intention of designing a system based on plastic scintillators capable of differentiating between radioactive sources. The benefits of such a system include high sensitivity and durability whilst retaining a moderately low cost.

1.2 Overview

Chapter 2 reviews the current radiation portal monitor technology being used, as well as some of the possible solutions to the false alarm rate problem being considered by various organisations. Common sources of radiation are categorised by their use into medical, industrial and nuclear applications as well as naturally occurring radioactive materials. The incident gamma-ray energy range of interest is defined by these sources as being from 30keV - 3.0MeV. The current use of plastic scintillators for gamma-ray detection in this energy range is studied with examples of its implementation in security portals. Other detector materials are also investigated including those with spectroscopic capabilities such as thallium doped sodium iodide scintillators and high purity germanium crystals with a discussion on their advantages and disadvan-

tages in comparison to plastic scintillators.

In Chapter 3 the key attributes of plastic scintillators are highlighted, with discussion of their intrinsic resolution and calibration techniques. Current portal designs are established as being a poor implementation of existing technology based on unrelated fields of study. Improvements to current plastic scintillator detector designs are defined with techniques on how to improve optical quality through the use of reflective materials, light guides, optical bonding and geometric considerations. The GEANT4 simulation tool-kit is also introduced as a means to explore new detector designs and quantify their benefits.

In Chapter 4 a new, small area plastic scintillator detector design is presented incorporating all the optical considerations presented in the previous Chapter. The result is a high performance plastic scintillator detector system capable of displaying excellent energy loss spectral quality. The performance of the detector system is quantified, including its optical characteristics, equivalent resolution and a comparison with the performance simulated using the GEANT4 tool-kit. Following the successful design of a small plastic detector, two new large area detector designs are also established. These two designs are presented along with their intrinsic characteristics, hardware profile and the software development required for their function. The resulting performance of each new design is compared with that of the smaller prototype design to ensure no significant degradation of spectral quality due to increasing the detection area.

Chapter 5 discusses the application of advanced spectrum processing techniques and identifies spectral deconvolution as an excellent candidate for processing the raw energy loss spectrum. Isotope classification and identification are discussed and software settings which must be used to process spectra from plastic scintillators are defined. New models used for processing spectra from plastic scintillators are established and an isotope identification library for use with plastic scintillators is established for the first time.

In Chapter 6 the isotope identification technology and spectral deconvolution techniques are applied to each of the new detectors designs established in Chapter 4. The results show the ability of these advanced plastic scintillator based detectors to not only detect but also identify a range of radioactive isotopes. A number of radioactive isotopes were tested and presented along with their raw and deconvolved spectra for comparison. A study is also completed which established that the identification success rate is heavily dependent on the number of counts present in each spectrum. With respect to this, a figure for the minimum number of counts per spectrum is published as 10,000 minimum counts to correctly identify isotopes with simple gamma-ray spectra such as Na-22, whilst those with more complex spectra, containing several distinct energies such as Eu-152, required a minimum of 22,000 counts per spectrum to identify with 100% success.

Chapter 7 investigates some the requirements for using the detector designs established in Chapter 4 inside a radiation portal monitor. Anomalies are addressed such as non-linearity in photomultiplier tubes and background scattering which can severely degrade the measured energy loss spectra. The impact of environmental factors such as temperature, shielding and background measurement is quantified. Automatic calibration techniques, positional sensitivity and multi channel analyser properties are also discussed, culminating in an extensive list of qualities which the components of the detector system must exhibit for effective use. The viability of neutron detection using only plastic scintillator was investigated, with specific emphasis placed on distinguishing neutrons from gamma-rays in the energy loss spectrum.

In Chapter 8 possible future PVT designs are outlined and evaluated for personnel portals and vehicles portals. The designs are based on the ANSI standards for the detection and identification of radioactive sources. The minimum volume of the detector system is established based upon the requirements of the ANSI standards for the identification of various isotopes with respect to the minimum number of counts required to identify such isotopes using the detector designs outlined in Chapter 4. Recent developments in photomultiplier tube technology are incorporated into the designs allowing for greater coverage area without spectral degradation. The results of

each system are presented along with limitations of use and comparisons with the previous PVT detector designs for verification of the spectral quality.

Chapter 9 summarises the work presented in the previous Chapters on plastic scintillators. The final configurations for an optimal design are outlined with the advantages and disadvantages that the system presents. Recommendations for possible future work are also outlined including the desire to fully test the work conducted in an industrial environment with proper field trials of the technology.

Chapter 2

Security Portals

2.1 Introduction

In Chapter 1, the problem of screening for radioactive materials using current radiation portal monitors was established. The following sections investigate this problem, defining the aims of radiation portal monitors and why the technology currently in use fails to achieve that aim. The problem is defined in two stages. Firstly the portal monitors can not initially distinguish between innocent and threatening sources of radiation leading to an alarm, and secondly once an alarm is triggered, resolving the source of the radiation requires time consuming identification techniques. A solution is therefore proposed that the portal monitor's ability to initially distinguish a radiation source should be improved. To achieve this aim, plastic scintillators are investigated with their interaction methods and compared to those of materials which are used in secondary screening techniques that can distinguish between radiation sources. A brief look at how other organisations propose to tackle this problem are given, and finally the intention to improve plastic scintillators as a possible solution is established.

2.2 Radiation Portal Monitors

2.2.1 The Aim of Radiation Portal Monitors

The threat of a nuclear based attack takes two main forms: a nuclear/atomic bomb, and a radiological dispersion device. A nuclear bomb is constructed using either plu-

tonium or highly enriched uranium (HEU) as its fuel, both of which are radioactive, releasing gamma-ray and neutron radiation. A nuclear weapon of this kind is most likely to be of a relatively crude, fission based design, but such a device is still capable of destroying an entire city. A radiological dispersion device is a device designed to disperse radioactive material over a designated target in order to cause harm. An example of this is a "dirty bomb" where a radioactive isotope is combined with a common explosive and detonated to spread the isotope over the desired area. Other devices could distribute radioactive material passively (non-explosively), such as spraying or spreading by hand. Alternately, a radiological exposure device could be used, which would simply involve placing a radioactive source in a public area to expose pedestrians passing by [Argonne National Laboratory, 2005].

Radiation portal monitors were designed to detect nuclear materials by measuring the incoming flux of gamma-rays or neutrons emitted by the radioactive material. The material inside radiation portal monitors responsible for the detection of gamma-rays is currently a polyvinyl toluene (PVT) based scintillator. PVT scintillator releases optical light upon interaction with gamma-rays which is then converted to an electrical signal by use of an attached photomultiplier tube. PVT based scintillators are popular for gamma-ray detection because of their relatively low cost, high versatility and excellent detection efficiency given the large areas they can be moulded into.

Gamma ray detectors of this type first arose in security applications with the use of PVT detector portals placed at a steel works [Lubenau and Yusko, 1995]. Orphaned radioactive sources used in the medical industry had been inadequately disposed of and became mixed with scrap metal which was then melted down into steel. After discovering the steel was radioactive it became worthless and the furnaces had to shut down whilst all radioactive traces were removed. The steel works suffered significant financial and productivity loss. Many similar incidents arose [Lubenau and Yusko, 1998] leading to the employment of relatively cheap plastic scintillator portals to detect any potential radioactive contaminants. The employment of PVT based portals at the steel works was a success.

Following the popularity and success of PVT based portals, the United States customs and borders protection placed PVT radiation portal monitors either side of traffic lanes for vehicles to drive between. The aim of these radiation portal monitors was to detect the presence of any radioactive materials present in the vehicle's cargo as it passed through. If an alarm sounded then the cargo would be flagged and the vehicle taken aside for investigation. The initial screening process of the radiation portal monitors was termed primary screening, whilst any more detailed follow up examinations were known as secondary screening.

2.2.2 How Radiation Portal Monitors Failed

Problems soon arose with these systems as they were initially designed to check for the presence of radioactive materials in an environment where none were expected. The primary screening technique could not distinguish between radiation produced by different sources and therefore gave an alarm when naturally occurring radioactive materials (NORM) such as bananas, cat litter, fertiliser or certain aggregates passed through a portal [Lipton]. Innocent alarms such as these, where no threatening material was present but the alarm was still triggered were termed "false alarms". The term "false alarm" is often used to cover two scenarios, one where an alarm sounded where there was no radioactive material, and one where benign material was present and sounded the alarm. Either scenario hinders the flow of traffic through borders unnecessarily. As a specific example, the Port of Los Angeles, adjudicated nearly 115,000 radiological alarms in 2007, which translates into between 400 and 600 alarms on a typical weekday [Winkowski, 2008]. Customs and borders protection officials report that on average plastic scintillators generate up to about 600 innocent alarms per day [Government Accountability Office, 2009], confirming that the majority of alarms are innocent in nature. The International Atomic Energy Association's (IAEA) illicit trafficking database (ITDB) 2007 also provides interesting figures from 1993 to 2007, reporting that:

> "As of 31 December 2007, the ITDB contained 1340 confirmed incidents reported by the participating States and a few non-participating States. Of the 1340 confirmed incidents, 303 incidents involved unauthorized possession and related criminal activity, 390 incidents involved theft or loss

of nuclear or other radioactive materials, and 570 incidents involved other unauthorized activities. For the remaining 77 incidents, the reported information was not sufficient to determine the category of incident."

[International Atomic Energy Agency, 2007].

These confirmed incidents originate from 100 countries around the world as defined in the ITDB 2007. Over 14 years 1340 confirmed incidents were reported, giving an average of around 95 threatening sources per year. This equates to far below one per day in any one country.

Each time a false alarm sounded, the vehicle and its cargo would be taken aside and investigated using secondary screening techniques. Such techniques involved the use of a small, hand-held detector which incorporated a spectroscopic quality scintillation crystal such as NaI(Tl). Gamma-ray spectroscopy with this hand-held detector subsequently confirmed the origin of the alarm. The secondary screening was effective but took a long time and overall costs were increased due to requiring two screenings for any alarm. Given that such a large proportion of alarms every day were false, the portal monitor operators reduced the sensitivity of the detectors to avoid the requirement for the secondary screening.

2.2.3 A Potential Solution

Following the high rate of false alarms, the decision was made to further investigate current radiation portal monitor technology to establish if the PVT scintillator material contained in them is capable of distinguishing between different radiation sources. Given that secondary screenings with spectroscopic materials such as NaI(Tl) have proven successful, the properties of similar materials are also investigated for comparison with PVT. If PVT can perform spectroscopy in a similar way that NaI(Tl) crystals can, then a form of spectrometry could be incorporated into the primary screening stage to distinguish radioactive materials. This would reduce the number of false alarms and thus the requirement for secondary screening techniques.

2.3 Detector Materials

2.3.1 Radiation Interaction

The method of how gamma-rays interact with PVT and spectroscopic materials must first be reviewed to understand how current secondary screening techniques can identify radioactive sources and primary techniques cannot. Gamma-rays interact with matter in 3 main ways: Photo-electric absorption; Compton scattering and Electron-Positron pair production. Each of these interaction processes takes dominance with respect to gamma-ray energy and the atomic number of the interaction material. The energy range useful for detecting gamma-rays from radioactive isotopes is up to around 3MeV. For energies less than 1.022MeV, the photo-electric effect and Compton scattering are both possible, whereas above 1.022MeV pair production is also possible [Knoll, 2000]. For plastic scintillator, the majority of the interaction is via Compton scattering, with only low-energy photons interacting via photoelectric absorption and a very small chance of pair production at high energies.

2.3.1.1 Photoelectric Absorption

In photo-electric absorption an incident gamma-ray is absorbed by an electron in the interaction material. The electron is then ejected with an energy equivalent to the incident gamma-ray minus the binding energy of the electron. The full energy of the incident gamma-ray is transferred to the scintillation medium via the interaction of the resultant electron with the scintillator. The probability of photo-electric absorption occurring is approximated using equation (2.1):

$$P_{p.e.} \propto \frac{Z^n}{E^{3.5}} \tag{2.1}$$

Where E is the gamma-ray energy, Z is the atomic number of the material and the exponent n ranges between 4 and 5.

2.3.1.2 Compton Scattering

In Compton scattering an incident gamma-ray of energy $h\nu$ is scattered off an electron in the interaction material, transferring energy $h\nu'$ in relation to the scattering angle θ

to the resultant recoiled electron. This process is shown in equation (2.2).

$$h\nu' = \frac{h\nu}{1 + \frac{h\nu}{m_e c^2}(1 - cos\theta)} \tag{2.2}$$

The full energy of the incident gamma-ray is therefore not deposited in the interaction material, with the scattered gamma-ray often able to escape from the material after interaction. The maximum energy deposited to the scintillation material is where θ = 180°, corresponding to a Compton edge in an energy loss spectrum. The angular distribution of scattered gamma-rays is predicted by the Klein-Nishina formula equation (2.3) and demonstrates a strong tendency for forward scattering at high energy values [Knoll, 1989].

$$\frac{d\sigma}{d\Omega} = \frac{1}{2}\alpha^2 r_c^2 P(E_\gamma, \theta)^2 (P(E_\gamma, \theta) + P(E_\gamma, \theta)^{-1} - 1 + cos^2(\theta)) \tag{2.3}$$

Figure 2.1shows a typical illustration of the angular distribution of scattered gamma-rays at various energies [Scraggs, 2009]. The energies shown are emitted by a range of isotopes such as Am-241, Na-22 and K-40, with the exception of 2.75eV which is in the blue region of the visual light spectrum and 10MeV which is in the energy region of gamma-ray bursts.

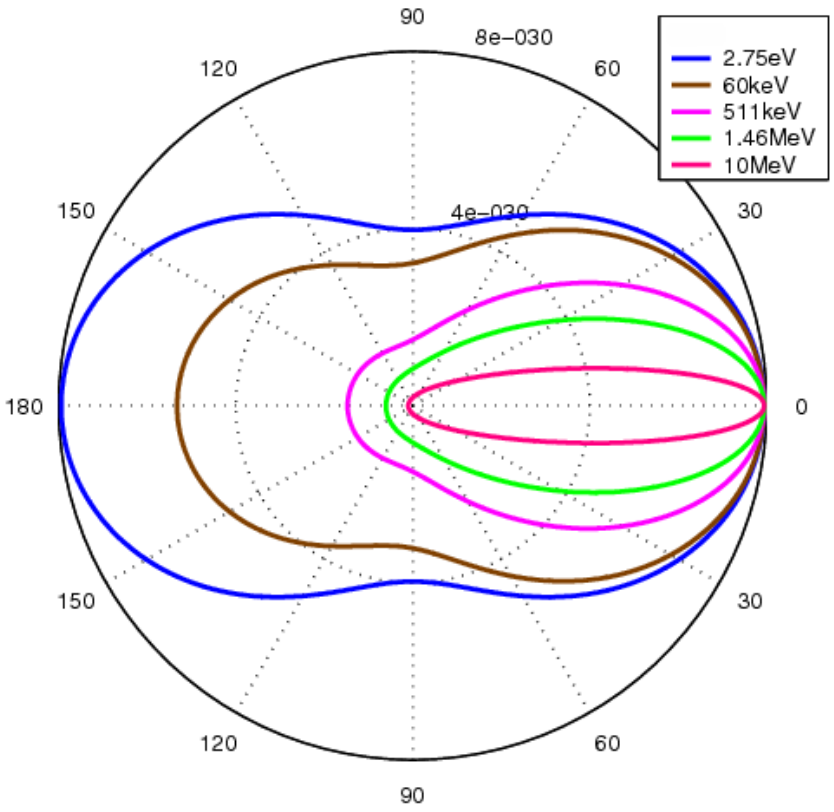

Figure 2.1: A typical angular distribution diagram of scattered gamma-rays predicted by the Klein-Nishina formula. The gamma-ray energies shown are emitted by a range of isotopes such as Am-241, Na-22 and K-40.

2.3.1.3 Pair Production

Electron-Positron pair production occurs at high incident gamma-ray energies. An electron and positron are produced when the incident gamma-ray has more than twice the combined rest mass of the particles, and interacts with a material's atomic nucleus. This never becomes a significant process for interaction with plastic scintillator over the energy range of interest due to the material's low atomic number.

2.3.2 Plastic Scintillators

Plastic scintillators consist of a base plastic such as polyvinyl-toluene (PVT) mixed with a number of fluors. The base plastic is responsible for the primary interaction

with gamma-rays, releasing a charged particle in the form of an electron. The high energy electron excites other electrons in the scintillator as it passes, causing them to radiate energy as they de-excite, a small percentage of which is in the form of optical photons. However, with the addition of a primary fluor, the dominant mechanism for the transfer of energy in PVT is not via radiation transfer, but via the Forster effect. In this mechanism, where a sufficient concentration of fluor is present, the distance between the PVT molecules and the fluor is around 100 Angstroms. A resonant dipole-dipole interaction occurs between the strongly coupled base PVT and fluor, sharply increasing the speed and the light yield of the plastic [Amsler et al, 2008]. A secondary fluor absorbs emitted light from the primary fluor and radiates at a longer, stokes-shifted wavelength, which is more suitable for less-attenuated propagation of the light through the PVT base. Figure 2.2 shows the mechanism of the PVT scintillation process. Various types of plastic scintillator are commercially available, each

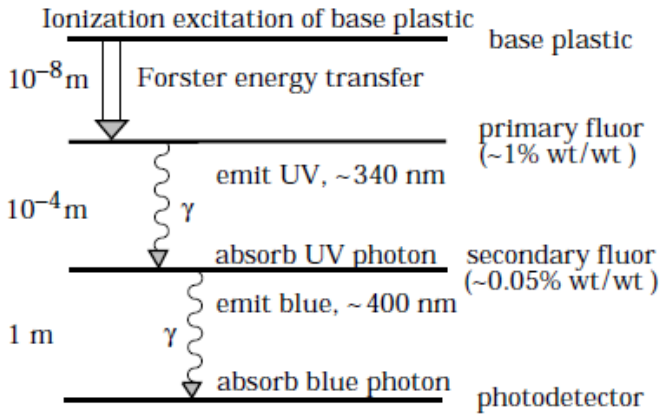

Figure 2.2: Mechanism of the PVT Scintillation Process. Figure from [Amsler et al, 2008].

incorporating unique properties such as fast timing, high tolerance to temperature and some that are loaded with materials such as lead for greater radiation stopping power. Each type of material is designed for a specific use. A general plastic scintillator with good all round properties is PVT based, usually quoted as similar in properties to nuclear enterprises (NE) Pilot F. The typical properties of such a scintillator are shown in table 2.1. PVT scintillators have a relatively low light output of just 10,000 photons per MeV of energy deposited. However, the wavelength of maximum emission

Table 2.1: Properties of a typical PVT Scintillator.

Scintillation Efficiency	10,000 Photons/MeV
Wavelength of Max. Emission	425nm
Rise Time	0.9ns
Decay Time	2.1ns
Density	1.023g/cc
Refractive Index	1.58
Bulk Light Attenuation Length	3.8m

ensures good compatibility with the optimal quantum efficiency of blue-sensitive photomultiplier tubes and the long light attenuation length means large volumes can be produced without significant light loss due to optical attenuation. The fast rise and decay times are also excellent for high count rates and timing applications. Due to the low atomic number of plastic scintillators, the majority of gamma-ray interaction occurs via Compton scattering, making them good candidates for gamma-ray detection, but having little or no spectroscopic quality. The combination of low light yield, low atomic density and low physical density are the major drawbacks of PVT scintillators.

2.3.3 Semiconductors

Semiconductors interact with gamma-rays via the photoelectric effect; the ejected high energy electron directly exciting further electrons from the valence band of the semiconductor into the conduction band and leaving holes in the valence band. These electrons and holes travel to applied electrodes where they are collected, the number of electrons and holes collected correspond to the amount of energy deposited in the semiconductor. Typical examples include high purity germanium (HPGe) and cadmium zinc telluride (CZT) detectors. Semiconductor based detectors in the form of HPGe offer the finest resolution available today at around 0.3% at 662keV. However, such instruments are expensive, costing many times more than that of an equivalent sized scintillation crystal. HPGe must also be cooled, usually with liquid nitrogen, as the thermal excitation at higher temperatures is enough for the valence band electrons to cross the band gap into the conduction band, rendering the detector ineffective.

Semiconductors of this type are only available in limited sizes; CZT detectors come in a pixelated array of small detectors, whilst improvements in HPGe production means that they are now available in sizes similar to that of small crystal scintillators.

2.3.4 Crystal Scintillators

Crystal scintillators are commercially available in many forms, the most common of which are thallium doped sodium iodide NaI(Tl), thallium doped caesium iodide CsI(Tl), bismuth germanate BGO and the more recent cerium doped lanthanum bromide $LaBr_3$(Ce). Crystal scintillators are often doped with activators such as thallium in the case of NaI(Tl) which enable a greater emission of scintillation light at an adjusted wavelength. In contrast to PVT, crystal scintillators are higher in atomic number and therefore photoelectric absorption is a major radiation interaction process over the energy range of interest. This, and their higher density make crystal scintillators excellent candidates for gamma-ray spectroscopy. Gamma-ray spectrometers using scintillation crystals such as NaI(Tl) are usually referred to as medium resolution, in comparison to the fine resolution available using semi-conductor based spectrometers. Table 2.2 shows the properties of some of the more commonly available crystal scintillators. Each crystal has unique properties that make it suitable for certain applications. Alkali halides such as NaI(Tl) and CsI(Tl) are popular for their good overall resolution. Whereas crystals such as bismuth germinate (BGO) have a lower light yield but a greater density and therefore greater chance of interacting with higher energy gamma-rays. The cost of these materials is a prime factor when considering the construction of gamma-ray detectors, the most popular of these crystals is NaI(Tl); it has good resolution at room temperature and a relatively low cost in comparison to other crystals. Cerium doped lanthanum bromide detectors give further improvements in resolution, but as this technology is relatively new they are currently only available in smaller sizes and cost significantly more than thallium doped sodium iodide.

Table 2.2: Properties of Various Crystal Scintillators

Material	Density	Emission Wavelength	Refractive Index	Decay Constant	Light Yield	FWHM @ 662keV	Hygroscopic
NaI(Tl)	3.67	415	1.85	230	38000	6.00	Yes
CsI(Tl)	4.51	540	1.8	1000	52000	8.00	Slightly
BGO	7.13	505	2.15	300	8200	10.00	No
LaBr	5.29	380	1.9	25	63000	2.80	Yes
PVT	1.02	423	1.58	2.4	10000	N/A	No
Units	g/cm^3	nm	N/A	ns	Photons/MeV	%	N/A

2.4 Portal Monitor Solutions Under Investigation

After overviewing the materials available and the methodologies involved in gamma-ray detection, the following is a summary of possible detection technologies that could help improve the situation at customs and borders. Some of these technologies are being studied extensively by other organisations. The current view in discriminating between NORM and threatening materials is to improve PVT scintillators (both physically or with software enhancement) to give them better discrimination abilities, or to use a different material with higher energy resolution to identify each material as it passes, thereby eliminating the need for secondary screening.

2.4.1 HPGe Portals

High purity germanium detectors provide the best spectroscopic information available, and therefore qualify as a key choice in radiation portal monitors with primary identification ability. Recent advances in mechanical cooling mean that HPGe based detector gain a degree of portability and reduce the costs associated with running them. The

main disadvantages of HPGe are the low detection efficiency given their small area and the high price of the detector and cooling required. Its advantages are its high resolution and primary interaction method. The cooling required also prevents against temperature based gain drifts often found with NaI(Tl) based systems. In 2004 Ely et al [Ely et al., 2004] complete a report comparing the benefits of HPGe detectors against that of a NaI(Tl) and PVT based equivalent. They state the price of an HPGe detector as $75,000 and further calculate that in order to match the same sensitivity as PVT portals can provide, the number of HPGe crystals required would be around 180. This would be a cost of around $13.5 million for each portal, and further running costs to cool the detector makes HPGe primary screening an extremely expensive and therefore unattractive option for primary screening.

2.4.2 Advanced Spectroscopic Portals

Advanced spectroscopic portals (ASP) using NaI(Tl) crystal arrays are under investigation as a primary screening method. In 2005 Siciliano et al [Siciliano et al., 2005] completed an overview comparing the benefits of using NaI(Tl) scintillators with respect to PVT scintillators in vehicle portal monitors. The PVT scintillator used was a 3.8cm$\times$36cm$\times$173cm (23.7 litres) panel with a single 2.5cm photomultiplier tube attached to one end, whereas the NaI(Tl) detector was a single 10cm$\times$10cm$\times$41cm (4"$\times$4"$\times$16") detector encased in a 0.05 cm thick steel shell. The authors investigate issues such as NORM discrimination, cost and durability of both systems. They found that when concerning NORM discrimination, limited results can be obtained using PVT by incorporating broad energy windowing (discussed further in Chapter 5) to discriminate between various isotopes. NaI(Tl) provided much better discrimination by directly identifying isotopes using its superior energy resolution and the presence of photo-peaks in the energy loss spectra. The authors found that NaI(Tl) crystals are prone to damage or drifts in gain due to temperature changes, whereas PVT scintillators are more durable in general. The estimated price for a NaI(Tl) based advanced spectroscopic portal in 2008, was around $822,000 for full deployment, whereas the PVT based radiation portal monitors were around $308,000 [Government Accountability Office, 2009] so the NaI(Tl) based portals are nearer the costs of PVT than HPGe, but still significantly more expensive. Certain situations would still re-

quire secondary screening however, such as masking of one isotope using another less threatening one, where the NaI(Tl) may still not have enough resolution to resolve conflicting energy peaks. Figure 2.3 shows a typical NaI(Tl) scintillator portal configuration with many NaI(Tl) detectors enclosed in each panel of the portal. Figure 2.4 shows a typical NaI(Tl) energy loss spectrum, in this case a spectrum of the isotope Radium-226.

Figure 2.3: A typical NaI(Tl) based portal configuration showing 4x NaI(Tl) detectors in each of the portal's panels [Pacific Northwest National Laboratory, 2009].

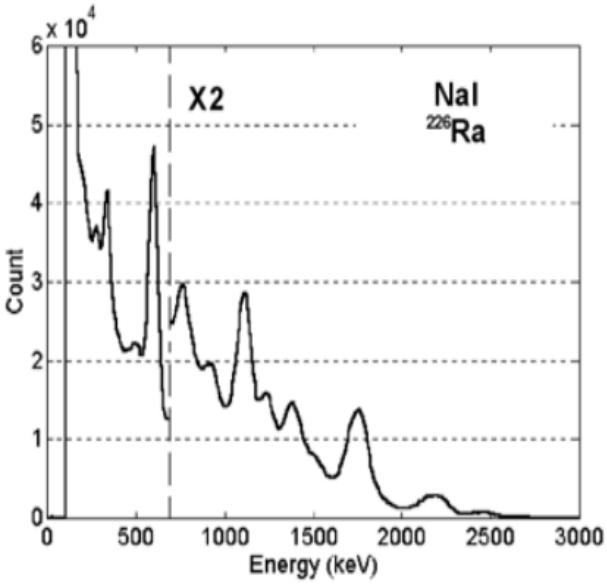

Figure 2.4: A Radium-226 spectrum taken using a NaI(Tl) based detector [MENG et al., 2002].

2.5 Current PVT Detector Designs

Current PVT detector designs give little thought to the quality of the resulting spectra they produce, typically consisting of large slabs of plastic with a one or two photomultiplier tubes attached to collect the scintillation light. These designs are intended purely for maximising the detector efficiency by increasing the volume of PVT; a typical 200cm×50cm×50cm design, for example, contains 500 litres of PVT. More recent designs are slightly more conservative, consisting of similar dimensions in height and width but being much thinner at around 4cm to 10cm. Examining the energy loss spectra produced by such a design may never have been an option given that plastic scintillators have always been considered a non spectroscopic quality product. If any sort of radioactive source discrimination is to be achieved however, the output of such devices should be closely examined. Figure 2.5 shows a variety of spectra taken by Siciliano 2005 [Siciliano et al., 2005] using a typical PVT detector of dimensions 173cm×36cm×3.8cm (23.5 litre). The detector used to produce Figure 2.5 had 1x

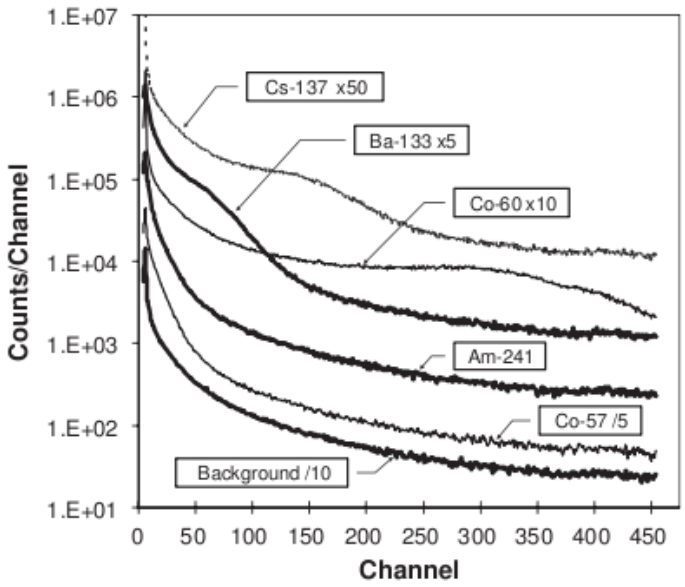

Figure 2.5: A variety of spectra taken with a PVT detector of dimensions 173cm×36cm×3.8cm

photomultiplier tube attached to the bottom to collect the scintillation light produced. The spectra are presented on a logarithmic scale and clearly show little discerning features for each of the spectra. The Compton edges that should be present are heavily broadened to the point that they cannot be recognised. The only useful information

that these type of spectra can provide are the shape of the spectra themselves and therefore a rough number of counts at high or low energies. The spectra of Am-241 and Co-57 are the same shape as the background spectrum, only at a higher number of counts. Ba-133, Cs-137 and Co-60 show slight humps where Compton edges should appear, but they are much too broad to be associated specifically with those isotopes. Other isotopes with spectral lines in a similar energy range could easily be misidentified as a range of other isotopes. Figure 2.5 represents a relatively average set of spectra taken with PVT, though many such detectors have a much greater thickness with the same light collection area, further degrading any signal produced. These spectra do not contain enough information to accurately distinguish between the sources they are measuring, it is therefore clear that the quality of information contained within them must be improved.

2.5.1 Targets For Change

As previously established, PVT based scintillators' dominant radiation interaction method for the energy range of interest is Compton scattering. Therefore the only uniquely identifying aspects of the energy loss spectra are the Compton edges produced. In order to reduce false alarm rates, the detector must be able to distinguish one radiation source from another. Spectroscopic detectors such as those based on NaI(Tl) already have this ability. Crystal scintillator spectrometers such as NaI(Tl) are often optimally designed to give maximum performance and therefore increase the detector resolution to its fullest potential in order to maximise the chances of identifying an isotope. Although NaI(Tl) based detectors rely on photo-peaks to identify spectra, the attention given to the detector design is far superior to that given to the PVT detectors present in current radiation portals. The optimisation principles applied to NaI(Tl) detectors could be applied to PVT to increase the quality of their energy loss spectra. Larger photomultiplier tubes and better proportionality between the light collection area and the detector dimensions are apparent in NaI(Tl) detectors as basic examples. Applying these qualities to PVT detectors could subsequently improve the chances of a system being able to discriminate one source from another. A PVT detector with improved resolution might also be properly calibrated. Finally, to save on the costs of introducing a whole new portal system, a refined PVT scintillator in-

corporating NaI(Tl) design principles could be retro-fitted to existing radiation portal monitors.

2.6 Conclusions

In a rush to implement counter terrorist technology after a series of terrorist attacks, the United States of America department of homeland security used PVT based radiation portal monitors to screen for potential radiological threats at its borders. Current PVT based radiation portal monitors detect threatening sources well but give rise to high false alarm rates during primary screening processes which then require extensive secondary screening to determine its cause. The high number of false alarms hinders commerce and wastes time and money. A range of possible solutions were reviewed including changing to spectroscopic detector materials for the primary screening process as well as improving upon the existing PVT systems to reduce the number of false alarms. High resolution systems such as HPGe offer the most desirable resolution but the high price and low sensitivity make this an extremely expensive and therefore non-viable option. Advanced spectroscopic portals in the form of NaI(Tl) scintillator detectors form one of the best alternatives with improved resolution, but at a cost of over double that of PVT. It is clear that not enough was done to ensure that PVT detectors were fully optimised for the task they were assigned to before such technology was commissioned. In the next chapter, PVT scintillators are studied in more detail with the aim of enhancing them to a point where analytical technologies can take full advantage of its improved characteristics. These improvements ensure the retention of good sensitivity and low cost that makes PVT based systems such an attractive option for radiation portal monitors.

Chapter 3

Enhancing Plastic Scintillators

3.1 Introduction

In the previous chapter a potential threat to the US and other NATO countries' national security by nuclear attack was outlined, as well as the preliminary measures taken by the United States department of homeland security to help prevent such an attack. Screening cargo and personnel for radiological threats was one such measure, but the screening technology was found to be flawed. It was concluded that the rush to implement whatever existing detector technology was available at that time was the main cause of this problem, leading to the present research into other technologies. A number of possibilities were discussed to improve upon the radiation portal monitor technology, with the decision to further investigate enhancing current PVT monitors for optimal performance during primary screening. Such optimised detectors could reduce the need for using secondary screening techniques to help discriminate threatening sources from benign sources. This detector optimisation will incorporate, amongst other attributes, the application of techniques used currently for NaI(Tl) detectors to improve the design and therefore performance of PVT based detectors.

3.2 Detector Optimisation

The quality of a detector system as a whole is limited by four factors: design requirement; price; available technology and build quality. Cheaper materials and poorer quality instruments can be used to lower the cost of the system, but doing so will

result in poorer performance. Conversely the latest technology could be used to get the best quality results but the overall design of the system in terms of its size and functionality would have to be reduced to compensate for the increase in price. For a successful system the design requirements must be met 100% with the best available technology available for a given price. The key factors affecting the design requirement of a radiation portal monitor are the sensitivity of the detector and the reliability of the system. The detector must be sensitive enough to cover the object being tested and give an acceptable margin of error in its measurements. Other design factors such as portability and ruggedisation vary depending on the detector application. The available technology is dependent on available materials for a given cost and the application of rigorous design principles and computational software to produce the best possible results. The following sections concentrate on using well established technology to improve detector performance at a reasonable price.

3.3 Scintillator Detector Resolution

The detector resolution of a typical crystal scintillator used in secondary screening techniques is a direct measurement of how well the detector can resolve incident gamma-rays at certain energies. A standard measurement is the full width at half maximum (FWHM) of a photo-peak in the energy loss spectrum. Increasing the resolution and thus decreasing the FWHM over the entire range of incident energies increases the chances of differentiating one isotope from another. The factors which effect the energy resolution of a typical scintillation crystal can be described using equation (3.1) [Meng et al., 2002].

$$R_{Total} = \sqrt{R^2_{Statistical} + R^2_{Noise} + R^2_{Intrinsic} + R^2_{VLCE}} \tag{3.1}$$

Where $R_{Statistical}$ is the contribution from statistical broadening, R_{Noise} is the contribution from electronic noise in the system, $R_{Intrinsic}$ is the contribution from the intrinsic variation in the light yield with respect to incident gamma-ray energy and R_{VLCE} is the contribution from a spatial variation in the light collection efficiency of the detector. In order to optimise the resolution of a scintillator, each of the above factors must be minimised. R_{Noise} is not usually a dominant factor due to the low noise

of modern photomultiplier tubes used in scintillation detector systems and $R_{Intrinsic}$ is assumed to be negligible for PVT, as the light output is stated to be relatively linear with respect to the incident gamma-ray energy [Knoll, 1989]. Although some reports [Brannen and Olde, 1962] suggest a non-linearity in the light yield of PVT below 125keV, this is discussed in more detail further in this chapter. The two main contributions to the resolution of the detector system are the spatial variation in the light collection efficiency, and the statistical broadening effects in the number of photo-electrons produced. $R_{Statistical}$ is defined in equation (3.2) as the statistical variation in the number of photo-electrons N_P received by the system per gamma-ray interaction.

$$R_{Statistical} = \frac{\sqrt{N_P}}{N_P} \tag{3.2}$$

The number of photo-electrons N_P received is defined in equation (3.3).

$$N_P = Q.E. \times L.C.E. \times L.Y. \times E_\gamma \tag{3.3}$$

Where $Q.E.$ is the average quantum efficiency of the photomultiplier tube, $L.C.E.$ is the average light collection efficiency of the detector, $L.Y.$ is the light yield of the scintillator and E_γ is the energy of the incident gamma-ray. It is therefore evident that in order to improve the detector resolution, the light collection efficiency of the detector must be maximised whilst minimising the spatial variation in the light collection. This combination will maximise the total number of photoelectrons received by the system and thereby reduce the statistical error; improving the detector resolution as a whole.

3.3.1 Light Collection Efficiency

The light collection efficiency of a detector is measured as the average percentage of light that reaches the photomultiplier tube(s) for each scintillation pulse created in the detector. Ideally, on each scintillation event 100% of the resultant optical light would travel through the detector material to reach the photomultiplier tube. This is not the case though, as the light produced is subject to factors which significantly reduce its chances of ever reaching the photomultiplier tube. These factors include light loss due to escape from the surface of the detector, optical attenuation from the scintillation

material and optical attenuation from any reflective materials applied to the detector's surface. As the light from each scintillation event is emitted isotropically, a proportion of the light inevitably escapes through the detector's surface if no reflective material is used to confine it, in this case the detector must rely on total internal reflection to transport the light internally. Light will escape if its angle of incidence is greater than the total internal reflection critical angle, which is around 39^o for a plastic scintillator surrounded by air. Scintillation material has an optical attenuation length (α), defined as the average length of the material that the scintillation light of a given wavelength can travel through before 50% of it is absorbed. The absorption of light through the scintillator is exponential as shown in equation (3.4).

$$I = I_0 e^{-\mu x} \tag{3.4}$$

Where I_0 is the initial intensity of light, I is the resultant intensity of light, μ is the attenuation coefficient and x is the path length. The optical attenuation length α is then defined in equation (3.5).

$$\alpha = -\frac{ln(0.5)}{\mu} \tag{3.5}$$

In NaI(Tl) the optical attenuation length is relatively short at just 0.3m, whereas PVT has a much better attenuation length of 3.8m. A longer attenuation length enables larger detector designs without radically reducing the average light collection efficiency due to optical absorption. The attenuation length also significantly affects the variation in the light collection efficiency of the detector, as the chance for the light from each scintillation event being detected is dependent on its average path length. This increases with initial distance from the photomultiplier tube and the number of times the light is reflected before detection. A short attenuation length results in greater variation of light received for the same shape detector. The geometry of the detector therefore has a great effect on the light collection efficiency and variation in the light collection efficiency of a given design, smaller sized designs have the best light collection efficiency and lowest variation in the light collection efficiency, but at the cost of lower detection area. The shape of the detector, regardless of its size, also has an important role to play in determining how much of the light escapes through its surfaces. Applying reflective coatings to detector's surfaces can dramatically reduce

the amount of light loss by forcing the light to reflect internally until it reaches the photomultiplier tube. Shaping the detector can minimise the number of reflections required, increasing the light collection efficiency and reducing the variation in the light collection efficiency.

3.3.2 Photomultiplier Tube Collection Efficiency

Equation (3.3) states that the number of photoelectrons received by the detector is a multiple of factors including the quantum efficiency of the photomultiplier tube. This quantum efficiency is the efficiency of the photo-cathode and is typically quoted by manufacturers to have a value of around 25%. However, this value if used by itself does not give an accurate representation of the collection efficiency of the photomultiplier as a whole. There are other factors affecting the overall collection efficiency. The first is that the emission spectrum of PVT is not a perfect delta function at 425nm, but a function of wavelength that varies mostly from 400nm to 500nm as shown in Figure 3.1. The quantum efficiency of the photo-cathode at these wavelengths is also not

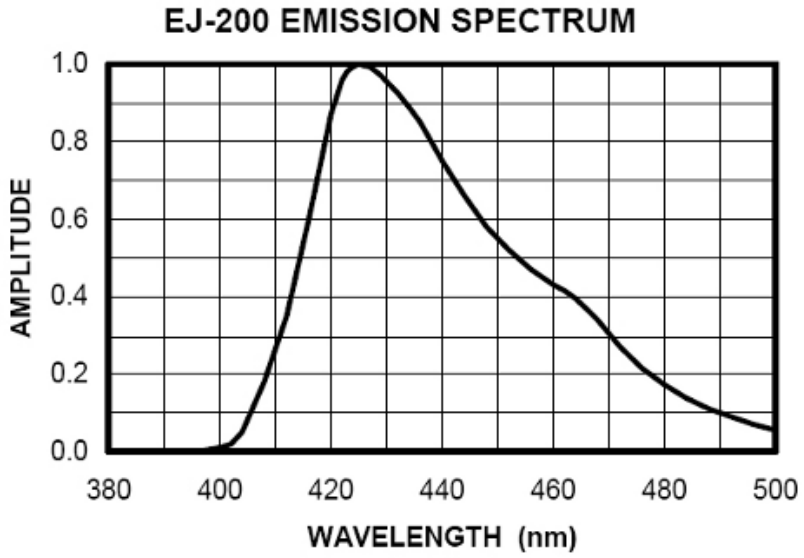

Figure 3.1: Emission spectrum of Eljen 200, a typical plastic scintillator

constant, but varies according to wavelength, as shown in Figure 3.2. Therefore to get the real photo-cathode collection efficiency when collecting light from PVT, the two spectra must be combined and the average value taken. In this instance a 5" Photonis XP3540 photomultiplier tube has a relatively good quantum efficiency of 27% at

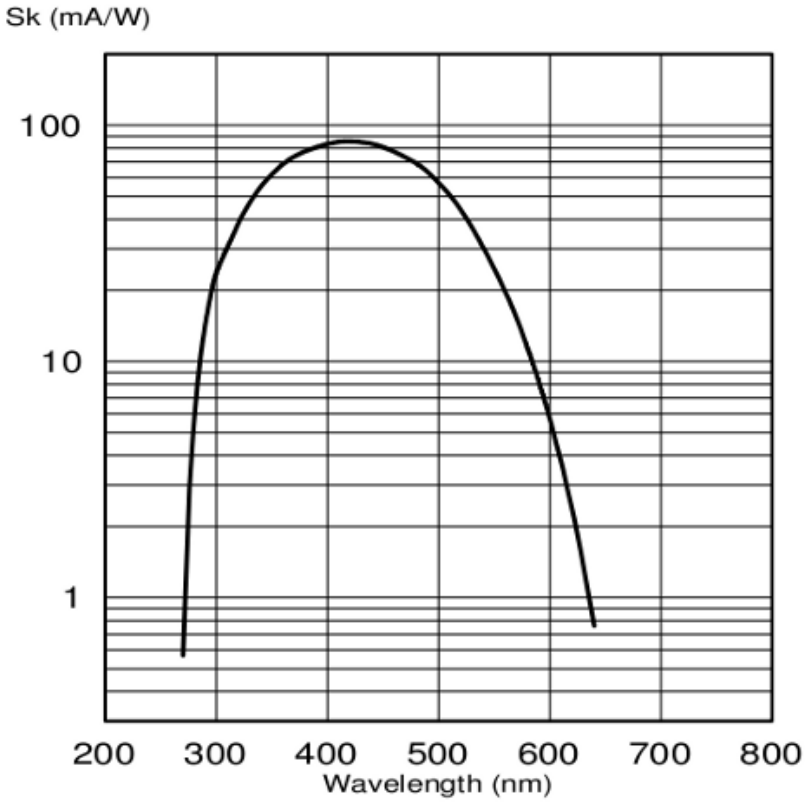

Figure 3.2: Photo-cathode quantum efficiency of Photonis XP3540 photomultiplier tube with respect to incident wavelength of light.

425nm. This value when combined however reduces to an average value of 23.5% for use with PVT.

The next factor is the photo-cathode to first dynode collection efficiency and the subsequent collection efficiencies of further dynodes. This value is difficult to measure and as of yet no manufacturer has supplied an accurate measurement. Hamamatsu however states that the efficiency of a typical first dynode increases with the applied voltage, and for voltages of over 100V the efficiency is over 95%. Typical values used by Hamamatsu for all the collective dynode efficiencies are estimated at around 90%. Finally, the spatial variation in the photo-cathode quantum efficiency for large area photomultiplier tubes is significantly large. Figure 3.3 shows the spatial variation of the photo-cathode quantum efficiency for the Photonis XP3540 photomultiplier tube. This figure shows variations for both the parallel and perpendicular axis of the tube with respect to the first dynode alignment. It has been noted on various photomultiplier tubes that an alignment parallel to the first dynode gives a slightly more uniform

response than other geometrical alignments. This value does not give a variance in the

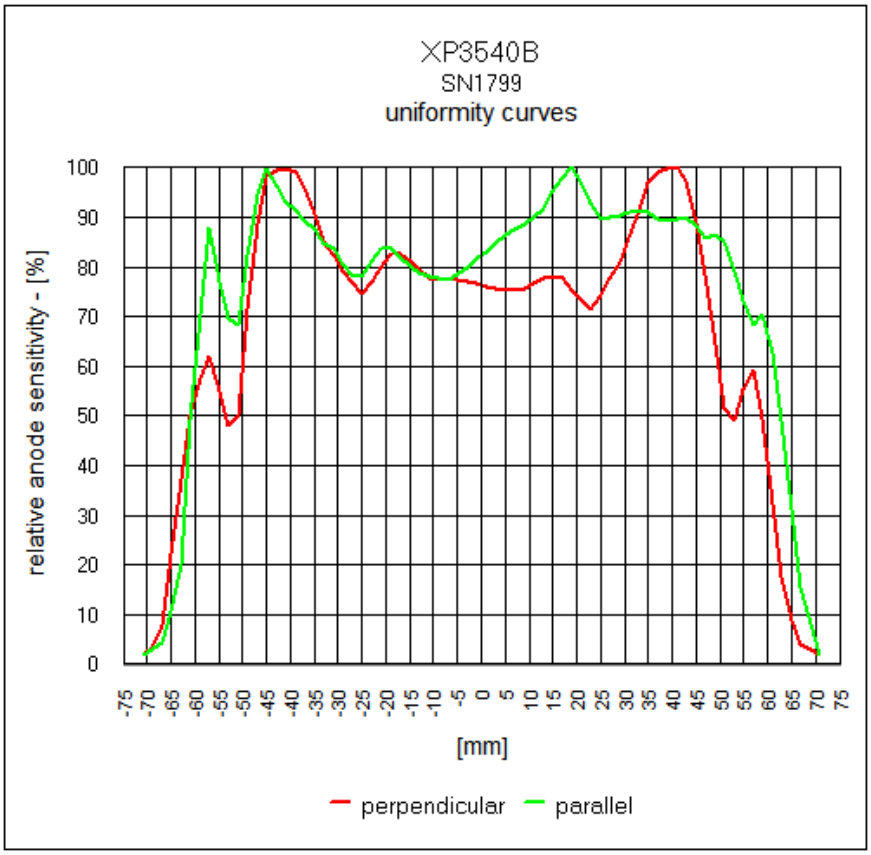

Figure 3.3: Spatial variation of the photo-cathode quantum efficiency for the Photonis XP3540 photomultiplier tube.

signal due to the even spreading of a high number of incident photons. Instead, the average value of the quantum-efficiency must be taken for the whole area. In this case the coefficient of variation for the 5" Photonis XP3540 photomultiplier tube is around 20%, with a mean photo-cathode quantum efficiency of 0.9x the peak quantum efficiency stated by the manufacturer.

The culmination of these factors gives a resulting photomultiplier tube light conversion efficiency of around 18%, a significant degradation to the initial 27% photo-cathode quantum efficiency which may have otherwise been used. Therefore choosing a photomultiplier tube which has a high quantum efficiency and a uniform response is of vital importance.

3.3.3 Reflective Materials

PVT designs have the benefit of an optical quality finish on their larger faces due to being cast, whereas crystal scintillators such as NaI(Tl) have to be milled into shape, leaving a rougher face. The scintillation light produced in PVT detectors is therefore subject to total internal reflection (TIR), where 100% of the light is reflected from its larger surface, given that its angle of incidence is less than the TIR critical angle. The smaller surfaces, or edges, of PVT detectors are usually milled to specification, leading to a poorer quality finish and therefore no TIR. Light reflecting from these rougher surfaces have an increasing chance of loss each time they reflect. For smaller detectors this is generally not a problem, but for the large area designs desired for radiation portal monitors, multiple internal reflections may occur before ultimately reaching the attached photomultiplier tube, further increasing the path length of the light. Current radiation portal monitors rely on total internal reflection to contain the scintillation light until it can be detected by the photomultiplier tube. Further reflective materials can be added to the detector to maximise the light collection. These materials are categorised as either specular reflectors or diffuse reflectors and have different efficiencies.

3.3.4 Material Type

Plastic scintillator comes in a variety of options for different applications. Many useful properties can be added to PVT to optimise the material for a certain task. For example, wavelength shifted scintillator that emits light in the green or red portion of the optical spectrum are suitable for coupling with photo-diodes and loading the scintillator with an extra element such as lead can increase its stopping power at lower energies. These refinements usually come at a cost however, the light output of wavelength shifted PVT is significantly reduced in comparison with standard PVT scintillator, having just 6,600 photons per MeV for red scintillator and 5,300 photons per MeV for green scintillator [Saint Gobain, 2009b].

Lead loading of the detector improves the stopping power at lower energies, but at a huge cost of light output. A typical 5% loading of the detector results in a light output of just 4,700 photons per MeV. The benefits are also restricted to energies around that of 200keV and below, where the light output is of greatest consequence with respect to

statistical broadening due to the number of available photo-electrons. Boron loading is also available for increased chances of Neutron detection, but again at a cost to light output.

The best possible type of PVT scintillator for gamma-ray detection has the highest light output with good durability. Current examples of such materials include Eljen EJ-200 and Bicron BC-400. In 2007 Campbell and Crone [Campbell and Crone, 2007] published details of a new plastic scintillator with over 3x the light output of current plastic scintillators. The authors achieve this by the inclusion of heavy metal phosphorescent dopants with concentrations measuring up to 35 wt % giving a peak light yield of 32,000 photons/MeV. This material has a much slower decay time at around 850ns and has only been prepared in microscopic films. It will therefore not be replacing standard PVT scintillator in the near future, but shows potential if costs can be kept low.

3.3.5 Light Guides

Optical light guides are classically used to pipe scintillation light from a scintillation material to a photomultiplier tube or diode. Light guides are useful when the photomultiplier tube is either smaller is size than the scintillation material, or if the dimensions of the scintillation material do not match that of the photomultiplier tube. Examples of light guide designs include "fish-tail" light guides, which couple a rectangular scintillator to a circular photomultiplier tube of roughly the same cross-sectional area, trapezoidal light guides which simply taper a large area matching the detector to a small one matching the photomultiplier tube, optical fibres for piping the light to distant receiver and twisted strip light guides, shown in Figure 3.4 that pipe light from a long thin sheet of scintillator to the circular area of a photomultiplier tube. Light guides are often used in particle detection experiments where the amount of light collected from the scintillator after an interaction is of lesser importance, as long as a measurable signal is received.

Figure 3.4: An example of a twisted light guide used for piping light from a thin sheet to a round surface [Saint Gobain, 2009a].

3.3.6 Variation in Light Yield

The response of plastic scintillators is largely stated to be linear with respect to the amount of energy deposited in them [Knoll, 1989]. The response to gamma rays over a suitable spectrum for gamma ray spectroscopy remains unseen however. In 1962 Brannen & Olde [Brannen and Olde, 1962] suggest that the response of plastic scintillator to external electrons is largely linear from energies above 125keV up to 2.5MeV, whereas their experiments suggest the response of internal electrons is linear down to around 20keV. They attribute any non-linearity of external electrons below 125keV to surface interaction effects of the scintillator. However, Birks previously defines a non-linear response in plastic scintillator due to the quenching of the primary excitation by the high density of ionised and excited molecules and gives the Birks equation, shown in equation (3.6), describing the response of the scintillator for various particle types [Badhwar et al., 1967].

$$\frac{dL}{dx} = \frac{S\frac{dE}{dx}}{1 + kB\frac{dE}{dx}} \tag{3.6}$$

Where $\frac{dL}{dx}$ is the differential light output, x is the path length of the charged particle, S is the unquenched sensitivity, $\frac{dE}{dx}$ is the collisional stopping power of the material and kB is Birk's parameter. Brannen & Olde's results suggest a contradiction to Birks equation for internal electrons when using a well-type detector, but appear to correlate for external electrons using a disk shaped detector. In 1967 Badhwar et al conducted further experiments with plastic scintillators and confirm the non-linearity

to be consistent with that predicted by Birks equation for low energy electrons. In 1994 Peron and Cassette study liquid scintillator cocktails at energies of 1 to 20keV and again confirm Birks equation with different values for kB. More recently, in 1999 Williamson et al [Williamson et al., 1999] study the response of plastic scintillators to low energy photons for use as a brachytherapy dosimeter. They conclude that plastic scintillators are largely linear above energies of 100-150keV, which is in agreement with the available literature. They also show an apparent non-linearity for energies below 100-150keV but note possible inaccuracy due to the use of bremsstrahlung radiation as opposed to a mono-energetic radiation source. In summary the literature suggests a definite non-linear response to external electrons below 125keV in energy, but whether or not this is due to surface effects is not yet known. No current data is available for the response of PVT based scintillator to low energy gamma-rays in terms of its linearity.

3.4 Detector Modelling with GEANT4

The GEANT (GEometry ANd Tracking) 4 simulation tool-kit is a collection of programming libraries, data sets and scripts written mostly in C++ that are used to construct and model physical events. Geant4 is native to the Linux operating system. With the addition of certain libraries, the theoretical models needed to successfully simulate a detector's response to incident radiation can be constructed. The same software can be used in a different mode to model the optical transportation of subsequent scintillation light within a detector. A virtual radiation source can be placed at different locations of the detector to determine spatial variations in the light collection efficiency and the detector geometry can also be altered to model any improvements in light collection efficiency. Materials can be added to simulate photomultiplier tubes with various quantum efficiencies, and a range of reflective materials can be added to the detector. The combination of gamma-ray and optical simulations is used to construct a full model of a detector system, with the ability to evaluate each detector's attribute for optimal performance. Background objects can also be factored in to determine how they might influence the response of the detector in a real-life environment. The initial version of Geant4 used was version 4.7.1, the software was

however updated regularly up to version 4.9.1. Each set of comparative simulations used the same version of Geant4, and all versions incorporated the G4LECS, low energy Compton scattering package, before the package was implemented as a Geant4 standard in version 4.9 and upwards.

3.4.1 Simulating Gamma-ray Interaction

Gamma-ray interaction models require only basic programming in Geant4, the scintillation material is defined along with each physics library that will be present to model interaction processes. Once this is complete the user can shoot particles at the detector and extract the response from the output, such as the energy absorbed by the detector for each event, the location of each interaction and the type of physical interaction process. For gamma-ray simulations, the response of the detector over the range of energies appropriate for gamma-ray spectroscopy is desirable. Therefore, a multi-channel analyser type model was created to build an energy loss spectrum for a complete range of incident gamma-ray energies. Shooting millions of mono-energetic gamma-ray photons at the detector slowly builds up an energy-loss spectrum for that given energy. Looping this simulation to encompass energies from 0keV to 3MeV in small increments results in a complete simulation of how the detector responds to all energies of interest. The gamma-ray simulation provides an excellent model of the detector material's initial response to radiation, but further modelling is required to predict the behaviour of the resulting scintillation light and its subsequent detection by photomultiplier tubes.

3.4.2 Simulating Optical Processes

Optical simulations to model the behaviour of scintillation light are more complex than those involved in gamma-ray simulations. In addition to the chemical composition, the detector medium must also be assigned various optical attributes, as must any other materials that are present in the simulation. The borders between each material must also be defined, and the interaction process describing how light should propagate from one material to the other. After the initial set up is complete, optical photons of a specific energy can be fired isotropically inside the detector at a specific location to simulate a scintillation event. The number of optical photons fired is representa-

tive of the light yield of the detector. An absorption material is defined at the same location as a photomultiplier tube would be in order to absorb and count the number of photons recorded for each scintillation event. The number of photons can then be used in conjunction with the quantum efficiency of the photomultiplier tube to give the total number of photo-electrons received for each gamma-ray fired at the detector. From these simulations, the total light collection efficiency and its the spatial variation can be determined by firing bursts of optical photons inside the detector at different locations. A two or three dimensional map is then created to show the number of photo-electrons received for each gamma-ray interaction point. This is extremely useful for evaluating the effects of reflective materials, detector geometry and the use of light guides on the quality of the energy-loss spectra.

3.4.3 An Integrated Model of a Complete Detector

Having obtained information on the gamma-ray interaction process and the behaviour of the resultant simulated light, an integrated model of the detector could be constructed. The figures extracted from the optical simulations were used to create a mathematical energy response function, as shown previously in equation (3.1). This equation was then used to broaden the raw energy loss spectra created from gamma-ray simulations, producing a realistic looking energy loss spectrum for any combination of incident gamma-rays. Geant4 comes with the ability to add a radioactive material to the simulation, which incorporates the complete model of radioactive decay and subsequent fraction of gamma-rays produced per decay. Therefore any possible scenario can be created in the simulated environment given enough time, which can prove very useful for investigating how the energy-loss spectra of a detector are affected by external influences such as shielding or scattering off nearby objects. The behaviour of a detector must be modelled accurately however and the simulated values obtained from optical simulations may not be accurate enough to account for any dissimilarity in one detector from the next. The simulation provides an ideal result given that the material is of perfect quality, that the reflective materials are perfectly uniform and perfectly bonded, and the response of any photomultiplier tubes are perfectly accurate. In practice this is not the case, as each individual detector has its own set of characteristics that deviate from that of an ideal detector. The simulation

does however provide an accurate tool for measuring relative changes in the quality of spectra with regards to any optical improvements.

3.5 A New Detector Design: Integration of Optimal Design Principles

There have been very few studies into the optimisation of plastic scintillators, especially for the use in gamma-ray detection. Pacific Northwest National Laboratory has conducted the majority of the available research into optimising plastic scintillators for use as gamma-ray detectors. Two such studies were undertaken, the Advanced Large-Area Plastic Scintillator project [Jordan et al., 2003] (ALPS) and a similar upgraded project called the ALPS-II project [Jordan et al., 2007]. The ALPS II project was the more advanced of the two projects and was conducted independently at the same time as the research presented in this thesis. This study has provided many useful results, confirming many of the findings presented in the following subsections.

3.5.1 Applying Light Guides

In applications such as gamma-ray spectroscopy the light collection is of paramount importance. Any extra material between the photomultiplier tube and the scintillation material will inevitably increase the number of light reflections, optical interfaces and the amount of material the light travels through, increasing the chances of absorption. This will reduce the overall light collection efficiency and increase the variation in the light collection efficiency. Scheu et al [Scheu et al., 2006] confirm this by attaching various shaped light guides to a scintillator and measuring the resulting performance. They conclude that:

> "The addition of plastic light guides of various shapes to one end of the scintillator results in a remarkable loss of light, almost independent of the used wrapping material."

Scheu et al further recommend direct coupling of the scintillator to the photomultiplier tube(s).

As the dimensions of the photomultiplier tube face are not too dissimilar from that of the face of a PVT scintillator used for gamma-ray detection, photomultiplier tubes should be directly coupled to the scintillator using an optical bonding agent to ensure minimal loss of light. Jordan et al [Jordan et al., 2007] also confirm this, simulating both fish-tail and trapezoidal light guides attached to a PVT detector with the Geant4 simulation tool-kit. Any configuration simulated resulted in a loss of light collection efficiency due to transmission losses through the light guides. Direct coupling of the photomultiplier tubes to the detector provided the highest light collection in each case. If the area of the detector face is large, a large photomultiplier tube or an increased number of photomultiplier tubes should be used to completely cover the surface with as much photo-cathode area as possible. However, if the number of photomultiplier tubes are limited, or the shape of the PVT is somewhat awkward for attaching multiple photomultiplier tubes, only short length, low ratio, trapezoidal light guides should be used to retain optimum light collection efficiency, as shown in Figure 3.5. These guides provide a slight gap between each photomultiplier tube which can be useful when designing clamps to hold the photomultiplier tubes firmly to a detector's edge. Each optical interface should be fixed using an optical bonding agent to eliminate any

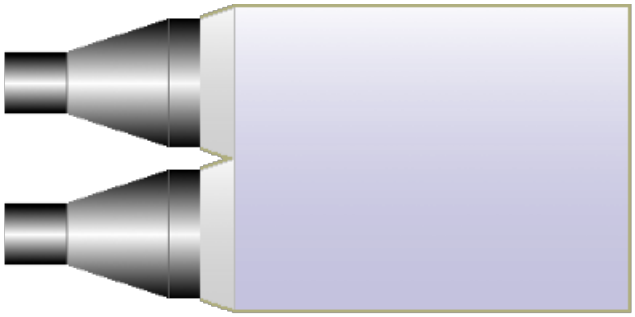

Figure 3.5: A diagram showing short, trapezoidal light guides connecting photomultiplier tubes to a scintillator. Such guides provide a slight gap between multiple photomultiplier tubes on a single detector edge which can be useful when designing clamps to hold the photomultiplier tubes firmly to the detector's edge.

air gaps, as the difference in refractive indices can cause light trapping between the two materials. This configuration ensures all of the detector face is covered and the loss of light due to extra material and optical interfaces is minimal. Using small light guides, up to a few centimetres in length, in this manner can also significantly decrease the variation in the light collection efficiency of the detector, given that gamma-ray interactions close to the photomultiplier tube(s) produce a much larger signal than that

of the rest of the detector, having a section of non-scintillating PVT reduces this large signal without adversely affecting the average light collection efficiency.

3.5.2 Applying Reflective Materials

Scheu et al [Scheu et al., 2006] study a range of these reflective materials on PVT scintillators in 2006 and give an efficiency for each material by measuring the yield of photoelectrons observed per 10mm of PVT in a scintillating bar of dimensions 700mm×20mm×6.4mm. The bar was composed of BC-412 from Bicron and read out at both ends using XP2020 photomultiplier tubes. The results by Scheu et al are shown in Table 3.1. The results clearly indicate that the best reflector for PVT is the

Table 3.1: Relative reflectivity of various scintillator reflective materials

Material	Relative Efficiency	Type
VM2000	100%	Specular
Tyvec (loose)	58%	Diffusive
Teflon tape	48%	Diffuse
Tyvec (tight)	48%	Diffuse
Aluminium foil	44%	Specular
Bare scintillator	41%	N/A
Black paper	34%	N/A

VM2000, a highly reflective ceramic reflector by 3M. Diffuse reflectors are somewhat useful if they are not tightly bound, and aluminium foil is only slightly better than using no reflective material at all. Given that PVT has optical quality faces, a highly reflective specular reflector should give the best results. If the material in use were NaI(Tl) the specular reflector would yield poor results due to its rough surface finish. The crevices in the rough surface of NaI(Tl) make the surface a diffuse reflector in itself so adding a specular reflector makes little difference. Surrounding the crystal with a diffuse reflector such as MgO is more desirable to contain the scintillation light. As NaI(Tl) crystals are typically small in size the light will eventually reach the photomultiplier tube without significant light loss.

Scheu et al's results were verified and expanded upon by conducting a similar experiment but with a circular disk of PVT scintillator. The PVT scintillator was EJ-200, manufactured by Eljen technology with a 5" diameter and 40mm thick. The disk's edges were milled, whilst the faces were cast to an optical quality finish. An Adit B133D01 5" photomultiplier tube was attached to one surface of the disk, whilst various reflectors were applied to the top as shown in Figure 3.6. For this experiment, the VM2000 specular reflector was replaced with 3M's Enhanced Specular Reflector (ESR), a ceramic film reflector with over 98.5% reflectivity in the visible light spectrum. The performance of each material was measured by observing the sharpness of

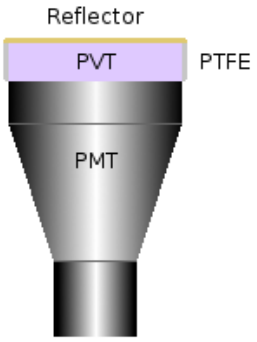

Figure 3.6: 5-inch 40mm PVT disk with reflector

a 662keV Compton edge from a Cs-137 source as it interacts with the PVT. The sharpness of the Compton edge was measured much in the same way as a typical full energy deposit is, in terms of a full width at half maximum. As a Compton edge technically has no FWHM in a strict sense given its shape, an equivalent was created by measuring the half width at half maximum of the leading edge and doubling the resulting value as shown in Figure 3.7. As well as testing various materials for performance, optical coupling was tested with the specular reflector to measure its effect on the performance. The coupling used for the experiment was silicone optical grease, and was also applied to the interface between the photomultiplier tube and the PVT to reduce the chances that light might become trapped between the photomultiplier tube's glass surface and the PVT disk surface. The results are shown in Figure 3.8. The results show that an optically coupled, highly reflective specular reflector gave the best performance. Using specular reflector without any coupling was less effective than using

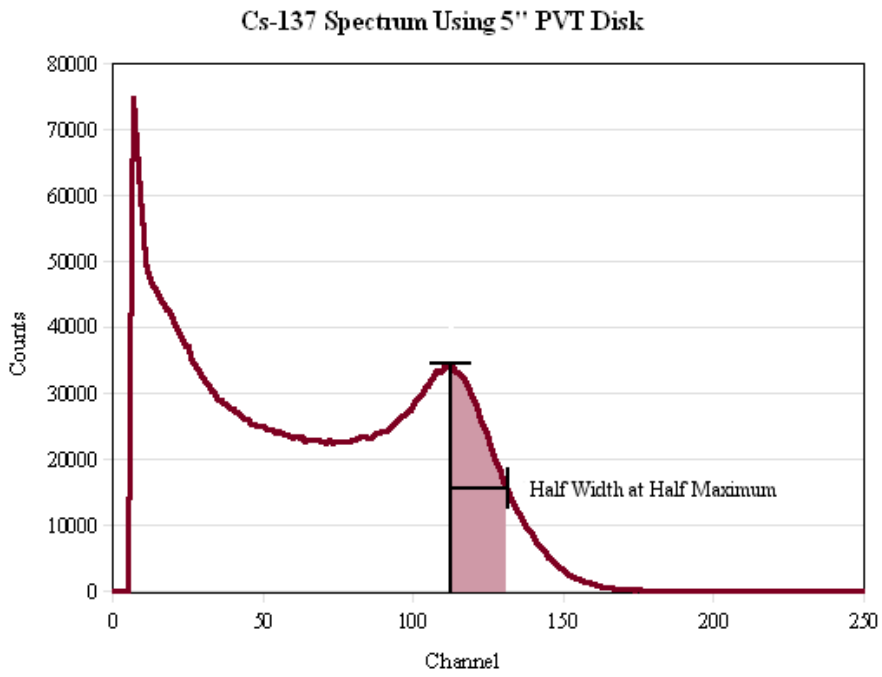

Figure 3.7: Half width half maximum of a Compton edge

a diffuse reflector. This is due to the air gap left between the specular reflector and the PVT, as the change in refractive index means that total internal reflection is the main process of reflection. This not only renders the specular reflector ineffective, but may also increase the chances that the light becomes trapped externally between the reflector and the PVT surface. The results show correlation with those presented by S. Scheu et al but it is not stated whether the VM2000 used by Scheu et al had any optical coupling.

Finally, the location of the reflective materials is also of great importance. A number of ways could be used to wrap a detector in reflective material. For smaller detectors like those of NaI(Tl) crystals, the material is fully contained on all sides by reflective material, except that of the photomultiplier. PVT however is generally much larger and benefits from a greater optical attenuation length and optical quality surfaces. This means that over large distances, even a high quality reflector might give significant light loss if the detector were wrapped on all faces. To confirm the optimal configuration for reflective materials, a series of Geant4 optical Monte Carlo simulations were performed. These include simulations for:

- Completely wrapped detector: The whole detector was wrapped except for the

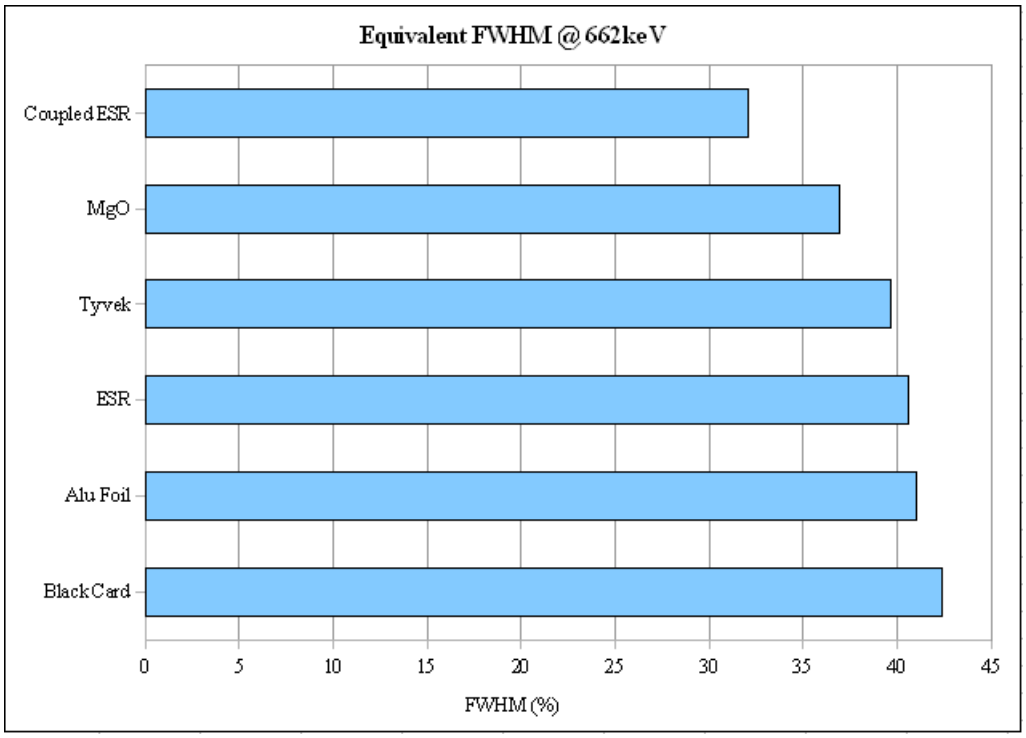

Figure 3.8: Comparison of reflector performance using the equivalent FWHM, shorter bars indicate better results.

photomultiplier tube interface.

- Completely unwrapped detector: No wrapping was used at all.
- Wrapping applied to the large faces only: Only the two large faces of the detector were wrapped.
- Wrapping applied to the edges only: Only the three edges were wrapped, as the final edge was attached to the photomultiplier tube.
- Wrapping applied to the end only: Only the edge on the opposite end to the photomultiplier tube was wrapped.

For these simulations, a detector with dimensions 150cm×25cm×4cm was used with photomultiplier tubes attached to one of the 25cm edges, as shown in Figure 3.9. The reflectivity of the wrapping was set to 98.5%, which is the average reflectivity of VM2000 and ESR. The detectors were simulated by firing 10,000 optical photons isotropically inside the detector at 10cm intervals in both the length and width dimensions. The results give an average light collection efficiency and spatial variation in that light collection efficiency for each design. The best configuration is the one

Figure 3.9: A detector with dimensions 150cm×25cm×4cm with photomultiplier tubes attached to one of the 25cm. This configuration was used for Geant4 simulations to confirm reflective material configurations.

producing the highest light collection without incurring a significant spatial variation. These results are shown in Table 3.2. The results indicate that the best configuration

Table 3.2: The effect of wrapping configuration on the light collection efficiency of a 150cm×25cm×4cm PVT detector

Configuration	Light Collection Efficiency	Spatial Variation
Completely Wrapped	31.3%	24.0%
Completely Unwrapped	26.2%	13.7%
Wrapped Faces	24.0%	28.2%
Wrapped Edges	35.3%	12.0%
Wrapped End	31.4%	10.0%

for wrapping PVT in reflective material in terms of light collection efficiency is wrapping only the edges of the detector. This configuration gives the highest light collection without significantly increasing the spatial variation. The configuration with the best collection uniformity at 10.0% appears to be the detector with a single wrapped end. However, this particular simulation is less accurate than the others by giving an overly optimistic result. This is because in reality the edges of the detector are not of an optical quality finish, but by default they are stated as optical quality in the simulation as part of the PVT's optical characteristics as a whole.

Wrapping the two large faces of the detector in any configuration produces poor results every time and therefore the faces should always be unwrapped. Although this configuration automatically results in a significant light loss through the large faces of the detector, light emitted at such angles would otherwise become highly attenuated by the number of reflections required to travel to the photomultiplier tube. Each re-

flection would subtract, at least, 1.5% of the light intensity on each reflection. Light reflecting at angles below the critical angle also becomes unnecessarily attenuated on each reflection, reducing the overall light collection efficiency and increasing the variation in the light collection efficiency. Finally, wrapping the whole detector would significantly increase the cost due to the high quality specular reflector used for optimum reflectivity. The edges of the detector are considered rough in comparison to the faces. Diamond milling of the edges would increase the quality of the surface finish enough to apply an optically bonded specular reflector for maximum reflectivity.

3.5.3 Geometry

The geometry of the plastic scintillator is important when considering the sensitivity and the cost of the detector. The primary goal in detector geometry is to retain optimal spectral quality whilst increasing the volume of the detector. The detector must therefore cover as large an area as possible without creating a huge decrease or differential in the light collection efficiency. Current detectors are bulky and high in volume with poor resulting light collection so this technique must be avoided. The first dimension of the detector geometry to be considered is its thickness. The thicker the detector is, the higher the detection efficiency with incident gamma-rays. However, a thicker detector will also result in a larger probability of multiple Compton scatters, which subsequently degrade the clarity of the Compton edge. The aim is to increase the clarity of the Compton edges in the energy loss spectra, and therefore the thickness should be restricted accordingly. To determine the trade off between detection efficiency and the amount of multiple Compton scattering, a Geant4 simulation was constructed using a Na-22 source placed above PVT slabs of dimensions 50cm$\times$12.5cm with varying depth. Two million gamma-ray photons were fired for each simulation, the results for which are shown in Figure 3.10. Figure 3.10 shows that for increasing depth the number of counts present from multiple Compton scattering events increases. This increase is quantified by measuring the total number of counts in the multiple scatter area of the 511keV induced Compton edge as a percentage of the total number of counts in the Compton edge as a whole. Figure 3.10 shows the boundaries used for this calculation labelled as “Marker” and represents the start of the Compton edge, the start of the multiple scatter region and the end of the Compton edge/multiple scatter

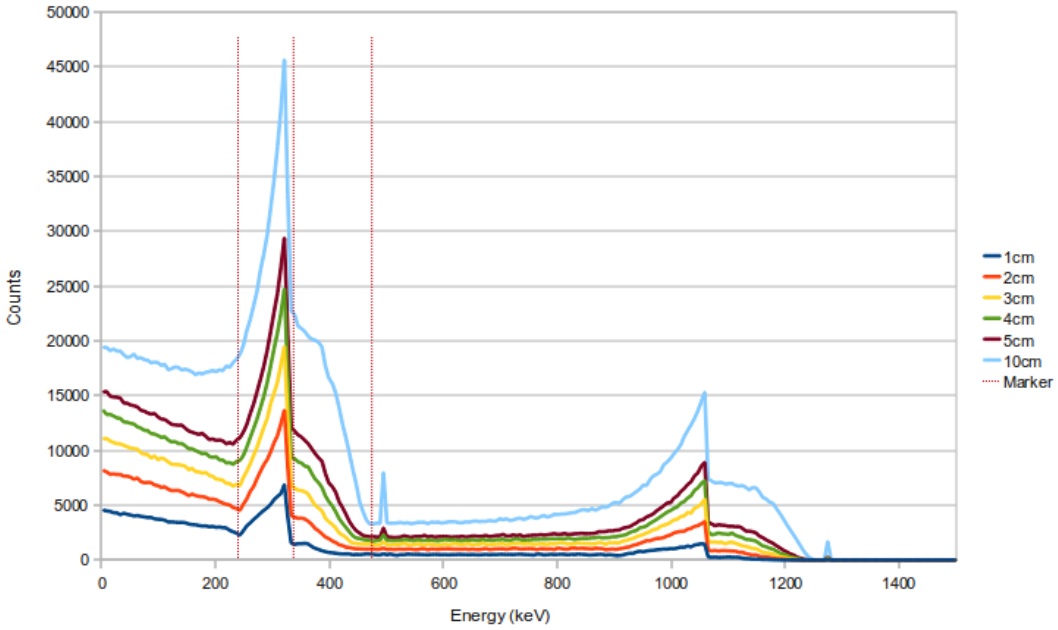

Figure 3.10: Geant simulations showing gamma-rays from a Na-22 source interacting with a 50cm×12.5cm PVT detector with varying depth.

region respectively. The amount of counts present as multiple scatter events are shown in Table 3.3. The results in Table 3.3 show that the percentage of multiple scattering

Table 3.3: Multiple scatters as a percentage of the total number of counts in a 511keV induced Compton edge for various depths of PVT scintillator.

PVT Depth	Multiple Scatters
1cm	25 +/-2%
2cm	30 +/-2%
3cm	34 +/-2%
4cm	36 +/-2%
5cm	39 +/-2%
10cm	46 +/-2%

events as a function of PVT depth is relatively linear. A depth of around 4cm is chosen as a trade off between detection efficiency and potentially clear Compton edges in the resulting energy loss spectrum.

The second dimension of the detector to consider is the width of the detector. The width of the detector is again a trade off, though this time between light collection efficiency, detection area and cost. Increasing the volume of PVT used by a small factor has little effect in the overall cost of a system in comparison to the extra electronics required to detect the scintillation light. Therefore if one edge of the PVT is covered with photomultiplier tubes, the detector width should be made in multiples of the photomultiplier tube diameter that is being attached.

The final dimension is the length of the detector. The length must be as long as possible to cover as greater detection area as possible without significantly degrading the light collection or its variation. If the ratio of length to width is too high, the detector becomes like a thin pipe, increasing the number of internal reflections required along the length of the detector before detection and increasing the volume of material traversed by the light. To keep an optimum light collection and spatial uniformity, the dimension ratio must be kept within certain limits.

The photomultiplier tube placement is also an important factor in deciding the detector geometry. Photomultiplier tubes could be placed at both ends of the detector, or at only one end of the detector with reflector attached at the other end. A configuration with photomultiplier tubes attached to one end, and reflector at the other, should give the same performance as using a photomultiplier tube at both ends of a detector twice the original length. This configuration is then purely optional based on the requirements of the detector system as a whole. As the thickness of the detector has already been established at a set value, the area must be altered to match the desired volume of material. In order to maximise light collection efficiency, the dimensions of the detector should match an optimum geometrical ratio for that area with a given number of photomultiplier tubes. Geant4 optical simulations are used to determine how the detector geometry, number of photomultiplier tubes and the configuration of those photomultiplier tubes affect the light collection and spatial uniformity.

First, it can be shown that for a set detection area or volume, covering an edge with as large a number of photomultiplier tubes as possible will increase the total light

collection efficiency. To show this, a simulation is constructed comprising of a PVT detector of dimensions 150cm×50.8cm×4cm with a varying number of 5" photomultiplier tubes attached to one end and ESR reflector covering all other edges. 10,000 optical photons are fired every 10cm along the width of the detector and every 10cm along the length of the detector. The average number of photons that are received by the photomultiplier tube(s) as a percentage of those initially fired give the average light collection efficiency, the results are shown in Figure 3.11. Pacific Northwest National

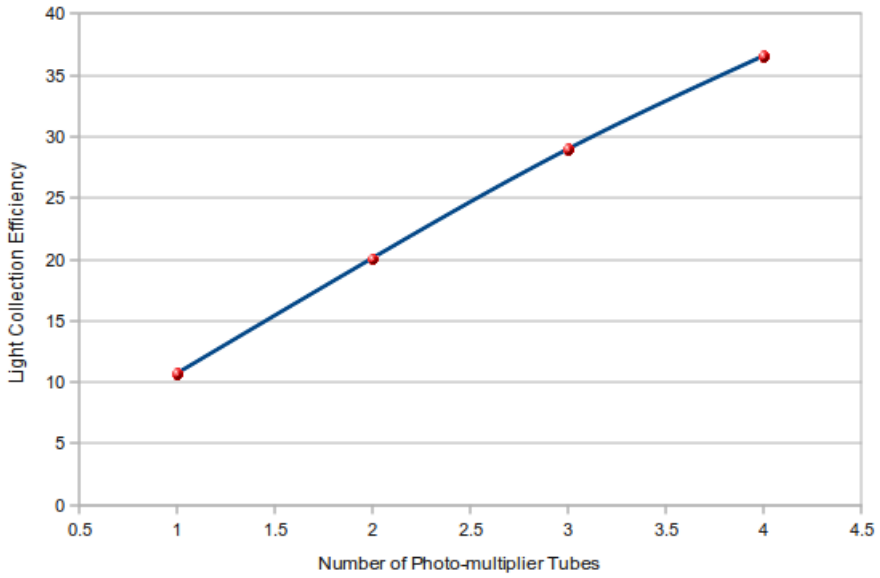

Figure 3.11: Light collection efficiency as a function of the number of photomultiplier tubes attached to one end of a 150cm×50.8cm×4cm PVT detector.

Laboratory's ALPS and ALPS II projects both provide insight into the light collection of a PVT detector with respect to the number of photomultiplier tubes attached. Table 3.4 shows some simulated results from the ALPS project, highlighting that the light collection efficiency of a 127cm×57cm×5cm PVT detector is heavily dependent on the number of photomultiplier tubes attached. The detector was simulated with loose aluminium foil wrapping, giving around 85% reflectivity. The "PMT Config." field has been adjusted to show how many 5" photomultipliers were attached at each end of the detector, "1+1" for example means that 1x 5" photomultiplier tube was used at each end of the detector. The results shown in 3.4 confirm the increase in light collection efficiency as a function of the number of photomultiplier tubes attached to the detector.

It can also be shown that increasing the volume of the detector decreases the light

Table 3.4: Simulated light collection efficiency of a 127cm×57cm×5cm PVT detector with respect to the number of 5-inch photomultiplier tubes attached. Data from PNNL's ALPS project [Jordan et al., 2003]

PMT Config.	No. of PMTs	L.C.E.
1 + 0	1	10.9%
2 + 0	2	19.9%
3 + 0	3	27.4%
2 + 2	4	30.7%
3 + 3	6	40.2%

collection efficiency for a given detector width and number of photomultiplier tubes attached. For these simulations the detector thickness and width are fixed, and therefore increasing the length of the detector increases the volume. This simulation is performed initially with a 25.4cm detector width covered by 2x 12.7cm diameter photomultiplier tubes. The detector is wrapped on all edges with ESR reflector. Once the simulations are completed for a 25.4cm width, the width is increased along with the number of photomultiplier tubes. A total of three widths are investigated, equating to using 2, 3 or 4 photomultiplier tubes each with 12.7cm diameter. Figure 3.12 shows how the light collection degrades with an increase in detector volume for these various width settings. For this simulation the increase in width is followed by an increase in the number of photomultiplier tubes to match that width. Figure 3.12 illustrates that at a fixed width, increasing the length, and thus volume, of the detector decreases the light collection efficiency exponentially. This result is expected as the optical attenuation equation predicts an exponential decay in signal over increasing length. The figure also shows that by adding more photomultiplier tubes to increase the detector width and decrease the length, whilst retaining the same volume, the overall light collection is significantly increased. Adding extra width to the detector to increase the overall volume will not degrade the light collection as long as additional photomultiplier tubes are added. Figure 3.13 shows the same simulation but for the variation in the light collection efficiency as the volume of the detectors increase. It can be seen for each detector that increasing the volume of the detector by its length increases the

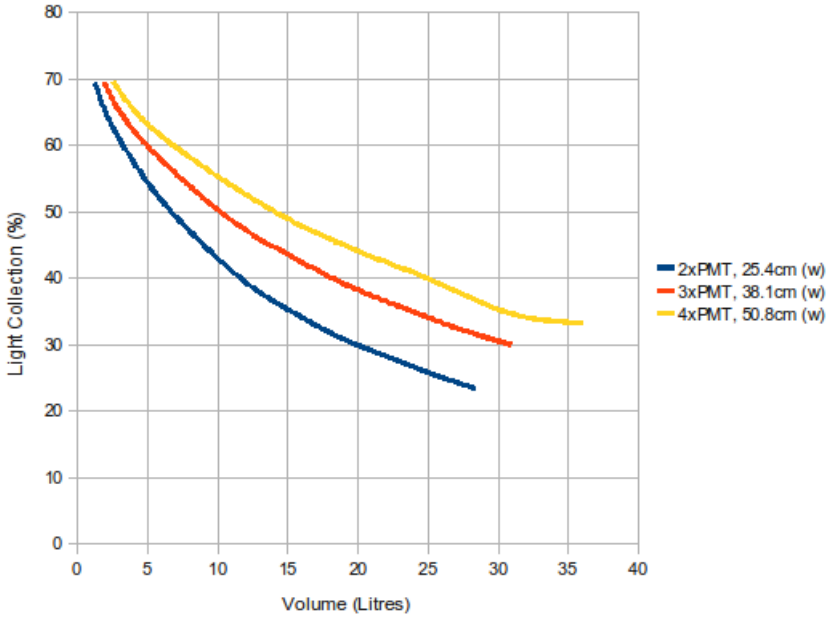

Figure 3.12: Light collection as a function of detector volume/length.

variation in the light collection efficiency. However, detectors at a set volume have a lower variation in the light collection if they have a lower length to width ratio with a greater number of photomultiplier tubes attached to that width.

Usually though the number of photomultipliers is fixed as they are a prime contributor towards to the overall cost of the detector. Therefore, if one needs to increase the detection area, whilst retaining the same number of photomultiplier tubes, the best technique must be established. By simulating 2x 5" photomultiplier tubes fixed to a varying sized section of PVT, the light collection as a function of detector dimensions can be measured. Figure 3.14 shows the light collection as a function of volume for different width detectors whilst all using 2x photomultiplier tubes with diameter 12.7cm. Figure 3.14 illustrates that for a given number of photomultiplier-tubes, increasing the width of the detector in order to increase the volume only degrades the light collection by a few percent. This shows that the aspect ratio of length to width for a fixed number of photomultiplier tubes is not a significant factor in determining the average light collection efficiency for lengths of up to 2m. Figure 3.15 however shows the variation in the light collection for the same set of detector geometries and clearly demonstrates that increasing the width for the same volume decreases the vari-

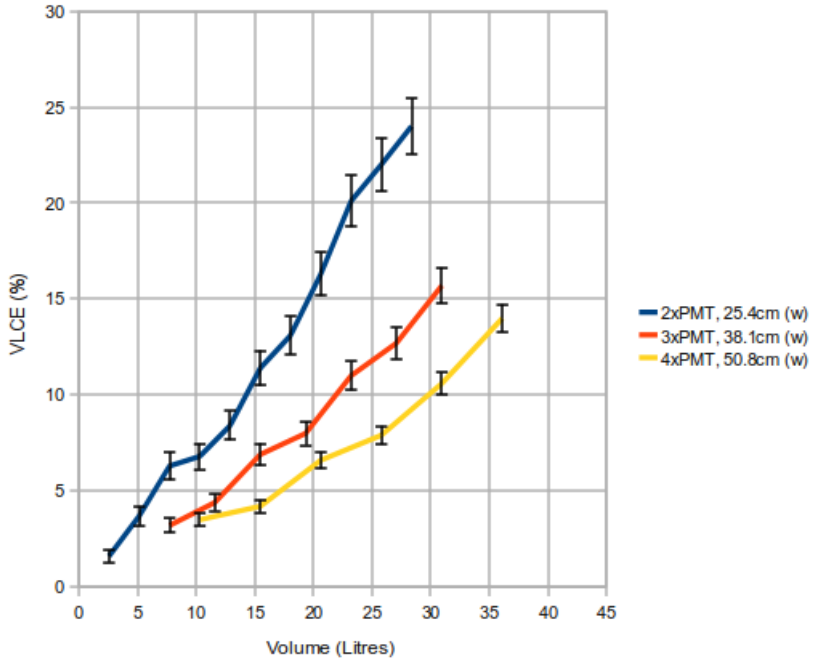

Figure 3.13: Variation in light collection as a function of detector volume by increasing detector length

ation in the light collection. Figure 3.16 shows the difference in the variation in light collection efficiency for the same geometry detectors but with a different number of photomultiplier tubes. One should expect that a detector with the same dimensions should have the same variation in the light collection regardless of the number of photomultiplier tubes attached. This is the case as 3.16 shows. The variation in the light collection efficiency is almost identical for the same geometry detector, showing no relevance to the number of photomultiplier tubes, but is based entirely on the shape of the detector. This is an important result as it allows a detector with a limited number of photomultiplier tubes to reduce the variation in light collection whilst increasing the detector volume by increasing its width. A high length to width ratio produces poor spatial uniformity along the detector.

The benefit of this result can only be seen when the effects on detector resolution are put into context. At lower energies for example the resolution of the detector will be dominated by the statistical variation in the number of photo-electrons, which in turn is a function of the light collection efficiency. At higher energies however there is more light available for each interaction, so the variation in the light collection plays a bigger role in broadening the detector resolution.

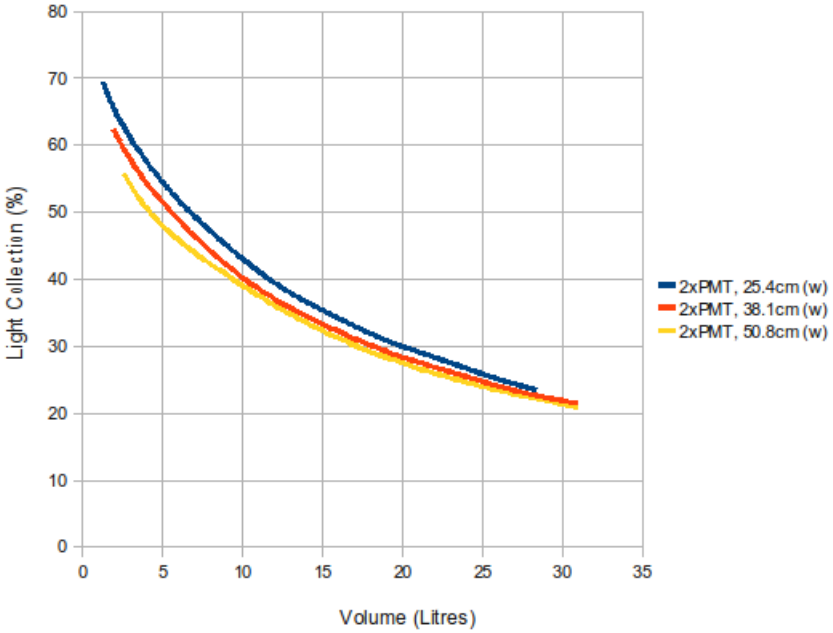

Figure 3.14: Light collection as a function of detector volume by increasing detector width

At higher volumes (>20 Litres) the detector has less than 30% light collection efficiency and starts to become impractical due to degradation of the signal. If high volumes of PVT are required then the only way to maintain good light collection is to add more photomultiplier tubes. Therefore the best configuration is to maintain a low aspect ratio of length:width whilst placing as many photomultiplier tubes along that width as financially possible.

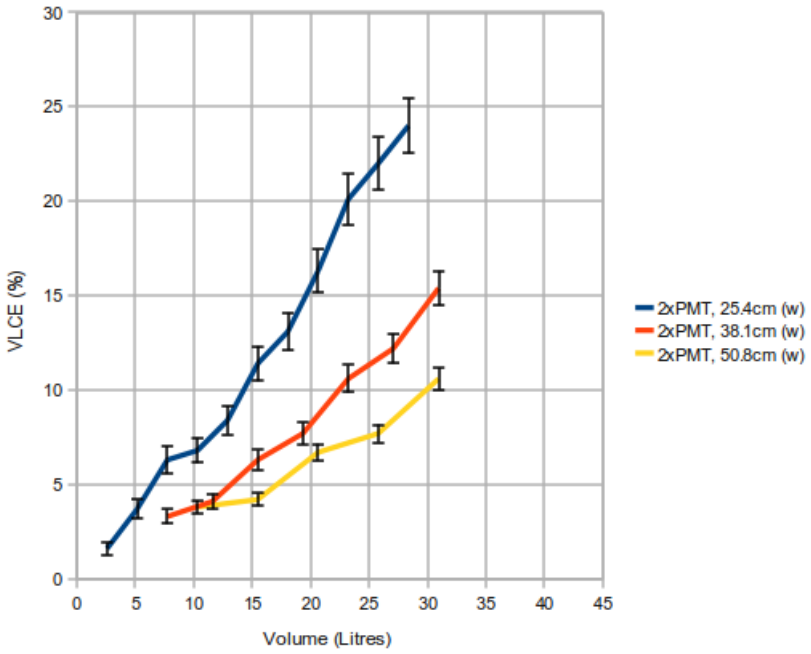

Figure 3.15: Variation in light collection as a function of detector volume by increasing detector width

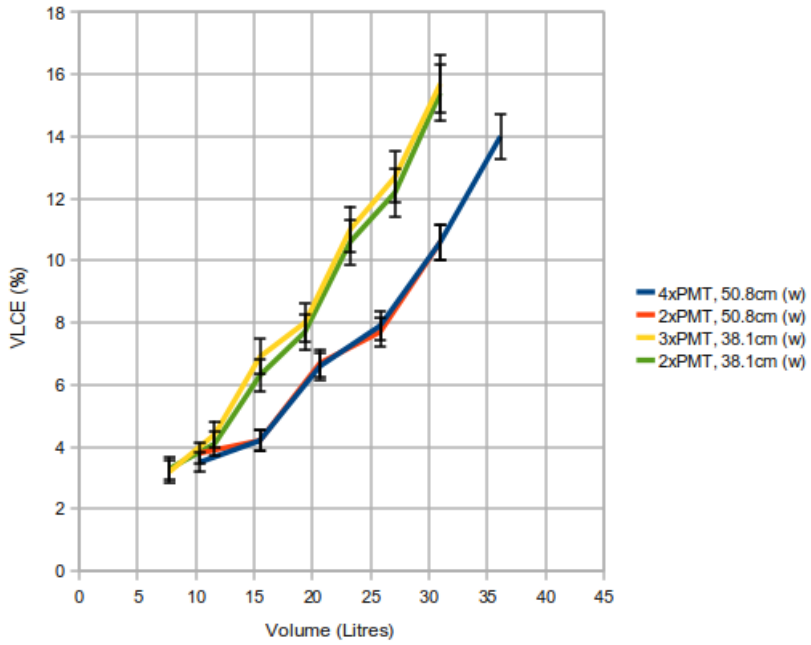

Figure 3.16: Variation in light collection as a function of detector volume by increasing detector width

3.5.4 Tapering the PVT

The final optimisation for a plank shaped PVT detector design is the inclusion of a taper along the length of the material. The taper keeps the same width at the photomultiplier tube end of the PVT to match its dimensions but gives a slightly narrower width at the opposite end. The function of this taper is to encourage the scintillation light trapped inside the detector to propagate towards the photomultiplier tube end on a straighter path by undergoing fewer reflections until it reaches the photomultiplier tube. This ensures that the light attenuation with respect to both self absorption by the PVT and absorption by the external reflective material is reduced. The amount of taper is investigated using Geant4 simulations of a 150cm×25.4cm×4cm PVT detector with 2x 5" photomultiplier tubes at one end. The detector has ESR optically bonded to its edges. The detector is initially simulated with no taper, then the taper is increased by decreasing the smaller end of the detector by 4cm per simulation until a 10cm decrement is reached. The results are shown in Table 3.5. Table 3.5 shows that any

Table 3.5: Simulated light collection efficiency and variation thereof of a 150cm×25.4cm×4cm trapezoidal PVT detector with a varying taper.

Narrow Width Dimension	Taper(%)	Volume	L.C.E.	V.L.C.E
25.4cm	0%	15.2 litres	35.3 +/-1.0%	11.5 +/-0.9%
21.4cm	16%	14.0 litres	38.0 +/-1.0%	10.0 +/-0.8%
17.4cm	31%	12.8 litres	40.0 +/-1.0%	9.4 +/-0.8%
15.4cm	47%	11.6 litres	42.0 +/-1.0%	9.2 +/-0.7%
9.4cm	63%	10.4 litres	43.8 +/-1.0%	8.9 +/-0.7%
5.4cm	79%	9.2 litres	45.2 +/-1.0%	9.0 +/-0.7%

size of taper gives a performance benefit over not having a taper. The light collection efficiency increases and the variation in the light collection efficiency decreases with taper size. The rate at which the variation in the light collection efficiency changes, however, slows as the taper is increased. Table 3.5 also shows that the volume of the detector also decreases with increasing taper, reducing the detector efficiency. Therefore a trade off between spectral quality and detector efficiency has to be met. For this

particular detector, up to 30% taper would seem a good choice, as it has a 5% increase in light collection efficiency, a 2.1% reduction in the variation in light collection but a 2.4 litre reduction in volume. The next setting at 47% taper however only gives a 7% increase in light collection and a 2.3% decrease in the variation of the light collection for a 3.6 litre reduction in volume. This would suggest that any taper gives a great improvement in quality, but to keep the taper relatively small as to not lose too much detector volume.

3.6 Conclusions

This Chapter has shown that there are many techniques available to optimise plastic scintillators, and a combination of these can drastically improve the factors which affect the quality of any resulting spectra. The number of photomultiplier tubes attached to a detector was found to be one of the largest contributors to the light collection efficiency. Light guides degrade this performance and therefore the photomultiplier tubes must be directly bonded to the detector's edge with a designated optical bonding agent. The best wrapping for a PVT detector was found to be an optically bonded, highly reflective specular reflector bonded to the edges of the detector, whilst leaving the large faces un-wrapped. The dimensions of the detector were the largest contribution towards the variation in the light collection efficiency, with long, thin detectors having the greatest variation in the light collection. Adding a taper to the detector increases the light collection and decreases the variation in the light collection, but also decreases the detector's volume. A small taper was found to be very beneficial. These results were mostly determined by Monte Carlo simulations using the Geant4 tool-kit. In Chapter 4 these principles were incorporated into detector designs and manufactured to test their performance experimentally.

Chapter 4

Optimised Prototypes

4.1 Introduction

Chapter 3 outlined the requirements and processes used to design optimised plastic scintillator detectors. The design needs to maximise light collection efficiency whilst minimising the spatial variation in the light collection efficiency. The design must be of a large enough area to provide good sensitivity, whilst also remaining relatively inexpensive. Expensive bespoke manufacturing techniques or large quantities of materials or electronics to operate should also be avoided to keep costs to a minimum. In the following sections three prototypes are outlined and tested for performance according to these specifications. The first is a small area detector designed both as a proof of concept as well as a potential hand-held detector, whilst the later two designs are larger in area are therefore more practical for use in a radiation portal monitor. Each detector is evaluated in terms of its light collection efficiency, spatial variance and the quality of the resulting energy loss spectra for a variety of measured isotopes.

4.2 Measurements

Here the process of measuring the light collection efficiency, spatial variation in the light collection efficiency and how the quality of spectra is determined are discussed. The techniques are those used to measure the attributes of spectroscopic crystals such as NaI(Tl), except for the light collection efficiency; which must be inferred, as discussed, in the following section.

4.2.1 Light Collection Efficiency

Ordinarily the light collection efficiency of a scintillation detector can be inferred by using the measured full width half maximum of a photo peak in an energy loss spectrum. From equation (3.1) established in Chapter 3, the resolution of a detector is a combination of factors including the light collection efficiency. Therefore by measuring directly all such factors, and observing the resolution from the FWHM of the photo peak, the light collection efficiency can be calculated. The light collection efficiency of plastic scintillators however, can be difficult to measure due to the lack of available photo peaks, and the potential unreliability of the photo peaks that are available due to possible variations in light yield at the low energies in which they are present. The light collection efficiency of a plastic scintillator detector can thereby be measured using two possible methods: by directly measuring the full width half maximum of an available low-energy photo peak and assuming the variation in light yield to be negligible; or by simulating an energy-loss spectrum for the detector using the Geant4 simulation tool kit. Given the number of known variables that form the detector resolution, the light collection can be estimated by fitting a Compton edge in an energy loss spectrum to a simulated equivalent from the Geant4 tool-kit. Using the energy loss spectrum of a Na-22 source as an example, the Geant4 tool-kit produces an energy-loss spectrum containing two distinct Compton edges. These Compton edges are for an ideal detector and must be statistically broadened by factors from light collection, variation in the light collection, electronic noise and variation in the light yield. The variation in the light collection is directly measured for each detector, as outlined in the following section. The electronic noise is assumed to be on the order of a few photo-electrons given the low noise performance of modern photomultiplier tubes. The variation in the light yield of PVT with respect to incident gamma-ray energy is initially assumed to be negligible for these measurements. Various figures for the light collection efficiency are then used to broaden the Compton edges and the most accurate match to the experimental data determines the most likely value.

4.2.2 Variation in the Light Collection Efficiency

The spatial variation in the light collection efficiency of a detector is measured directly using a collimated, mono-energetic gamma-ray source. Typically Cs-137 is used as it

has an isolated gamma-ray emission at 662keV. The Cs-137 source is placed inside a large, lead collimator measuring 4cm diameter$\times$2cm thick. An indent is cut into the top of the lead to allow the Cs-137 source to sit inside. The collimated source is then placed at various locations on the detector depending on the detector's dimensions, but typically every few centimetres along its length and width. For each source location on the detector, an energy-loss spectrum is acquired, resulting in a two-dimensional map of a detector's response with respect to the source location. The central channel that the Compton edge (or photo-peak in the case of a NaI(Tl) crystal detector) appears in is recorded for each source location. The result is the relative light collection efficiency of the detector at each location. The standard deviation of these readings as a percentage of the overall mean gives the coefficient of variation, which is taken as the variation in the light collection efficiency.

4.2.3 Spectral Quality

The spectral quality of the detector measured relatively by the equivalent FWHM of the Compton edges in an energy-loss spectrum, as shown in Figure 3.7 from Chapter 3. Typically the energy-loss spectra from isotopes which produce resolved Compton edges are used for this. Isotopes which produce many spectral lines will often have overlapping Compton edges making accurate measurements of their FWHM impossible. A wide range of incident energies is desirable, so many isotopes are used to construct a picture of the detector's performance. These isotopes include Cs-137, Na-22 and Eu-152. The 662keV induced Compton edge from a Cs-137 source is used to give an absolute figure for the performance. This Compton edge appears at 478keV in an energy loss spectrum.

4.3 The 50cm V-Plank

As a prerequisite to the construction of a large area detector, a smaller area design incorporating the same optimised attributes was produced. This design was 50cm long$\times$12.5cm wide and the shape is trapezoidal, using a total of 2.5cm to taper the width of the detector downwards along the length of the plank. The detector is therefore 12.5cm wide at its broader end in order to match the area of a 5" photomultiplier

tube; the largest area photomultiplier tube available with good quantum efficiency. The narrow end of the detector is 10.0cm (4") wide and the thickness is 4cm, making the total volume 2.25 litres with a 20% taper. The tapered design, as described in Chapter 3, allows for more efficient propagation of optical scintillation light from the narrow to the broader end of the detector. The detector relies on total internal reflection from its larger faces to reflect scintillation light internally, whereas the surrounding edges of the detector have highly reflective specular reflector optically bonded to their surfaces. The design was named the 50cm "V-Plank" design according to the detector profile roughly matching the shape of the letter 'V'. Figure 4.1 shows an illustration of the 50cm V-Plank.

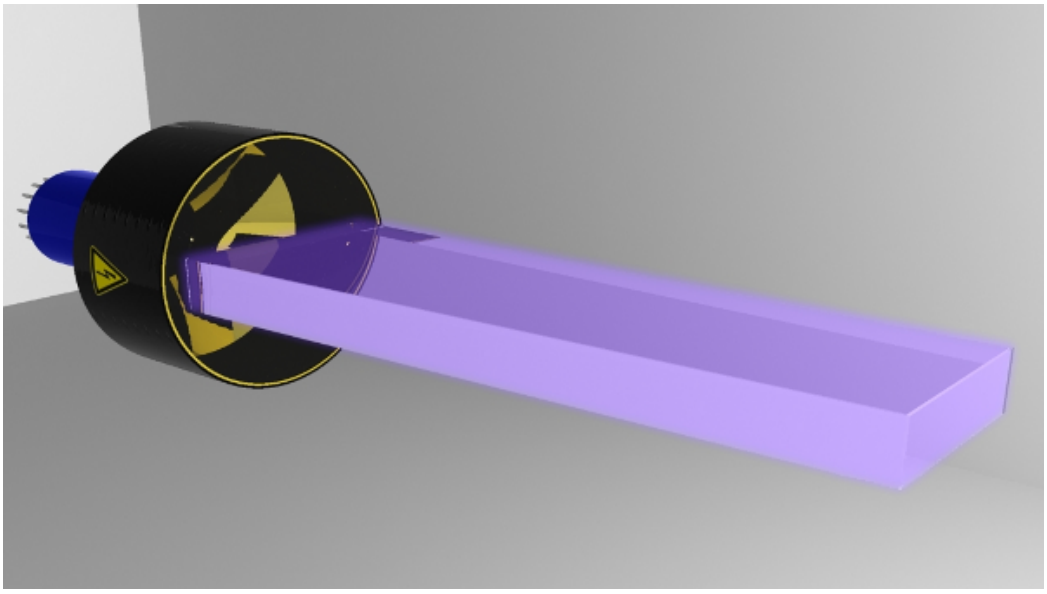

Figure 4.1: A 3D rendered illustration of the 50cm V-Plank.

4.3.1 Simulated Performance

An optical simulation was designed to test the performance of the 50cm V-Plank using the Geant4 tool-kit. The simulation comprised of the plastic volume, its reflective coatings and the equivalent of a photomultiplier tube attached to the larger end. In order to simulate the light collection efficiency, a burst of optical photons was released at various points inside the detector to simulate gamma-ray interaction events. Each burst released 10,000 optical photons at 2.93eV, equivalent to a 1 MeV gamma-ray being fully deposited within the detector. The location of these events was varied along the length and width of the detector, with events fired every 1cm along the

Table 4.1: 50cm V-Plank Simulated Performance

Mean LCE	57.0 +/- 1.0%
VLCE	2.8 +/-0.3%

Table 4.2: 50cm Straight Plank Simulated Performance

Mean LCE	52.8 +/- 1.0%
VLCE	3.9 +/-0.4%

length of the detector and every 1cm along the width. For each optical burst, the number of photons which reach the collecting end of the detector was measured. A two-dimensional map of the detector's light collection was then constructed, along with the mean light collection efficiency and the spatial variance therein. This map of the variation of the light collection efficiency is shown in Figure 4.2. The spatial

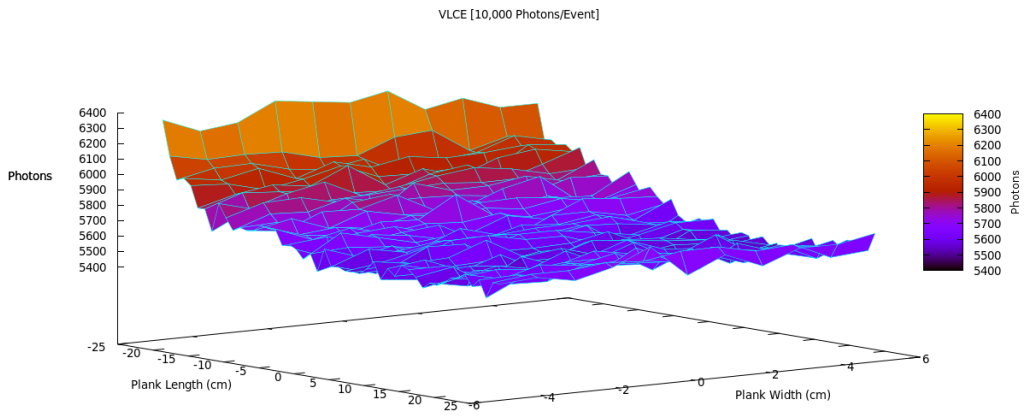

Figure 4.2: A map of the simulated variation in the light collection efficiency of the 50cm V-Plank.

variance was taken as the coefficient of variation, using the standard deviation in the number of optical photons detected as a percentage of the total mean. The results of the simulated performance are shown in Table 4.1. To illustrate the improvement that the taper makes over a standard plank-shaped design, the same detector was simulated without the taper enhancement. Table 4.2 shows the results.

4.3.2 Measurements

The detector was connected to an Ortec digiBASE which in turn was connected to a PC using a USB link. Maestro-32 software was used to capture energy loss spectra which were then exported to a tabular format and plotted. The voltage of the photo-multiplier tube was set to the manufacturer's recommended voltage of 940V with the default MCA gain settings on 1 coarse and 0.7 fine. The MCA had a channel range of 1 to 1024 channels. The low level discriminator was initially set to channel 2. The shaping time was set to the lowest possible time setting which was 0.75μs. To measure the spatial variation in the light collection efficiency of the V-Plank, a Cs-137 source was placed first in a Tungsten collimator and then on the surface of the V-Plank. The channel number of the 662keV spectral line from Cs-137 was then recorded as a function of the source location on the V-Plank. The source was placed in three equidistant locations along the width of the plank for each of 5cm increment measurements along the length of the plank. The V-Plank was connected to an Ortec Scintipack and MCA Card. The variation in the light collection efficiency was minimal at less than 2%. The Monte Carlo simulation for the prototype predicted a variation of less than 3%.

4.3.3 Energy Calibration

The 50cm V-Plank was the first PVT based scintillator to undergo energy calibration. It was calibrated by taking a high count, background subtracted, Na-22 spectrum. The Na-22 spectrum was exported into a text format where it was plotted in a spread sheet. A corresponding simulated spectrum generated using the Geant4 tool-kit for 511keV and 1275keV incident gamma-rays was then over-laid onto the measured spectrum. The simulated data was normalised in number of counts to match that of the experimental data. A linear equation was then used to stretch the channel number axis until the experimentally acquired spectrum matched the simulated data. The two Compton edges at 511keV and 1275keV were used as the main reference points for closeness of fit. Once the channel number was matched to the correct energy scale the calibration was complete. The fitting process was initially measured by eye, but later a program was written to match the spectra based on minimising the difference between the two sets of Compton edges. The resulting linear equation between the channel number and energy scale is the calibration equation and was manually applied to the subsequent

spectra taken in order to calibrate them. This method of calibration was first outlined by Kudomi in 1999 [Kudomi, 1999].

4.3.4 Resulting Spectra

The following are a sample of some spectra taken with the 50cm V-Plank. For these measurements, each source was placed above the detector at a height of around 15cm to ensure a flood illumination of the detector. Figure 4.3 shows the first of the spectra, which is a Cs-137 spectrum. Figure 4.3 shows a well defined Compton edge induced

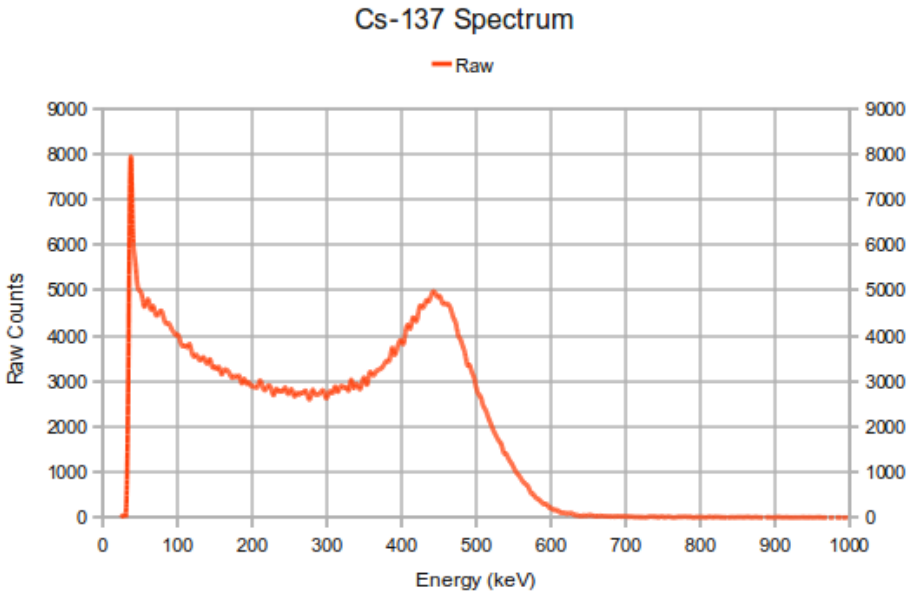

Figure 4.3: Cs-137 spectrum taken with 50cm V-Plank.

by the 662keV gamma-ray. The voltage and gain settings for this measurement do not allow the resolution of the 32keV X-ray present from the Cs-137, though a high number of counts can be seen at the low energy scale. Given the range of Compton scattering angles it is expected that there be a large number of low energy counts in the spectrum, though this should be at a variety of energies and not all concentrated at the low channel numbers seen here. As this spectrum is background subtracted, the only explanation for such a high number of counts is either backscattered gamma-rays from surrounding material, or unresolved 32keV X-rays. The possibilities of noise or a light leak in the detector was eradicated as a background spectrum shows no such spikes at low energies. The second spectrum acquired was that of Na-22, shown in Figure 4.4. Figure 4.4 shows two clear Compton edges resulting from the 511keV and

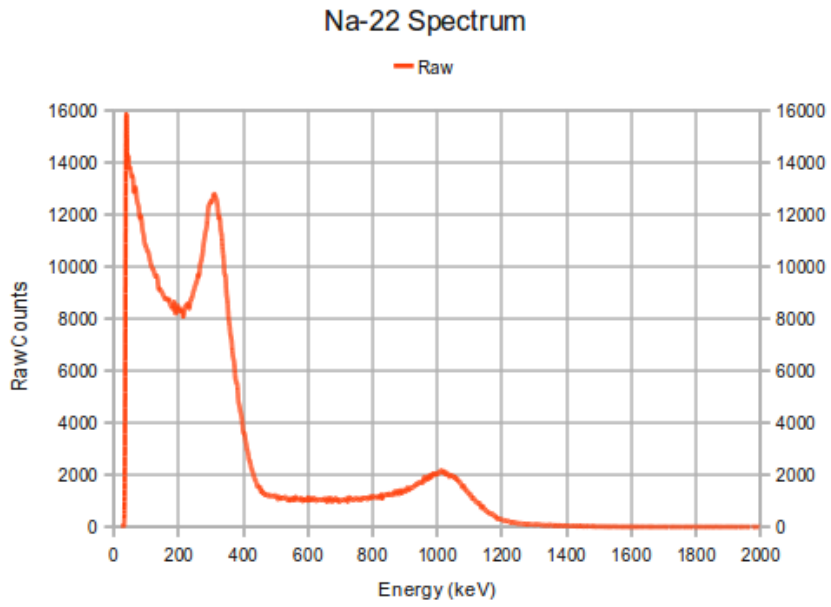

Figure 4.4: Na-22 spectrum taken with 50cm V-Plank.

1275keV incident gamma-rays. The low energy spike seen in the Cs-137 spectrum is not present, with only a minor low energy presence which suggests that the previous spike in the Cs-137 spectrum was from the 32keV X-rays. The final spectrum shown here is that of Eu-152 in Figure 4.5. Figure 4.5 shows many Compton edges, most

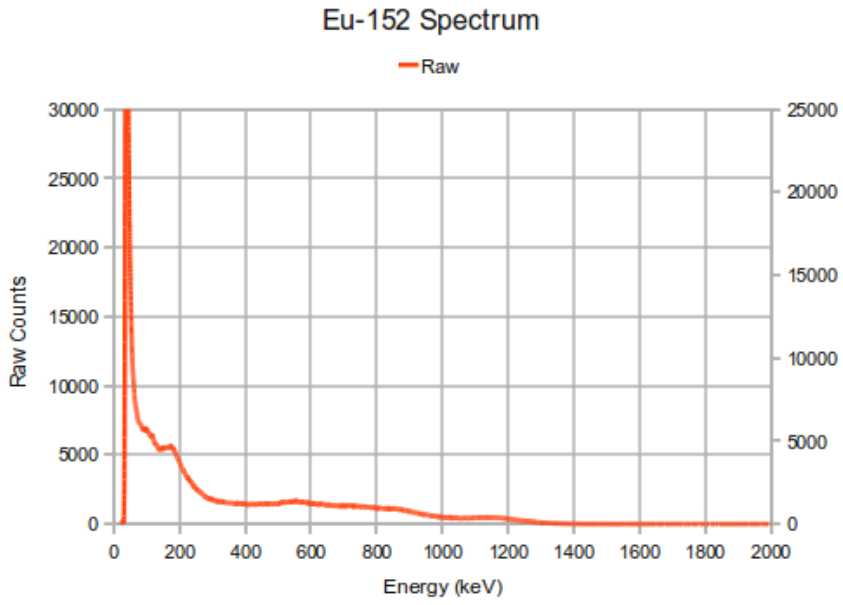

Figure 4.5: Eu-152 spectrum taken with 50cm V-Plank.

of which are unresolvable. Eu-152 has a range of dominant gamma-ray emissions spread relatively evenly from 122keV up to 1.4MeV. The 40keV X-ray emission is relatively strong and is absorbed much more efficiently in the PVT than the higher

energy gamma-rays. The 122keV gamma-ray will Compton scatter down to produce a narrow Compton edge at around 39keV. The 40keV and 122keV emissions therefore show as one large, combined peak in the spectrum. The extent of the intensity is not displayed in this figure however, as the count scale is adjusted to show the range of Compton edges present.

4.4 The 1m V-Plank

The first of the larger area designs was the 1m V-Plank. This design was 100cm long$\times$25cm wide and the shape was also trapezoidal, using 5cm to taper the width of the detector downwards along the length of the plank. This design was the same shape as the 50cm V-Plank, only with four times the volume by doubling the width and length, making a total of 9 litres. The detector was therefore 25cm wide at its broader end in order to match the area of two 5" photomultiplier tubes, whereas the narrow end of the detector was 20.0cm (8") wide, showing a 20% taper. Figure 4.6 shows an illustration of the 1m V-Plank. As the design used multiple photomultiplier tubes to

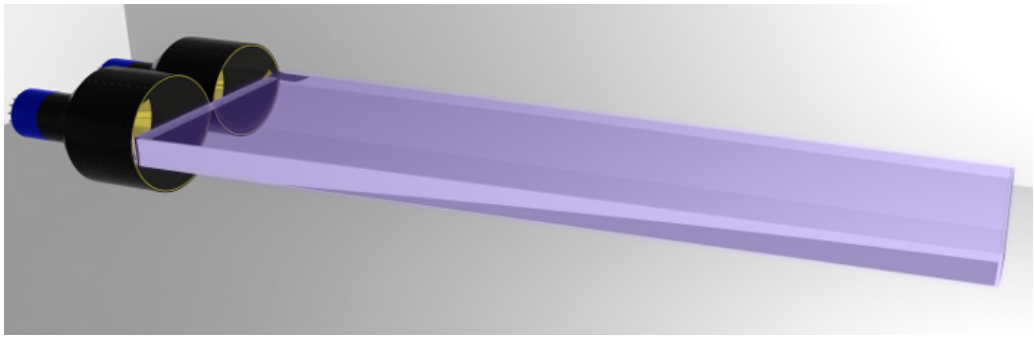

Figure 4.6: A 3D rendered illustration of the 1m V-Plank.

cover the full collection area, extra electronics and software were required to operate the detector. An extra digiBASE was used to cover the extra photomultiplier tube, and a large software development project was created as the two MCAs must be run in coincidence mode. The mode available for this using the Ortec digiBASEs is called List Mode and simply outputs each event detected by each MCA as an amplitude along with its time stamp. The digiBASE has a microsecond resolution internal timer that it uses for the time stamping process, though both digiBASEs must be synchronised manually to ensure they are set to exactly the same time. The software produced

must then coincide these time stamped events and add them accordingly to produce a coincident event. Given the relatively uniform response of the detector, the amplitudes from each MCA event were simply added together. A more detailed overview of the software and techniques developed for multiple photomultiplier tube detectors is discussed in Chapter 7.

4.4.1 Simulated Performance

A two-dimensional map of the detector's light collection was constructed, along with the mean light collection efficiency and the spatial variance. The procedure for simulating the variation in the light collection are kept the same as with the 50cm V-Plank design, only with 2cm points along the width of the plank, and 2cm points along the length. The simulated variation in the light collection efficiency is shown in 4.7. The

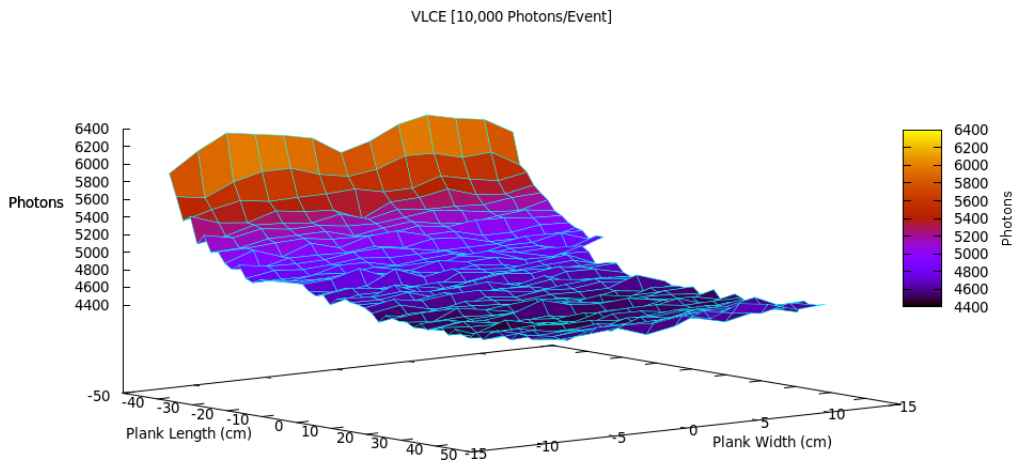

Figure 4.7: A map of the simulated variation in the light collection efficiency of the 1m V-Plank.

resulting figures of the simulated performance are shown in Table 4.3.

Table 4.3: 1m V-Plank Simulated Performance

Mean LCE	47 +/- 1.0%
VLCE	5.6 +/-0.6%

4.4.2 Measurements

To measure the spatial variation in the light collection efficiency of the 1m V-Plank, a Cs-137 source was used inside a lead collimator and then placed on the surface of the 1m V-Plank. The measurement locations used for this experiment were every 5cm along the width of the detector and every 15cm along the length of the detector, making a total of 21 measuring points. The variation in the light collection efficiency was found to be around 2%, much lower than that simulated by Geant4. A range of isotopes were measured using the 1m V-Plank, all of which were placed in turn at around 40cm above the centre of the detector to ensure flood illumination.

4.4.3 Resulting Spectra

The same selection of spectra is presented here as were presented with the 50cm V-Plank. The first is Cs-137 shown in Figure 4.8. Figure 4.8 shows the Compton edge

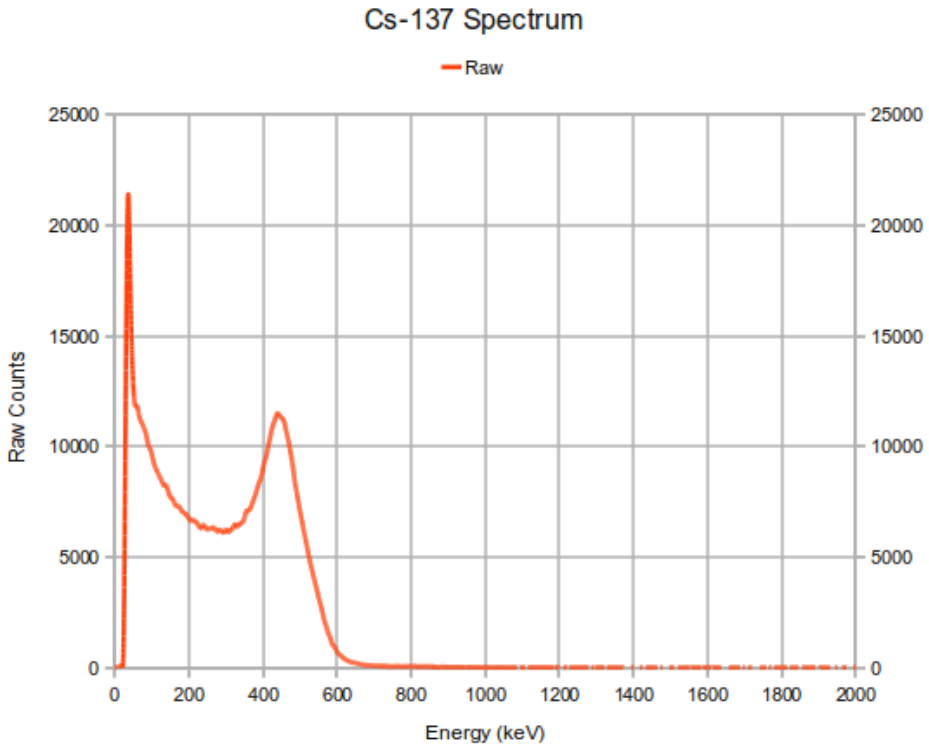

Figure 4.8: Cs-137 spectrum taken with 1m V-Plank.

from the 662keV incident gamma-ray has excellent clarity, indicating that increasing the volume of this detector did not significantly degrade its performance. The low energy spike seen in the same spectrum for the 50cm V-Plank is not present in this

spectrum. This is because the low level discriminator was raised slightly to reject any signal below that equating to around 35keV in energy in order to reduce the dead time of the detector. Figure 4.9 shows the next spectrum, which is Na-22. Figure 4.9 again

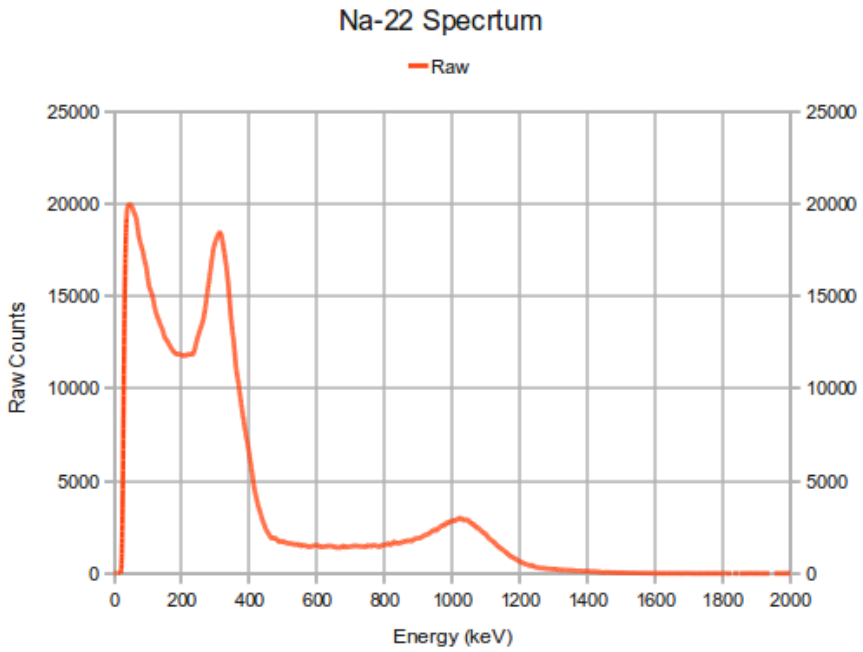

Figure 4.9: Na-22 spectrum taken with 1m V-Plank.

shows good clear Compton edges, similar to those in the 50cm V-Plank. Figure 4.10 shows the spectrum for Eu-152. Figure 4.10 shows a similar Eu-152 spectrum to the 50cm V-Plank, though with many unresolved Compton edges, it is difficult to quantify any detailed degradation from this spectrum.

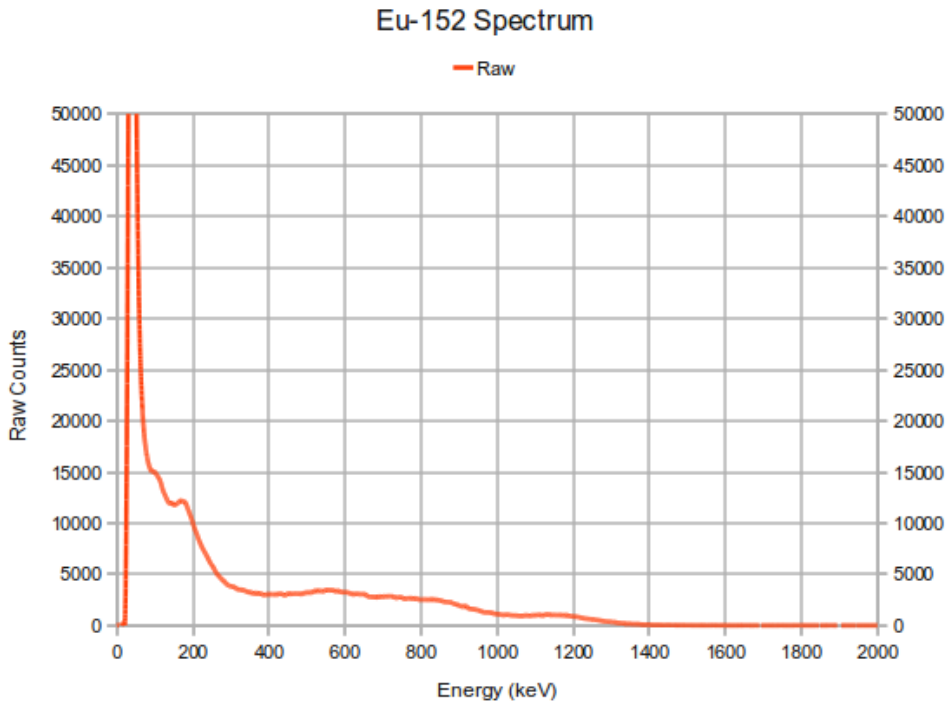

Figure 4.10: Eu-152 spectrum taken with 1m V-Plank.

4.5 The 2m X-Plank

The second of the larger area designs was the 2m X-Plank. This design was 200cm long$\times$12.5cm wide and the shape was a double trapezoidal, using 2.5cm to taper the width of the detector downwards along the length of the plank to the middle, then taper outwards again to the other end. This design was similar to two V-Planks placed end to end, only with a greater length to width ratio. The volume of this design was also 9 litres. The detector was 12.5cm wide at both ends to fit a 5" photomultiplier tube at either end. This design like the larger V-Plank used multiple photomultiplier tubes to cover the full collection area and therefore uses the same set up as the 1m V-Plank. The benefit of using this design however, is the larger coverage area from top to bottom, whereas the 1m V-Plank has a better sensitivity at the mid level. In a personnel portal for example, this design would give a better sensitivity for sources concealed in a hat or shoe. This design also required the same software used for the 1m V-Plank to coincide the signals from each photomultiplier tube. In this case the signals were simply added together as with the 1m V-Plank, this is because the taper gives a relatively uniform response across the length of the detector. A straight plank of similar dimensions would require that the signals be added differently to minimise the

variation in the signal. By taking into account the ratio of the pulse height between the two ends of the detector, the signal could be reconstructed according to the attenuation profile from one end to the other due to optical attenuation. Figure 4.11 shows an illustration of the 2m X-Plank.

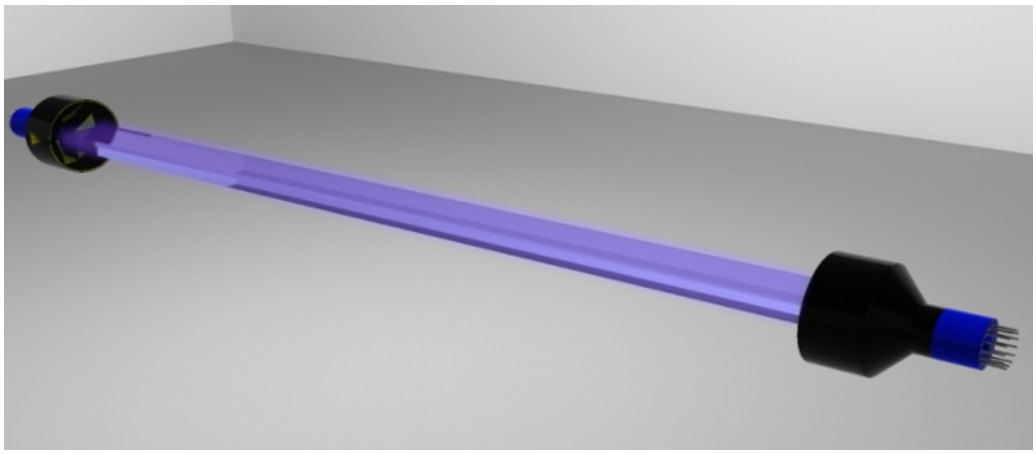

Figure 4.11: A 3D rendered illustration of the 2m X-Plank.

4.5.1 Simulated Performance

A two-dimensional map of the detector's spatial variation in the light collection was constructed for the 2m X-Plank, along with the mean light collection efficiency. The procedure for simulating the variation in the light collection are kept the same as with the 50cm V-Plank design, with 1cm points along the width of the plank, and 1cm points along the length. The simulated variation in the light collection efficiency is shown in Figure 4.12. The results of the simulated performance are shown in Table 4.4.

Table 4.4: 2m X-Plank Simulated Performance

Mean LCE	46 +/- 1.0%
VLCE	5.5 +/-0.6%

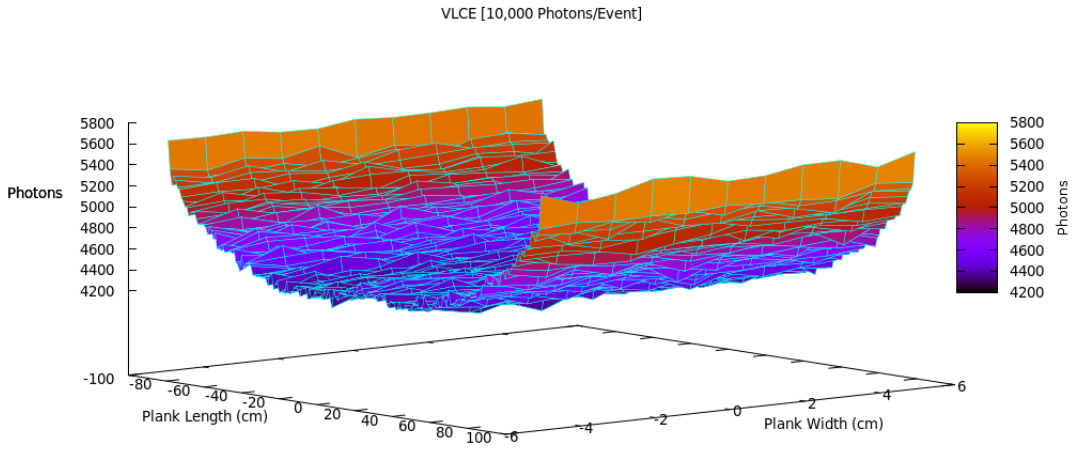

Figure 4.12: A map of the simulated variation in the light collection efficiency of the 2m X-Plank.

4.5.2 Measurements

The spatial variation in the light collection efficiency of the 2m X-Plank was initially measured using the same collimated Cs-137 at 39 points; every 15cm along the length of the detector for 3 equidistant points along the width of the detector. The variation in the light collection efficiency was found to be 3%, again much lower than predicted by the Geant4 simulation.

4.5.3 Resulting Spectra

For the 2m X-Plank Cs-137, Na-22 and Eu-152 spectra were taken to observe the quality of the Compton edges produced. The first is Cs-137 shown in Figure 4.13. Figure 4.13 shows a similar spectrum to the one created by the 1m V-Plank. Initial observation shows a similar shaped Compton edge, which was expected due to the similar simulated results of the detector. The next spectrum is Na-22 shows in Figure 4.14. Figure 4.15 shows the Eu-152 spectrum taken with the 2m X-Plank. Both the Na-22 and Eu-152 spectra are similar to that of the 1m V-Plank. It is again difficult to differentiate between the quality of the spectra without a more detailed analysis of the Compton edges, which is provided in the next section.

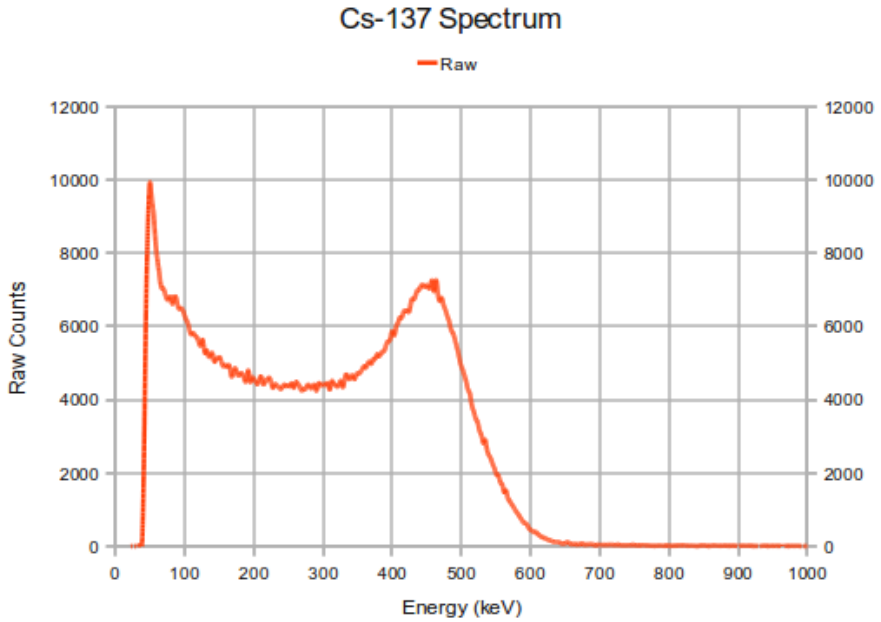

Figure 4.13: Cs-137 spectrum taken with 2m X-Plank.

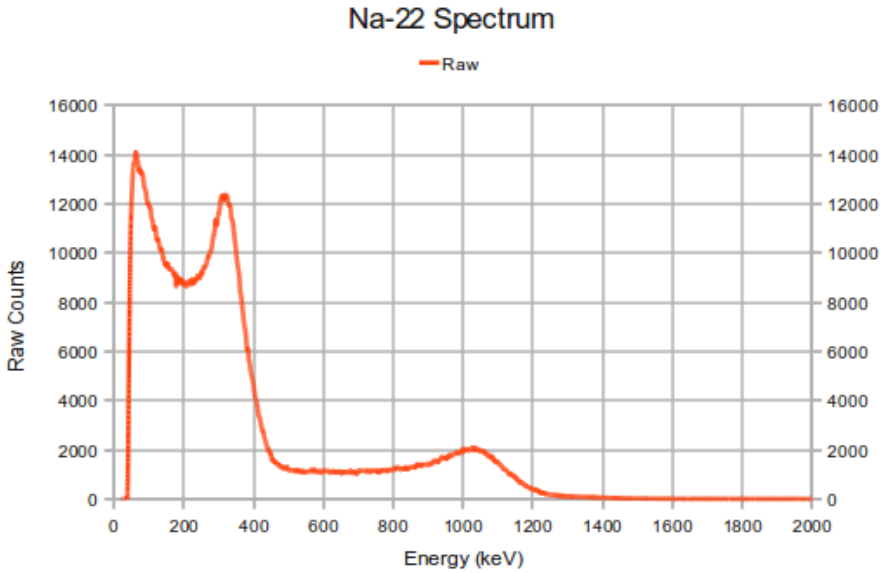

Figure 4.14: Na-22 spectrum taken with 2m X-Plank.

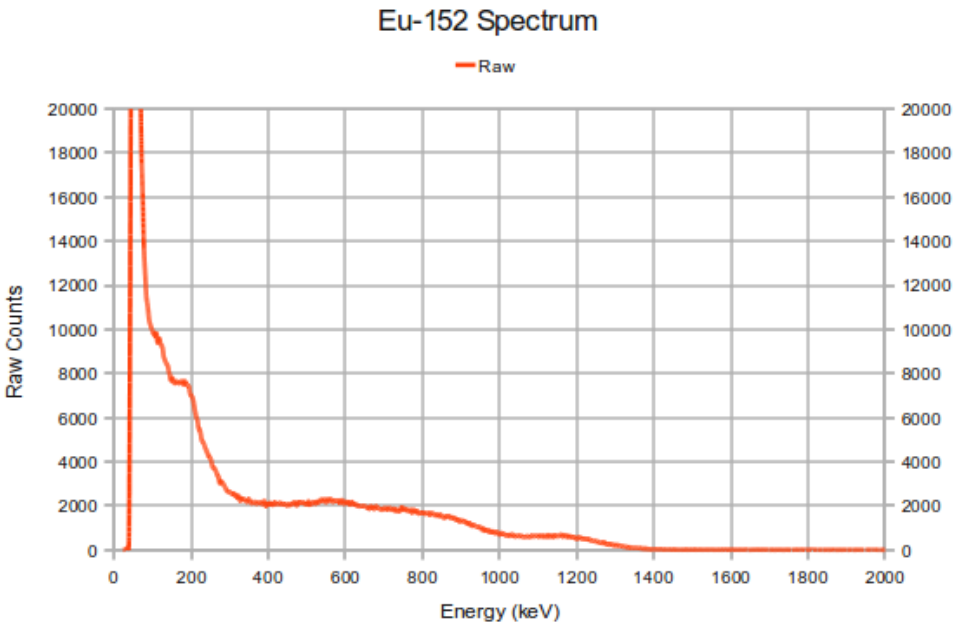

Figure 4.15: Eu-152 spectrum taken with 2m X-Plank.

4.6 Relative Performance of Each Design

In order to evaluate the relative performance of each detector design, two methods were used. The first was simply to quantify the equivalent resolution of each detector by measuring the equivalent full width at half maximum at the 662keV induced Compton edge. The Compton edge from a 662keV gamma-ray appears at 478keV. To measure the FWHM, a Gaussian function was generated with mean value equal to that of the location of each of the Compton edges. The standard deviation in the mean was then altered manually until the difference between the data and the model was minimal. This method is not entirely accurate as only the Compton edge itself follows a Gaussian type distribution, rather than the rest of the Compton continuum. It does however provide a relative method for comparing the resolution of each detector design. Figure 4.16 shows the Gaussian fitting process to a 662keV induced Compton edge from the 50cm V-Plank. Table 4.5 shows the results of all the detector designs.

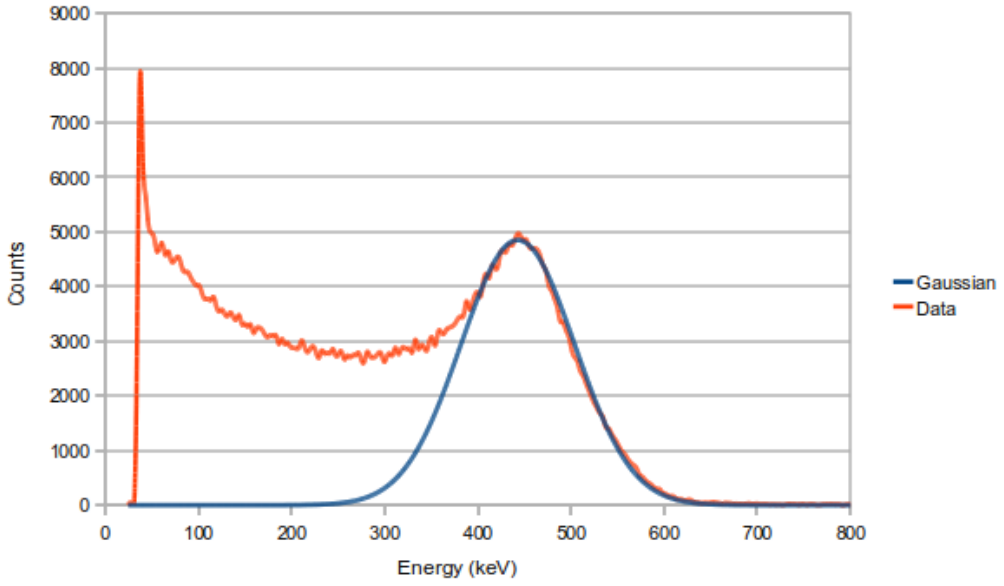

Figure 4.16: An example of the Gaussian fitting process, in this case a 662keV induced Compton edge from the 50cm V-Plank.

The second method for evaluating the detector performance was to simulate a portal type scenario where each of the larger designs were tested against each other and also a standard sized NaI(Tl) based detector. The simulation was constructed in a Geant4 environment to determine the performance of each detector design in a walk-through personnel portal scenario. In each portal simulation two detectors were used; one

Table 4.5: Equivalent FWHM of each detector design at 662keV induced Compton edge

Detector	Equivalent FWHM @ 478keV
2m X-Plank	34 +/-1%
1m V-Plank	33 +/-1%
50cm V-Plank	32 +/-1%

each side of the portal. The portal consisted of the two detectors placed exactly 1m apart and in vertical alignment. A simulated source was then passed through the portal system and information such as the number of counts and the quality of the resulting spectra were recorded. A 16μCi Cs-137 source was passed through the detector portal at a typical walking speed of 1.2 m/s. The maximum height of the portal unit was taken to be 2m high, and therefore the detectors were placed mid-way at a height of 1m above the ground. The source was then walked through the portal starting from 2m behind the portal to 2m in front of the portal in a series of 40 incremental steps which averaged a speed of 1.2 m/s. Each simulation was completed at heights of 1m and 180cm above ground. These heights were ultimately designed to test the limits of each detector since some designs had the majority of their volume localised in one region. Physically, the heights could represent a person with a concealed source either on their mid-section, or perhaps hidden in a shoe or hat respectively. For this simulation, the two large area detector designs were compared with a standard 4"$\times$2"$\times$16" NaI(Tl) crystal detector. The resulting number of counts recorded in each detector, along with the corresponding relative sensitivity compared to the NaI(Tl) crystal, are shown in Table 4.6. The results of the simulation show that both PVT designs were more sensitive than the NaI(Tl) crystal in a portal setting. This was expected due to the larger area covered by each of the PVT designs. The 1m V-Plank had the best overall sensitivity, as the total number of counts for both centre and 180cm runs was equal to 32,018 counts whereas the 2m X-Plank was slightly less at 29,393 counts,

Table 4.6: Radiation Portal Simulation Results

Detector	Counts +/-2% (Centre)	Counts +/-2% (180cm)	Relative Sensitivity (Centre)	Relative Sensitivity (180cm)
2m X-Plank	16946	12447	1.44	3.27
1m V-Plank	22219	9799	1.89	2.57
4"×2"×16" NaI(Tl)	11759	3806	1.00	1.00

though as predicted the 2m X-Plank was slightly more sensitive towards the ends of the detector. The NaI(Tl) has a total number of counts of 15,565 making it on average half as sensitive as the PVT designs. However, although the sensitivity of each design is important, the quality of the resulting spectra is crucial to any attempt at identifying the source. The spectra associated with each simulation were also recorded, and are presented in Figure 4.17. There is little difference in the overall shape of the spectra for the 2m X-Plank and the 1m V-Plank designs with designs showing a clear Compton edge at 470 keV from the incident 662keV gamma-ray, enough for the human eye to recognise as a Cs-137 source. The PVT based designs show their disadvantage at this point as although they are more sensitive, a large proportion of their counts occur outside of the Compton edge which are therefore wasted counts in the context of determining the source producing the spectra. In contrast, the NaI(Tl) design has a high photo-fraction, showing its advantage of a clear 662keV photo-peak, which was where the majority of the counts were recorded, making them more useful for isotope identification or classification.

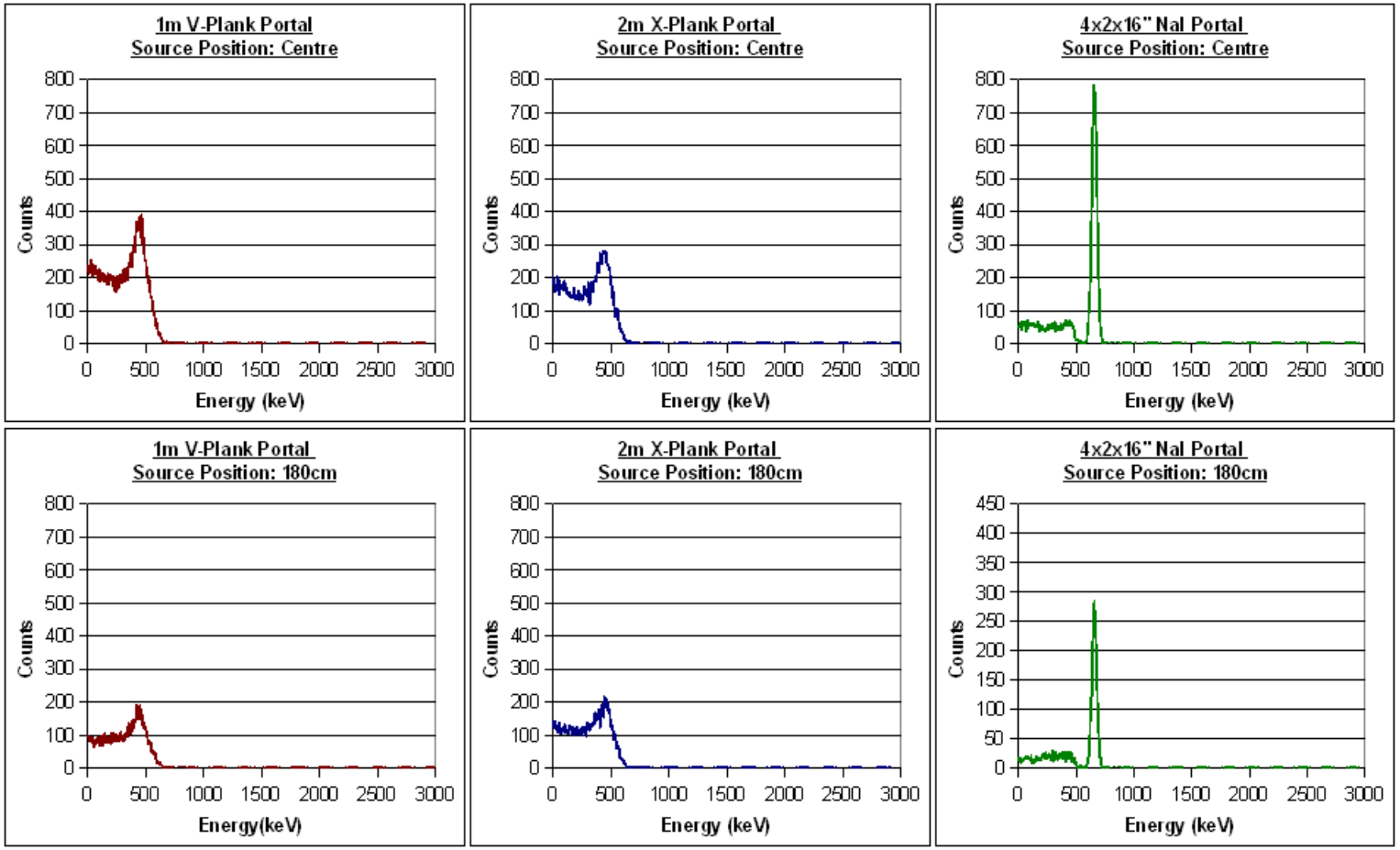

Figure 4.17: Comparison of Spectral Quality from Portal Simulations

4.7 Comparison With Traditional PVT Designs

For comparison with traditional PVT designs results were used from a previous experiment conducted by M. Dallimore at Symetrica Ltd, in which the performance of a 91cm× 25cm× 4cm PVT design was measured. This design was similar in dimensions as the 1m V-Plank, but had a single 2.5" photomultiplier tube for light collection, crinkled aluminium foil as surrounding reflector and the design did not incorporate a taper. This design is somewhat optimistic over other designs, as although it has only one small photomultiplier tube, the ratio of the length to the width of the detector is quite reasonable and the length itself should not allow for much light attenuation. The results for this detector are shown in Table 4.7 This design clearly shows the

Table 4.7: 1m Straight Plank Measured Performance

Mean LCE	2.5%
VLCE	8%
FWHM (662keV induced Compton edge)	52%

weakness of using a single small photomultiplier tube and no reflective coating. A combination of reflective edge coatings and larger coverage by photomultiplier tubes would bring the variation in the light collection down and increase the light collection efficiency dramatically. Figure 4.18 shows an example Cs-137 spectrum from the 91cm×25cm×4cm PVT design.

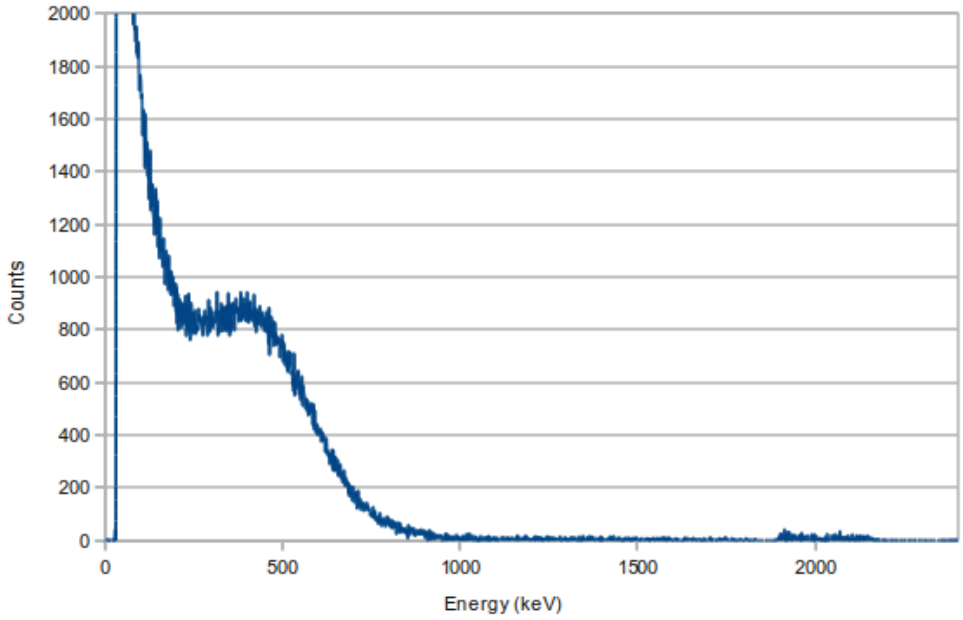

Figure 4.18: An example Cs-137 spectrum from the 91cm×25cm×4cm PVT design.

4.8 Conclusions

In this Chapter, all three of the new PVT designs were found to perform very well giving excellent quality spectra. The 50cm V-Plank gave the best performance due to its much higher light collection, followed by the 1m V-Plank and lastly the 2m X-Plank. The performance of the 1m V-Plank and 2m X-Plank was very similar, but the higher variation in the light collection efficiency of the 2m X-Plank gave slightly poorer performance. The equivalent FWHM for each design at the 662keV induced Compton edge was 32% for the 50cm V-Plank, 33% for the 1m V-Plank and 34% for the 2m X-Plank. Portal simulations were conducted for each design and included a NaI(Tl) based design for comparison. The PVT based designs outperformed the NaI(Tl) based design in terms of raw number of counts in the spectra, but the NaI(Tl) based detector had the advantage of a high photo-fraction, with more counts placed in photo-peaks rather than counts wasted in the Compton continuum as was present in the spectra of the PVT based designs.

Chapter 5

Spectral Processing

5.1 Introduction

In the previous chapters the physical design of PVT detectors were investigated and an optimal solution for the detector design was discovered. To gain any further significant improvements in performance of the detector, or for the detector to gain the ability to distinguish between isotopes, spectral processing was required. Various techniques are available for processing spectra, most of which have been used with NaI(Tl) based detectors. However, given the lack of photo peaks in the energy loss spectra from PVT, a different approach was required. One of the more common approaches with PVT given the current lack of resolution in mainstream devices is to section off each part of the spectrum into a window. This technique is more commonly known as energy windowing. Another more recent addition is the use of neural networks to attempt to discern radioactive sources. This set of algorithms is programmed to learn a pattern based on a number of input variables or samples. In this context a number of sample spectra are given for the network to learn and the network can then match a current spectrum. The final type of spectral processing covered here is spectral deconvolution, a process which attempts to account for the flaws in a detector system and subsequently eradicate their effects to produce a reconstructed most likely incident gamma-ray spectrum from an energy loss spectrum.

5.2 Energy Windowing

Although PVT scintillator has little useful spectroscopic capability, limited information of incident gamma-rays are preserved in the Compton edges of resultant energy-loss spectra. The Compton edges are relatively broad however and therefore cannot be used to accurately determine the incident gamma-ray energy. Using broad energy windows can give some discriminatory ability to the detector, for example, one can check the number of counts in high or low energies and compare that to what is expected for various NORM spectra. After a primary screening alarm, one would not expect to find a large percentage of high energy gamma-rays from a source that the transporters declared was medical in nature. Energy windowing can be used to check gross energy differences without the need for high resolution. Ely et al at PNNL give an overview of one such technique in their paper "The use of energy information in plastic scintillator material" [Ely et al., 2008]. In this paper the authors measure fertiliser and plutonium and compare them with background radiation, measuring the gross number of counts in the spectrum for each source and the proportion of counts in the high and low energy ranges. Figure 5.1 shows the results. The authors conclude

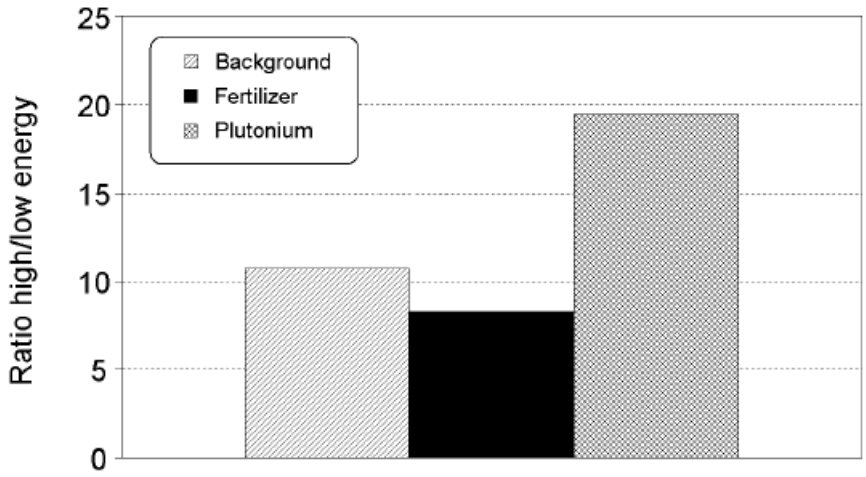

Figure 5.1: Ratio of low to high energy count rates for background, background plus fertiliser, and background plus plutonium. Figure taken from [Ely et al., 2008]

that this method can give limited success, but only for isotopes that have both high and low energy components. The majority of isotopes such as those used in the medical industry have only low energy spectra and therefore this method would be ineffective in distinguishing them.

The number of windows used for the energy windowing method to be successful would need to be large enough to give a wide range of energies without being unrealistic about the resolution of the detector. Ely et al in their paper "The use of energy windowing to discriminate SNM from NORM in radiation portal monitors" [Ely et al., 2006] give examples of both 3 window and 5 window systems for isotope discrimination. A small range of sources were used in these experiments, which include HEU, WGPu, fertiliser, and tile. Figure 5.2 shows the results of the 3 window approach, whereas Figure 5.3 shows the results of the 5 window approach. The

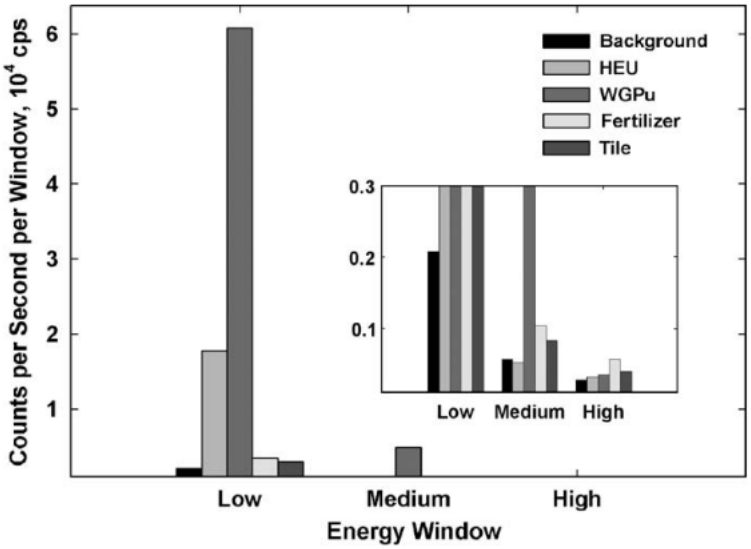

Figure 5.2: Count rates in counts-per-second (cps) per energy window in the three energy bins (low, medium, and high energy) for background, HEU, WGPu, fertiliser, and tile. Figure taken from [Ely et al., 2006]

authors conclude that the 3 window system has limited success as with the simple 2 energy windows system and is not very effective at discriminating SNM from NORM. The 5 window system provides better results, in discriminating SNM from NORM by using a more complex set of ratios between the 5 energy windows. The authors note than neither system successfully discriminates between other sources such as those from the medical industry. In such methods the main principle is to compare the overall shape of the energy-loss spectrum to that of a typical background spectrum. As the number of windows increases, the processing technique becomes more and more like spectroscopy rather than a simple discrimination. Energy windowing systems can therefore provide a relatively simple, cost effective solution for discriminating SNM

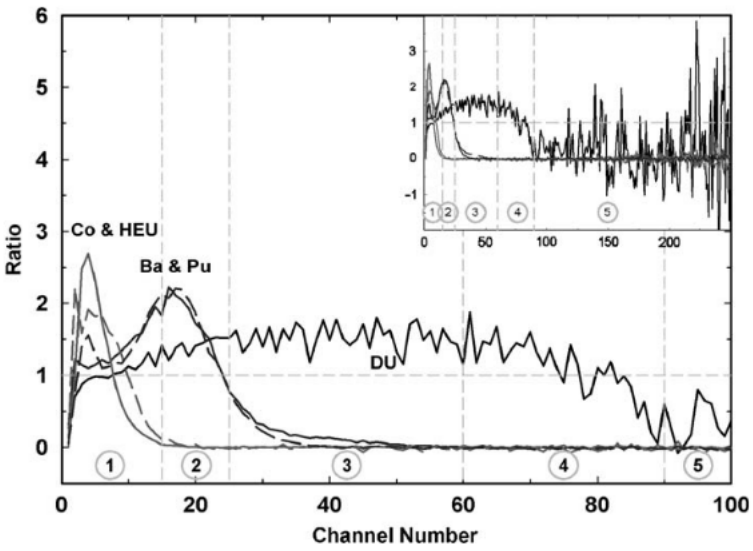

Figure 5.3: The channel-by-channel ratio of the counts in a net-source spectrum to the counts from a background spectrum for spectra from Co-57, HEU, Ba-133, WGPu, and depleted uranium. The circled numbers are the window numbers referenced in the text. Figure taken from [Ely et al., 2006]

from NORM, but cannot discriminate other sources from NORM.

5.3 Neural Networks

Artificial neural networks have also been examined as a way of discriminating between sources using existing PVT technology. This technique involves teaching a computer system how to correctly distinguish a threatening from a non-threatening isotope based on previous sets of accurate spectra. The system learns from samples of threatening and non-threatening energy loss spectra by finding patterns in each data set. Ultimately the system can analyse new spectra to determine if they fall within these pre-defined patterns and therefore if they are from threatening sources or not. Like energy windowing, this system has the advantage of being an inexpensive add on to existing technology. The process is also relatively fast, requiring little time during to process each new spectrum. The disadvantages of this system are the large number of spectra required during the learning phase to construct a reliable system, an unpredicted spectrum falling outside of the system's patterns are therefore not being able to identify properly, and the system's discriminatory ability being limited by the resolution of the PVT.

Kangas et al [Kangas et al., 2008] conducted an initial feasibility study into such a system. The authors used simulated sample spectra during the learning phase to establish identification of various other simulated spectra. They found that in order to increase the chances of detecting a specific source whilst maintaining the same false alarm rate, the system had to be provided with a minimum number of counts per spectrum. An example of this was with identification of a simulated cobalt-57 spectrum. 100% identification could be achieved in simulation with a 0.5% false alarm rate using simulated spectra with over 1000 counts. The authors concluded that the number of spectral samples required for the system to correctly learn were practically impossible to attain without the help of such simulated data. Neural networks become heavily reliant on the accuracy of the simulated model during the learning phase and also suffer from the need to cover all possible shielding/masking scenarios for every radiation source of concern. Neural networks applied to PVT scintillators is still a relatively new area of work. Whilst some of the results presented by Kangas et al look promising, more in-depth studies are required and therefore an accurate conclusion cannot be made on their viability at this time.

5.4 Spectral Deconvolution

Spectral deconvolution attempts to reverse engineer the effects of performance degradation due to inherent flaws in the detector system and compensate for them accordingly. Using this technique on crystal scintillators such as NaI(Tl) and CsI(Tl) has proven to be successful with a significant increase in detector resolution. Such techniques have seen the FWHM improve from 12% at 662keV in the raw spectrum of a 3"x3" NaI(Tl) detector to 3% after software deconvolution [Meng and Ramsden, 2000]. The possibility of using deconvolution techniques for plastic scintillators was investigated and the results were found to significantly increase the functionality of PVT detectors for spectroscopy. Isotope identification techniques were also developed to make use of the improved functionality as well as a system for classifying detected isotopes into appropriate categories. The isotope category system is a more useful approach to identifying any potential nuclear threat as the operator of the detector system does not need to translate the identification of an isotope into a corresponding threat level. Unidentifiable isotopes can also be placed into relevant categories based on similar patterns in their spectra.

The resultant energy loss spectrum produced from a gamma-ray source is the composition of the incident gamma-ray spectrum combined with the response function of the detector measuring it. By calculating the response function of a detector the incident gamma-ray spectrum can be reverse engineered from the energy loss spectrum. In order to do this the response function must be calculated for each individual detector as each detector has its own unique set of characteristics. The process of spectral deconvolution is an advanced data-processing technique which can be executed with either stand alone software or with the aid of dedicated hardware. A standard personal computer is required to undertake the necessary iterative processing of raw energy loss spectra.

5.4.1 The Models Required

The method of deconvolution employed requires a response function which is assembled using Monte Carlo methods in the Geant4 simulation tool kit. Typically the

response of a detector must be modelled for every single energy gamma-ray of interest, in this case from 3keV to 3000keV. The model used for this work consisted of 512 files numbered from n = 1 to n = 512, each containing a normalised spectrum of incident energy E shown in equation 5.1:

$$E = (n * 6keV) - 3keV \tag{5.1}$$

This gives a maximum energy of 3069keV for the final 512th file. This set of files represents the complete detector response for a given material at all incident gamma-ray energies without any broadening due to detector characteristics. Typically to model the response of a detector to each gamma-ray energy around 2 million gamma-ray photons are fired into the detector. The computation of these files can therefore take from 24 hours to 72 hours on a standard 3.0 GHz, single core, personal computer depending on the model being constructed. This time can however be reduced using a modern multi-core PC, or many individual PCs, by distributing the number of files across each processing core to simultaneously process their own range of files. Once the raw energy files are complete they must be broadened with the detector response function, which is determined by both simulation and by measurement, as outlined in Chapter 3, to give a new set of files, termed a "q-matrix". The q-matrix gives an accurate representation of the response of the whole detector system to any incident gamma-ray. The number of files for the q-matrix is limited to 512 to reduce the computational load that the deconvolution process requires. As processing the spectrum would need to be done in real time when used in a portal, the computational load and therefore the time to process each spectrum must be minimised. 512 energy bins is enough to provide an increased energy resolution for NaI(Tl) based detectors, whose current resolution is much greater than that of PVT. Using 1024 files, the next step up in resolution, has previously provided no additional energy resolution to NaI(Tl) based detectors whilst significantly increasing the computational time required for spectral processing.

The factors required for the broadening the raw data files into q-files were outlined in Equation 3.1 from Chapter 3. The photomultiplier noise was typically assumed to be very low and estimated at a few photoelectrons RMS. Three or four photoelectrons

were taken as the noise value, though in some simulations this number was increased to around six photoelectrons to quantify the noise effects in an energy loss spectrum. The variation in light yield was assumed to be negligible for PVT for the time being given the lack of definitive agreement of such effects. Both these values are used for all range of PVT detectors using the standard 5" Adit photomultiplier tubes. The variation in the light collection must be measured experimentally for each detector used. This was measured by placing a collimated Cs-137 source at various locations along the length of each detector and measuring the resulting percentage shift in the Compton edge produced by the 662keV gamma-rays, as outlined in Chapter 4. The overall light collection efficiency cannot be accurately measured from a photo peak in PVT and is therefore estimated from optical Monte Carlo simulations. The light yield of the PVT and collection efficiency of the photomultiplier tubes are given by the manufacturers and are combined with an optical simulation of the light propagation through the detector medium. Once all the characteristic values for the detector have been obtained, a new table of resolution values can be created to represent the amount of broadening that a spectrum of each energy gamma-ray would receive. These values are represented as the full width at half maximum of the expected photo-peak at a given energy. The FWHM values are plotted with respect to the incident energy to give a graph of how the detector's resolution changes with incident gamma-ray energy. The function of the graph is extracted as the detector's response function. Statistical broadening routines are finally employed to broaden the raw energy files with the response function to give the final q-matrix.

5.4.2 Deconvolution Algorithm and Process

A complex analysis of the deconvolution algorithms will not be covered here as this work has been covered in detail by Ramsden and Meng [Meng and Ramsden, 2000] who discuss and compare in length various algorithms used for gamma-ray spectral deconvolution. Ramsden & Meng conclude that of the algorithms they compared the Maximum Likelihood by Expectation Maximisation (ML-EM) algorithm gave the best overall performance on a tested NaI(Tl) detector. This conclusion was based on the best peak resolving power, the best peak to valley ratio and the narrowest peak widths of the resultant deconvolved spectra. Ramsden & Meng did however note at

the time that some small artefacts were present in the deconvolved spectrum due to discrepancies between the simulated and real response of the detector. Symetrica Ltd has since built a large collection of deconvolution libraries and software based around the ML-EM algorithm for their various crystal based scintillation detectors. A framework was therefore already in place for the deconvolution of PVT spectra. Figure 5.4 shows a graphical representation of the deconvolution process used to process raw spectra. The process of deconvolution is iterative. To start with an initial guess is made on the incident gamma-ray spectrum based on the raw peaks found in the energy loss spectrum. In the case of plastic scintillator where there are no photo-peaks, the resolution window is widened so that the algorithm looks at the sharp Compton edges as photo-peaks. Once this initial guess at the spectrum is complete, the estimated energies are run through the q-matrix of the detector to produce a simulated energy-loss spectrum. This simulated spectrum is compared to the energy loss spectrum for precision. A modifying function then adjusts the initial estimate to a more accurate one, which is then in turn combined with the q-matrix and tested against the energy loss spectrum. This process repeats until the similarity between the simulated estimate and the real energy loss spectrum is acceptable and the difference from one estimate to the next becomes negligible. The accuracy of the deconvolution processes' ability to reconstruct the energy loss spectrum is represented by the full width half maxima of each peak produced in the deconvolved spectrum. Meng and Ramsden [MENG et al., 2002] give a good example of spectral deconvolution on their Scintisphere, a spherical CsI(Tl) crystal scintillator 100cc in volume. The source measured was Radium-226 and is shown in Figure 5.5. Figure 5.5 already shows good resolution due to the design of the detector, but the positive effect of the spectral deconvolution produces an excellent result, with many spectral lines identified that were previously not resolvable. This particular detector had a raw resolution of 7.7% at 662keV and a deconvolved resolution of 1.4% at 662keV.

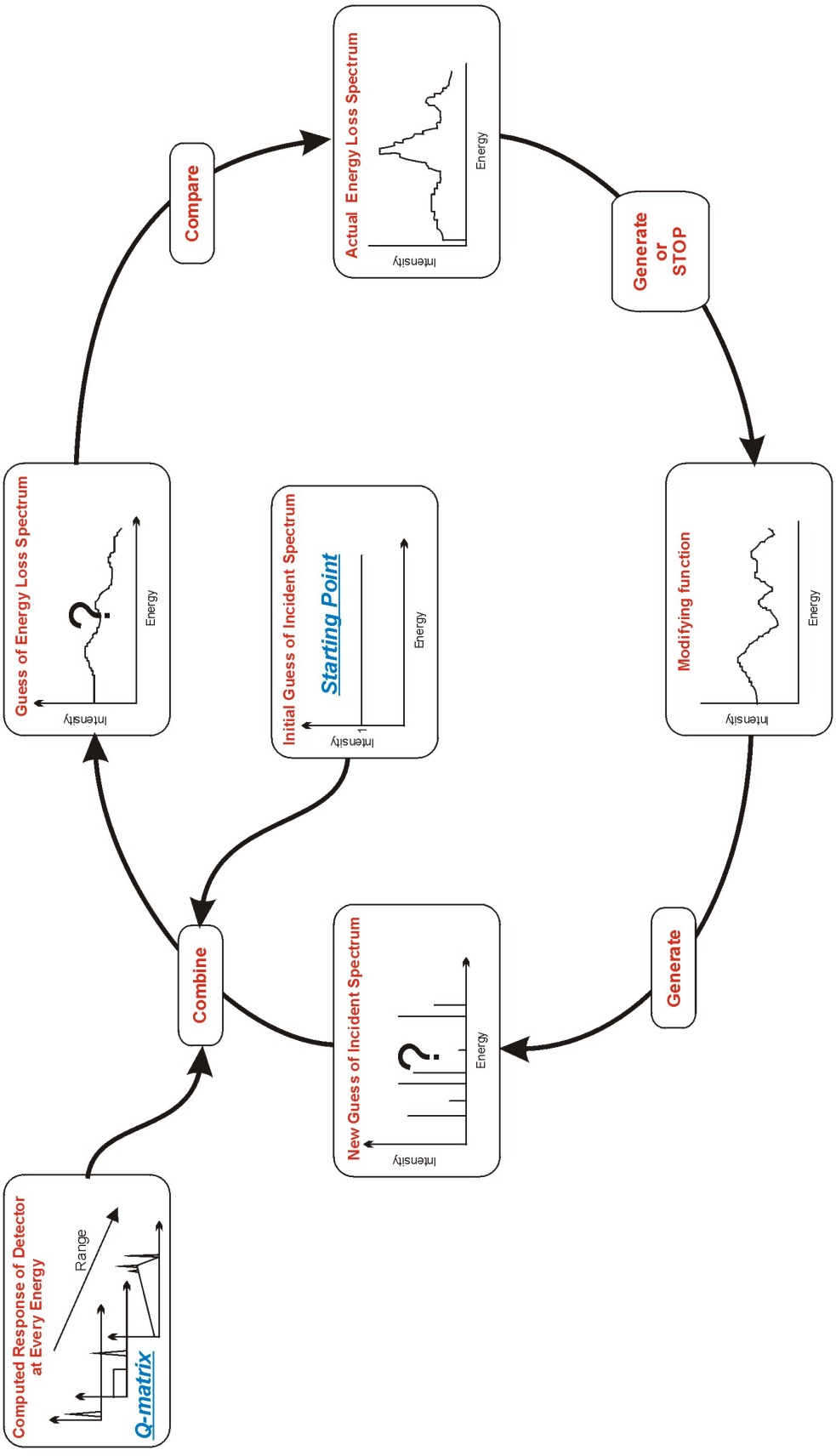

Figure 5.4: A graphical representation of the deconvolution process

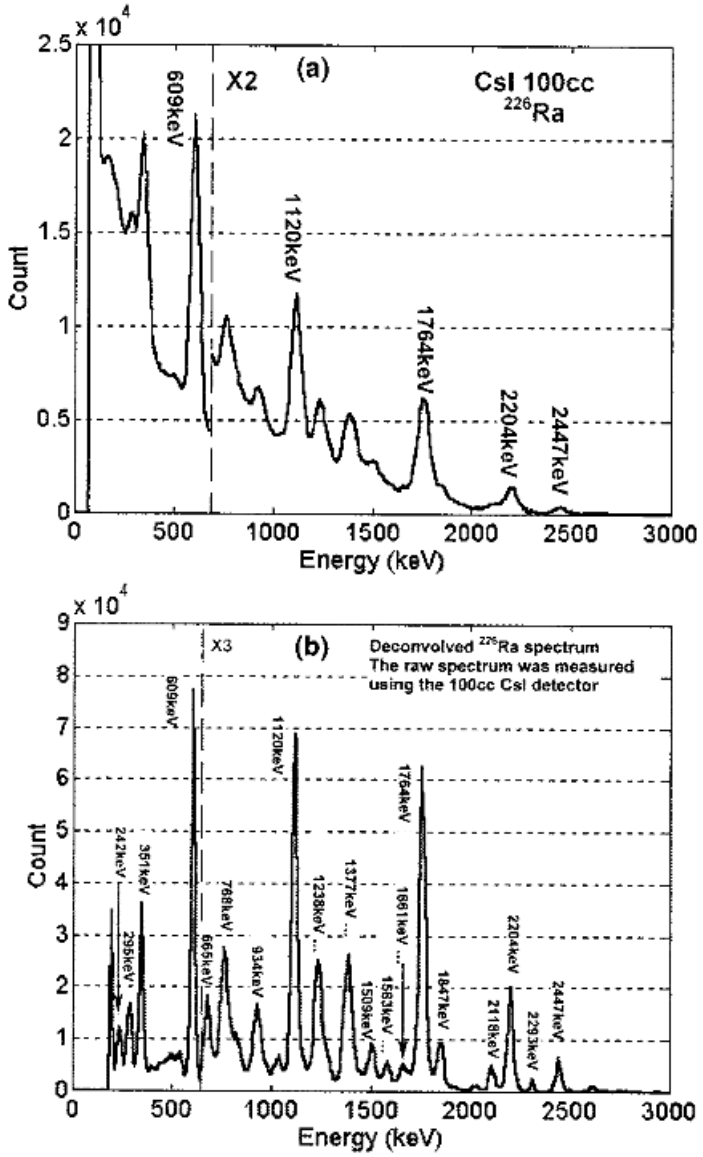

Fig. 4. (a) The measured and (b) the deconvolved spectra using the 100 cm^3 Scintisphere and a ^{226}Ra point source.

Figure 5.5: (a) The measured and (b) the deconvolved spectra using the 100 cm Scintisphere and a Ra-226 point source.

5.5 Isotope Classification & Identification

The entire process of identifying an isotope using deconvolution software is outlined as follows:

- Detector measures source radiation
- Raw spectrum compiled
- Raw spectrum deconvolved
- Deconvolved spectrum run through identification process
- Isotope identified and classified

In order to categorise or identify an isotope, that isotope must first be programmed into an identification library. This library contains the names and spectral information of all possible isotopes of interest, and also which of the following major categories they belong to based on their typical usage. The categories used for classification by the Symetrica deconvolution and identification software are the same as those present in the ANSI N42.38-2006 standards for spectroscopy based portal monitors [IEEE, 2006b] and are shown in Figure 5.6. Figure 5.6 also shows which isotopes belong to which classification. These categories can also be divided into shielded and un-

— Special nuclear materials: Uranium (used to indicate ^{233}U, ^{235}U), ^{237}Np, Pu

— Medical radionuclides: ^{18}F, ^{67}Ga, ^{51}Cr, ^{75}Se, ^{89}Sr, ^{99}Mo, ^{99m}Tc, ^{103}Pd, ^{111}In, Iodine (^{123}I, ^{125}I, ^{131}I), ^{153}Sm, ^{201}Tl, ^{133}Xe

— Naturally occurring radioactive materials (NORM): ^{40}K, ^{226}Ra, ^{232}Th and daughters, ^{238}U and daughters

— Industrial radionuclides: ^{57}Co, ^{60}Co, ^{133}Ba, ^{137}Cs, ^{192}Ir, ^{204}Tl, ^{226}Ra, and ^{241}Am

Figure 5.6: Isotope list and classification according to the ANSI N42.38-2006 standards for spectroscopy based portal monitors.

shielded sources, producing a much larger library. Typically the identification library must contain entries for energies of spectral lines expected for that isotope, the intensity proportion of those lines for the given isotope and the resolution of those lines in an energy loss spectrum. This library is different for each detector as the resolution and attenuation coefficient change with detection material. An ideal isotope identification algorithm can pick out photo-peaks, measure their resolution and intensity,

compare it to the identification library and suggest possible isotopes with a certain confidence level. Multiple isotopes in a spectrum should have no bearing on each of the isotopes' identification as the algorithm should be able to match each spectral line to a range of possible isotopes. Such algorithms are very effective with high resolution detectors like HPGe based detectors and NaI(Tl) based detectors. A basic level of identification can be reached by sorting incident spectra into one of the above major categories based on the number of counts in a given energy region based on a process of elimination and likelihood. Proportions of counts appearing in certain regions of the energy loss spectrum are common amongst many isotopes of a specific category. Medical isotopes rarely have many counts in the high energy region of a spectrum for example, so anything with a large proportion of counts in that area can eliminate the possibility of a medical isotope.

For PVT based detectors the spectrum must first be deconvolved to produce photo-peak like lines in the processed spectrum. These peaks/lines represent the best estimate of the incident spectrum and have a resolution, intensity and expected energy similar to that of the photo-peaks of a crystal based detector. The identification and deconvolution algorithms used here were provided by Symetrica's bespoke software. In addition to the identification libraries required, a variety of software settings were also present. These include the minimum and maximum raw energy for deconvolution, the maximum expected resolution of each resultant peak for identification and the maximum accepted offset of each peak from its expected location. All these settings were specifically targeted towards NaI(Tl) based detectors, and were therefore not relevant for PVT based detectors, given their much poorer resolution. Settings relevant to PVT based detectors were somewhat reverse engineered, starting with the original NaI(Tl) based settings and decreasing the resolution until the system was able to identify the spectral lines from a variety of test sources. The settings used for the deconvolution after this point were as follows:

- Linear resolution: 4%
- Offset: +/- 8keV
- Minimum Energy: 25keV

- Maximum Energy: 3000keV

These settings make allowances for both the deconvolution and isotope identification algorithms. The deconvolution will work from 25keV to 3000keV and the peak search algorithm will look for peaks within 4% of a specific energy +/- 8keV. These settings are quite broad to allow for the decrease in resolution of the detector over one based on NaI(Tl). An isotope identification library was also created specifically for use with PVT based detectors, as discussed in the next subsection.

5.5.1 Isotope Library Creation

To successfully identify an isotope, a library containing all isotopes of interest was used as a reference. This library contains the isotope name along with the expected incident gamma-ray energies and the corresponding intensities for a given detector. Such a library was already employed successfully for NaI(Tl) and other crystal scintillator detectors, but had to be recalculated for use with PVT given its poorer resolution and differing interaction processes. To complete this task a program was written in C++ to automatically transmute commonly available, high resolution isotope gamma-ray libraries into suitably broadened files for use with PVT detectors. This program worked by merging incident energies or spectral lines that would normally be present with high efficiency detectors such as high purity germanium. It completes this process according to specific detector attributes and settings that must be supplied to the program. The program initially loads a list of gamma ray line energies and intensities from an isotope file and weighs the line intensities with the corresponding detector efficiency at that energy. The program then simulates a Gaussian broadening of each line energy according to the detector resolution at that energy. This resolution is taken from the q-matrix calculated earlier for that detector. If any spectral lines are unresolvable after broadening, then the lines are combined according to their respective intensities. Weak lines with less than 1% intensity are also removed as they do not appear in the subsequent energy loss spectra. The line combination process is iterative, with priority always given to the two closest lines in a given spectrum for each iteration. In this manner several spectral lines in the same energy region can be combined accurately. The program also compensates for the Compton scattering process by accounting for Compton edges that will appear at energies in the same region that

low energy photo-peaks might appear. It is able to predict the merging of low energy photo-peaks with that of a similar energy Compton edge produced from a higher energy gamma-ray. The whole process results in a reduced isotope library relevant for PVT taking into account both its poorer resolution and the merging of photo-peaks and Compton edges. Weak intensity spectral lines or lines that are out of the energy range of the detector that will not appear in the spectrum are also removed from the library. The program does not however predict the existence of phantom peaks (described in Chapter 6) within the spectra, this is done manually and added with a flag in the library to allow the user to see that the peak should not exist at that energy for the isotope being measured. An example of the isotope Cs-137 is used to demonstrate the creation procedure, with the initial data from the Berkley laboratory Isotopes Project library [Firestone1 and Ekstrm, 2004]. Table 5.1 shows the data for X-rays and gamma-rays. Table 5.2 shows the library entry after the program has merged and removed the necessary spectral lines.

Table 5.1: Spectral energies of X-rays and gamma-rays emitted by Cs-137. Taken from Berkley laboratory isotopes project library.

Energy (keV)	Intensity
3.95	0.0143%
4.33	0.0064%
4.45	0.040%
4.47	0.36%
4.83	0.226%
4.85	0.023%
4.93	0.039%
4.99	0.0030%
5.16	0.074%
5.53	0.033%
5.8	0.0065%
5.81	0.0093%
31.45	0.000263%
31.82	2.04%
32.19	3.76%
36.3	0.352%
36.38	0.680%
36.65	0.0079%
37.26	0.215%
37.35	0.0481%
283.53	0.001%
661.66	85.100%

Table 5.2: Spectral energies of X-rays and gamma-rays emitted by Cs-137. Adjusted for identification with plastic scintillator based detector.

Energy (keV)	Intensity
661.66	85.1%
32.0615	5.8%

The library creating process removes all the lines with less than 1%, leaving the lines at 31.82keV, 32.19keV and 661.66keV. The 31.82keV and 32.19keV lines are combined according to their intensities as they are unresolvable on their own. This leaves the 662keV and 32keV lines present in the adjusted library.

5.6 Conclusions

In this Chapter spectral processing techniques were reviewed and the deconvolution process discussed. The creation process of an isotope library was also presented with values for the identification algorithms specific to PVT based scintillators. It was shown that although some success has been made using basic energy windowing techniques with PVT, the process can only distinguish NORM from SNM and not identify any other radioactive material. This is due to the majority of radioactive sources of interest having spectral lines in regions that are similar to that of NORM, and with no further resolution to separate these lines identification cannot be made. The use of artificial neural networks looks to be restricted by the same factors as energy windowing, but this is still a work in progress and needs more research before a proper conclusion can be made. Spectral deconvolution has been proven with NaI(Tl) based scintillators to drastically improve the resolution of a detector, and therefore this technique has been optimised for use with PVT based detectors. Settings were optimised and an isotope identification library created based on the limited resolution of PVT. In the following Chapter the results of the deconvolution of various isotopes for each detector design are presented along with an analysis of the detector performance.

Chapter 6

Spectrometry with PVT

6.1 Introduction

Having investigated spectral processing techniques and the optimisation of PVT scintillators, in this Chapter spectroscopy is investigated with PVT using Symetrica's spectral deconvolution software. Each of the detector designs previously outlined are tested with a variety of radioactive sources. Complex and simple radioactive sources such as Eu-152 and Na-22 are measured, deconvolved and identified. A dependence of the identification ability on the minimum number of counts in a raw energy loss spectrum is established and investigated for Eu-152 and Na-22 sources. The factors which affect the ability to correctly identify these two sources are shown with the prime cause given. An overview is also given on the detection of neutron sources and the possibility of differentiating neutrons from gamma-rays using PVT detectors.

6.1.1 Sources Measured

The radioactive sources measured were those that were available at both the University of Southampton and at Symetrica Ltd's laboratory. They represent a range of gamma-ray energies from sources across the board of isotope classification; Medical, Industrial, NORM and daughter products from Special Nuclear Materials. Table 6.1 shows a list of the isotopes measured along with their most dominant gamma-ray/X-ray spectral lines as would be found using a NaI(Tl) based detector. All sources used for testing were below 10μCi in activity.

Table 6.1: List of Sources Measured with their Line Energies.

Source	Line Energies (keV)
Am-241	59
Ba-133	53, 80, 276, 302, 356, 384
Co-57	122, 136
Co-60	1173, 1333
Cs-137	32, 662
Eu-152	40, 122, 244, 345, 779, 964, 1100, 1408
Na-22	511, 1275
Ra-226 (1)	47, 76, 88, 186, 242, 295, 352, 511
Ra-226 (2)	609, 772, 934, 1152, 1389, 1759, 2204

6.2 The Phantom Peak

During the deconvolution of spectra from PVT based detectors, a curious phenomenon was noted due to the changing of dominant radiation interaction mechanisms with the PVT. At lower gamma-ray energies and X-ray energies of up to around 20keV, the dominant interaction process for electromagnetic radiation interacting with PVT is the photo-electric effect. X-rays and gamma-rays up to this energy produce photo-peaks in the energy loss spectrum if the threshold is set low enough. Above this energy, the dominant interaction mechanism shifts to Compton scattering. However, the Compton edge associated with gamma-rays up to around 80keV will not be seen in most of these spectra, as the Compton edges appear below 20keV in the energy loss spectra. This means that isotopes with emissions of up to around 70keV will give photo-peaks in the spectrum and no Compton edge. Emissions of around 80keV will give no entries in the spectrum at all as the photo-peak is too weak in intensity and the Compton edge is too low in energy for them to register. A problem occurs around these energies due to the sharper Compton edges of optimised PVT detectors. That is, there exists a region where a higher energy Compton edge looks similar in shape and is located in the same channel as a lower energy photo-peak. This can be seen in Eu-152 spectra and is illustrated in Figure 6.1 where a simulated 122keV gamma-ray produces a Compton

edge roughly in the same place as a 40keV photo-peak. Because the Compton edge looks remarkably like a photo-peak, isotope identification systems can have trouble distinguishing the two. This is exactly the case with deconvolution of energy loss

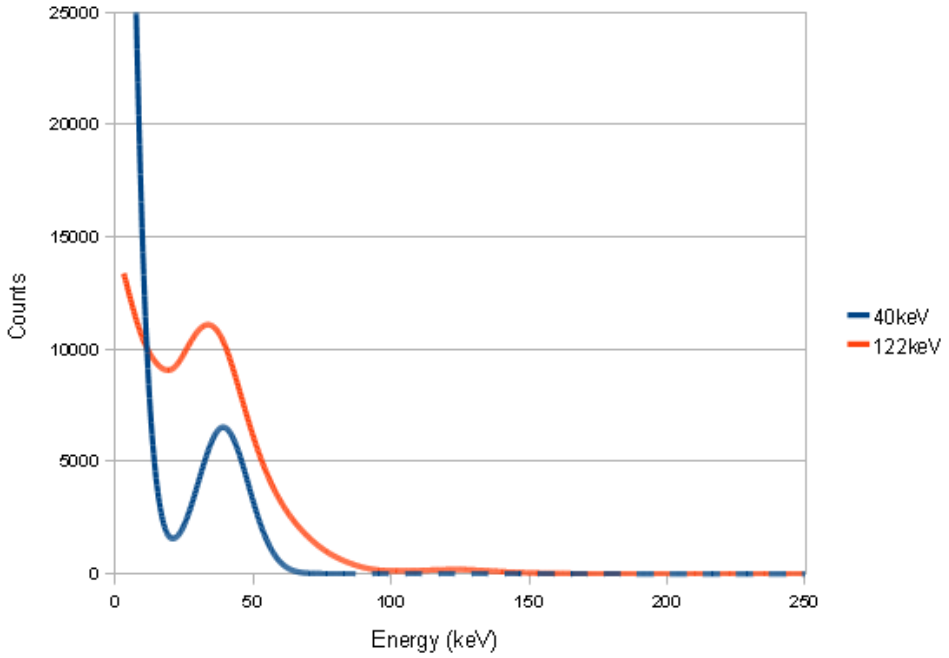

Figure 6.1: A Simulation showing a 40keV X-Ray photo-peak covered by a 122keV Gamma-ray Compton edge. This occurs in Eu-152 Spectra.

spectra. A 40keV gamma-ray or X-ray can produce a peak at around 120keV in the deconvolved spectrum as the software mistakes the 40keV photo-peak for a 120keV gamma-ray which would produce a Compton edge at 40keV. This Compton edge of course does not exist and therefore the peak present in the deconvolved spectrum is termed a "Phantom Peak" for quick reference to this phenomenon. The energy of a potential phantom peak can be calculated as the inverse Compton scatter of the photo-peak that would cause it. Phantom peaks can appear in the PVT spectrum at anywhere from 100keV to 150keV. This represents photo-peaks from around 25keV to 50keV. The 60keV photo-peak from Am-241 does not produce a phantom peak if the lower energy threshold of the detector is set low enough. Phantom peaks can also occur at slightly higher energies if a partial photo-peak is present. Setting the low energy threshold at 35keV for example will enable the higher energy part of a broadened 30keV photo-peak to exist in the spectrum and produce a phantom peak at various energies due to the software's in ability to predict accurately where this entry came from.

Many of the following spectra presented were taken before this information was deciphered and therefore phantom peaks appear in some of the initial spectra before the problem was addressed. Phantom peaks can be compensated for by adding their entries into the isotope library with a special tag alerting the operator that the peak produced does not really exist and to ignore it when trying to identify the isotope.

6.3 Spectral Deconvolution of 50cm V-Plank

Symetrica's propriety deconvolution software required the construction of a computer generated q-matrix as outlined in Chapter 5. This model was constructed for the small 50cm V-Plank using Geant4 Monte Carlo simulations. Once the model was constructed, the q-matrix was loaded into the software and deconvolution of the raw spectra was given as one of the resulting output files. For these measurements the 50cm V-Plank was operated at the same settings as described in Chapter 4 for the initial spectra. The photomultiplier tube voltage was set to 940V and a Na-22 spectrum was first taken as a reference for the calibration. Background spectra were also taken for the same duration of time that each spectrum was taken for. These background spectra were then subtracted before the deconvolution process. The deconvolution software settings were set to a linear resolution limit of 4% +/-8keV for identification of a spectral line.

6.3.1 Resulting Spectra

A variety of spectra were taken using the 50cm V-Plank and subsequently deconvolved. Initially the sources were each placed around 15cm above the centre of the detector for flood illumination and spectra taken for 60 seconds. The spectra are shown in the following figures. The first spectrum is of Na-22 shown in Figure 6.2. This figure shows excellent clarity, the two Compton edges have been deconvolved into what look like two photo-peaks at the correct spectral energies. The deconvolution process has also added some counts towards the lower end of the spectrum, these are assumed to be from a small amount of back scatter. Figure 6.3 shows a deconvolved Cs-137 spectrum. The spectrum shows a clear peak at the correct energy of 662keV. A small number of counts are again shown at the lower end of the spectrum, these counts are

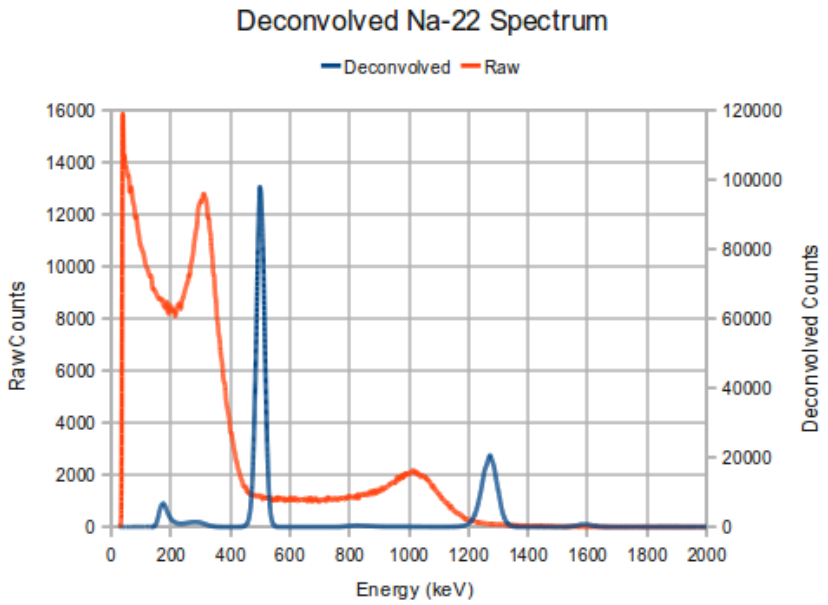

Figure 6.2: A Deconvolved Na-22 Spectrum from the 50cm V-Plank

consistent with back scatter as the energy is too high for the 32keV X-ray. Figure

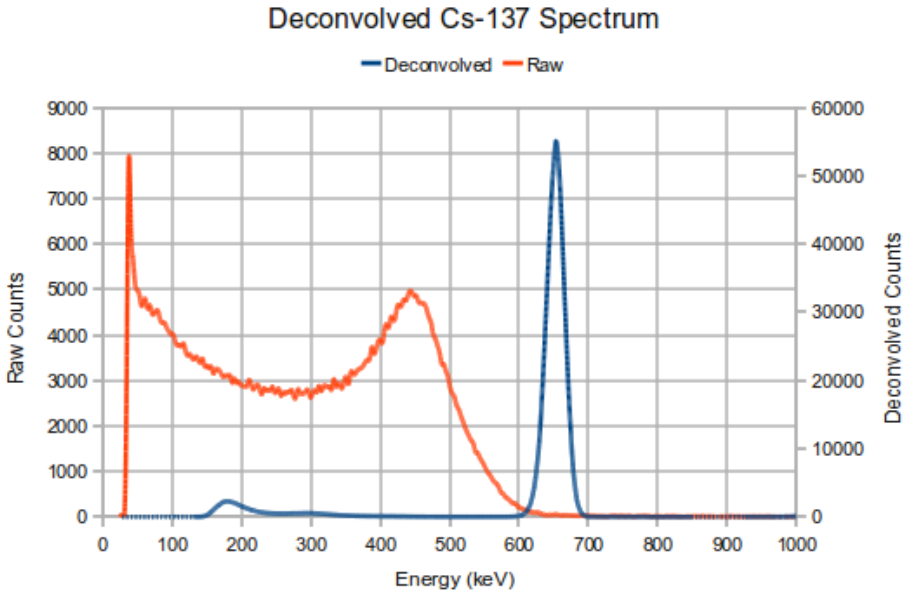

Figure 6.3: A Deconvolved Cs-137 Spectrum from the 50cm V-Plank

6.4 shows a deconvolved Am-241 spectrum. This spectrum is the first example of a phantom peak. In this case the photo-peak produced by the 60keV gamma-ray is mistaken as a Compton edge from a much higher energy. This occurred because the low energy threshold was set too high and can be avoided by fine tuning this setting and some of the deconvolution and calibration settings as evident in the next section, where the Am-241 spectrum is successfully deconvolved on the 1m V-Plank using

updated software. Figure 6.5 shows a deconvolved Ba-133 spectrum. This spectrum

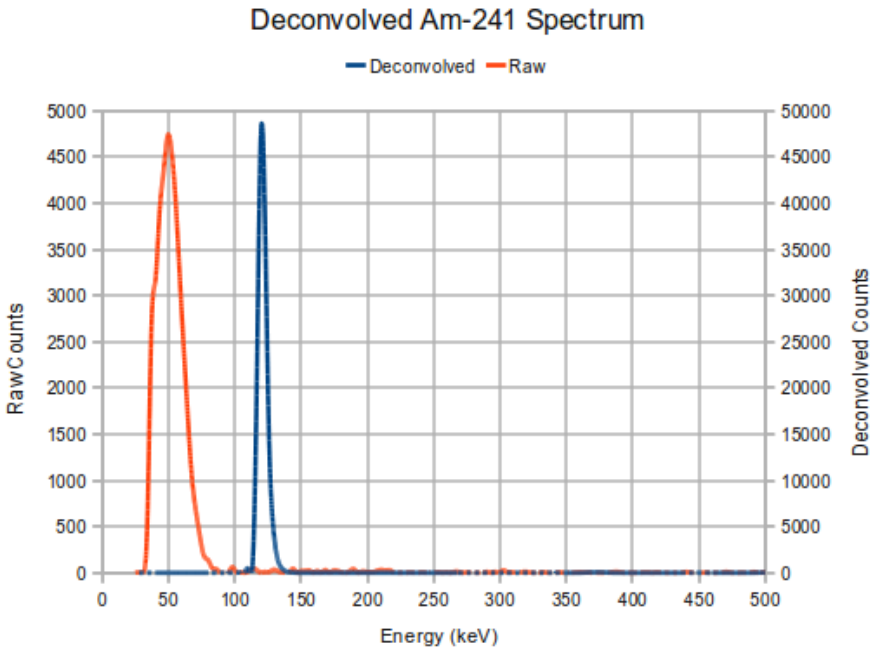

Figure 6.4: A Deconvolved Am-241 Spectrum from the 50cm V-Plank

shows only two peaks present for Barium-133 as the others were unresolvable given the PVT's limited resolution. The 356keV peak is easily identifiable. The 80keV peak however is not, and appears as a Compton edge at around 20keV, which therefore will not show up in the spectrum as the deconvolution lower limit was set to 35keV. There is however a strong collection of 31keV X-rays which would produce a photo-peak. These X-rays would produce a phantom peak at 105keV. Although 31keV is slightly below the threshold, the uppermost edge of the photo-peak would still be present in the spectrum and therefore causes the phantom peak to appear. Figure 6.6 shows a deconvolved Co-57 spectrum. Along with Am-241, Co-57 proved one of the more difficult isotopes to successfully deconvolve. Co-57 produces only one gamma-ray resolvable by PVT which is detected at 122keV. The Compton edge for this energy occurs at around 40keV and can therefore become confused with a photo-peak at a similar energy. As was the case with Am-241, a finely tuned range of settings ensures that this spectrum deconvolves properly each time. Figure 6.7 shows a deconvolved Co-60 spectrum. This spectrum is perhaps one of the most impressive showing two very clear, well defined peaks at the correct spectral energy. Some back scatter can be seen at the lower end of the energy scale. Figure 6.8 shows a deconvolved Ra-226 spectrum. The Radium-226 spectrum could sometimes prove a relatively difficult

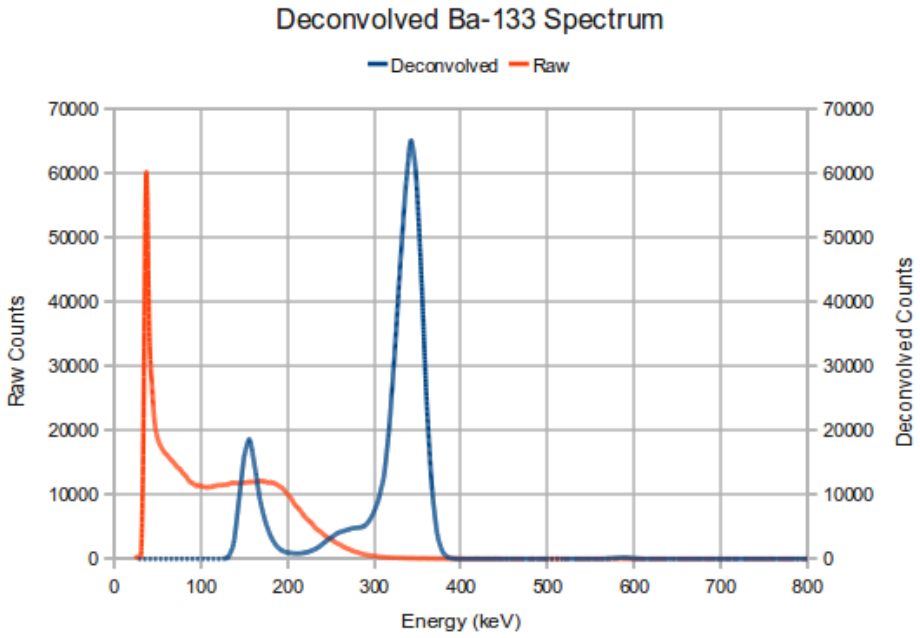

Figure 6.5: A Deconvolved Ba-133 Spectrum from the 50cm V-Plank

spectrum to identify. This is not due to the issues experienced with low energy spectra however, but more due to the sheer complexity of the spectrum. A number of closely spaced spectral lines mean that only some of the gamma-rays can be identified, though only a small number are required for positive identification. The final spectrum measured was Eu-152, shown in Figure 6.9. This is a well defined spectrum, showing nearly all the same peaks as a raw NaI(Tl) detector shows. The only problem with the Eu-152 spectrum is that the 122keV Compton edge appears exactly in the same channel as the 40keV photo-peak. In this rare case, the phantom peak induced by the 40keV X-ray is in the location of an existent gamma-ray Compton edge. This can cause confusion in the deconvolution process which often places all the counts in either the 40keV bin or the 122keV bin, but rarely in both, although this is not a problem for identifying Eu-152. Some success has been made by fine tuning the software to place at least some of the counts in both spectral lines, though the correct intensity for each is very difficult to achieve.

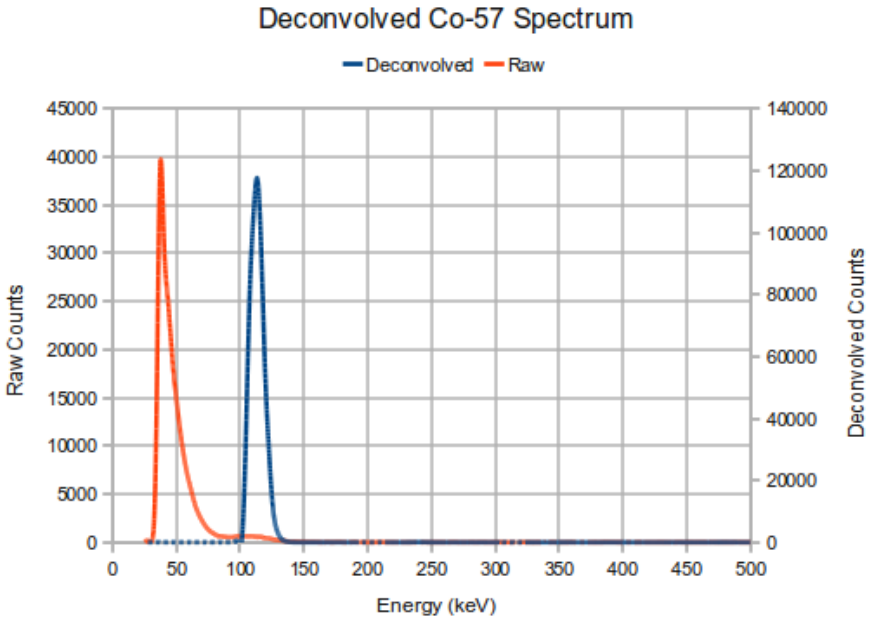

Figure 6.6: A Deconvolved Co-57 Spectrum from the 50cm V-Plank

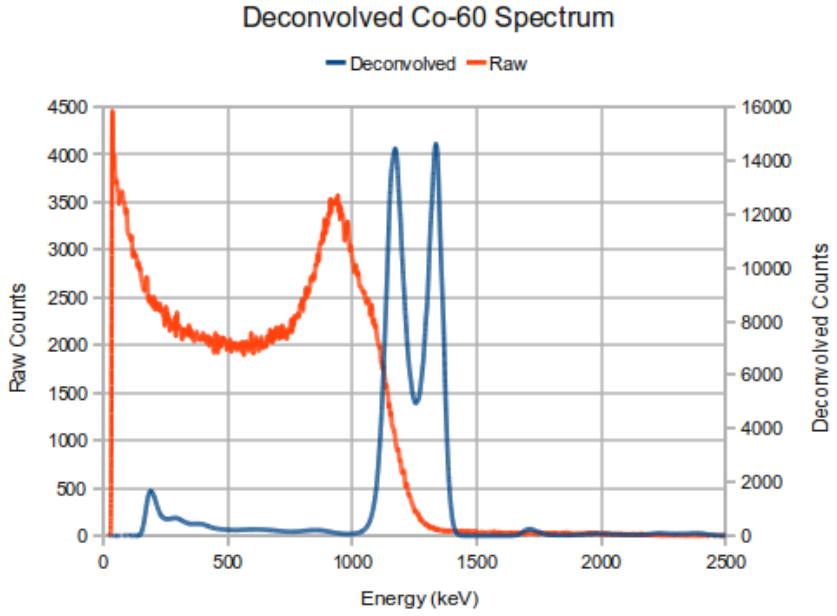

Figure 6.7: A Deconvolved Co-60 Spectrum from the 50cm V-Plank

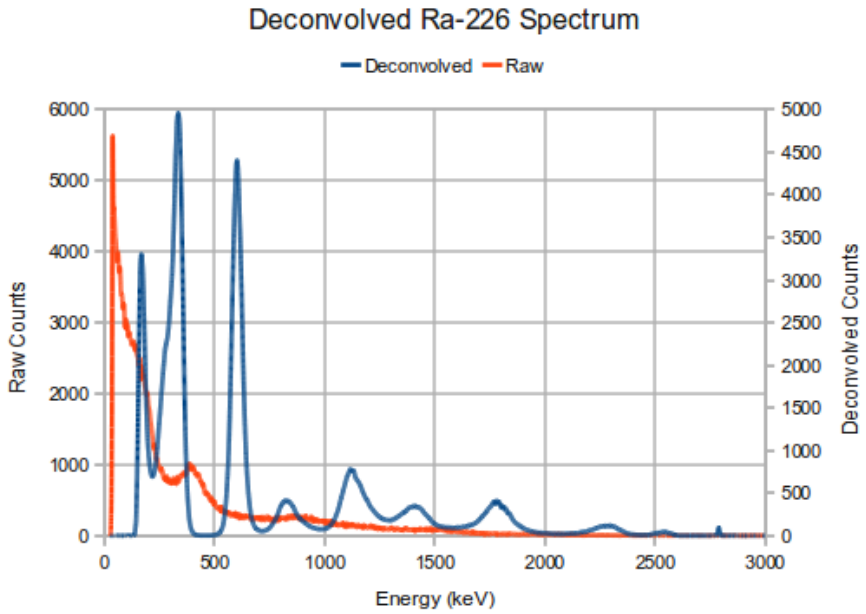

Figure 6.8: A Deconvolved Ra-226 Spectrum from the 50cm V-Plank

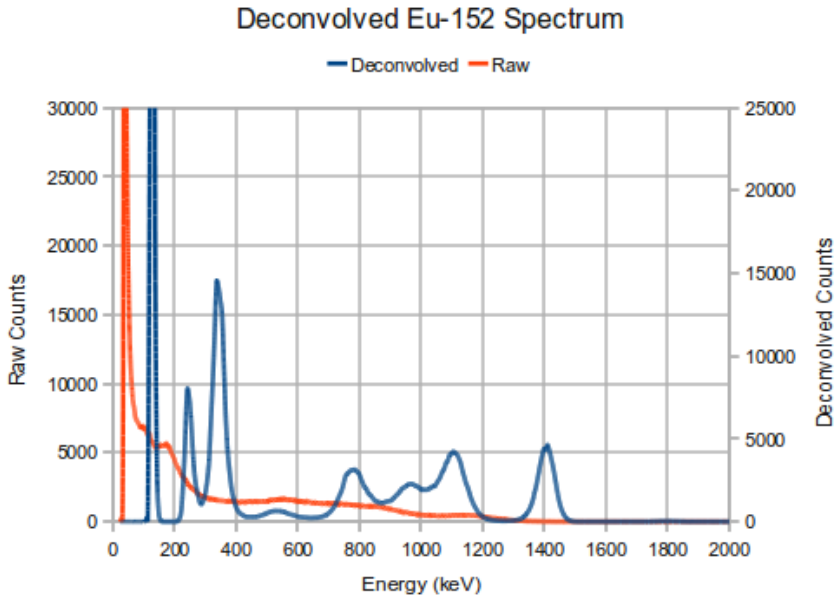

Figure 6.9: A Deconvolved Eu-152 Spectrum from the 50cm V-Plank

6.3.2 Refined Energy Calibration with Plastic Scintillators

The calibration of the detector can be fine tuned by deconvolving a spectrum and using the resulting peaks in the deconvolved spectrum to shift the gain of the system until these peaks match their correct energies. Whilst this procedure is not recommended for general use and was therefore not incorporated in the final software developed for PVT based detectors, it can be useful for determining why a particular calibration routine might not be working correctly during development. This technique was temporarily employed to slightly refine the calibration technique, as matching a Geant4 simulated spectrum to a measured one can produced a slight offset if the emphasis is not placed on the negative gradient of the Compton edge itself and not the preceding Compton continuum. This offset can be responsible for misidentifying isotopes, especially at lower energies where the calibration is most sensitive.

6.4 Large Area Detectors

For the two large area detectors similar procedures were used to deconvolve various spectra as were used with the 50cm V-Plank. Given the large detectors' slightly lower light collection, different q-matrices were used for each detector accordingly. Both of these detectors were placed horizontally above the ground at a height of around 60cm, suspended between two stands. Previous measurements have shown that given the coverage area of these detectors, they are both susceptible to a high amount of back scatter. The sources were placed around 40cm above the centre of each detector for the measurements. A weak Th-232 source became available at the time of testing the large detectors and spectra for this source are provided in the following sections. This source was in the form of thoriated welding rods containing 2% thorium oxide and required around 300 seconds of acquisition time to generate a useful spectrum given their relatively low activity.

6.4.1 2m X-Plank

The 2m X-Plank has the slightly lower clarity of the two larger detectors with 3% variance in the light collection efficiency. It also produces a lower number of counts for any given acquisition time as its volume is more spread out. The first spectrum

displayed is Na-22 shown in Figure 6.10. This figure shows good clarity of the Compton edges and subsequent peaks from deconvolution. Some back scatter can be seen at lower energies, this is a common occurrence with large area detectors in this configuration. Cs-137 is the next spectrum shown in Figure 6.11. The Cs-137 spectrum again

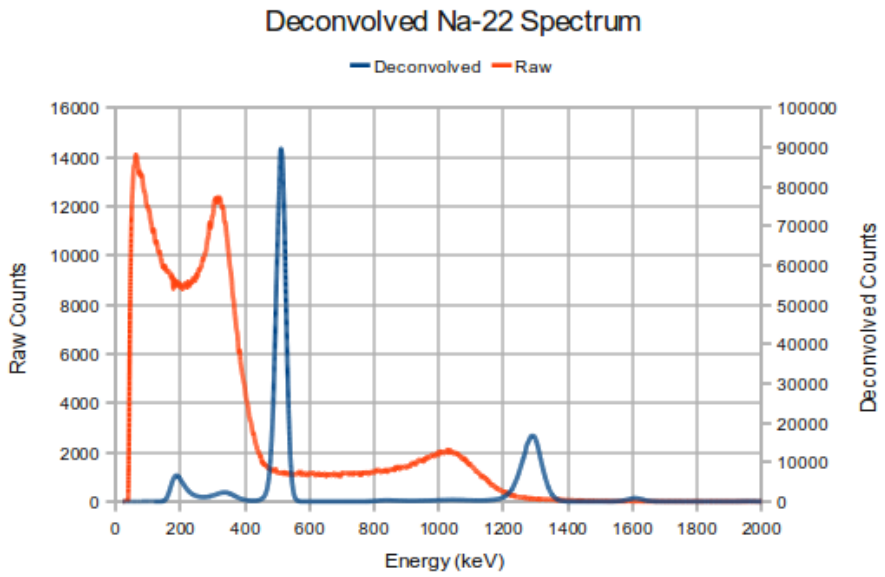

Figure 6.10: A Deconvolved Na-22 Spectrum from the 2m X-Plank

shows a good quality peak from the deconvolution. This spectrum however shows two peaks from the back scatter. This could simply be how the deconvolution algorithm is interpreting the back scatter, or the 32keV X-ray could be producing a partial photo-peak at low energies which is being misinterpreted as a higher energy Compton edge. The low level cut off energy for this spectrum is 35keV, so it is possible that part of a 32keV photo-peak is producing a shifted phantom peak in the deconvolved spectrum. Figure 6.12 shows a deconvolved Am-241 spectrum. In this spectrum the 60keV photo-peak is easily observable and the deconvolution algorithm has no problem interpreting its correct energy. A high intensity peak is created at 60keV giving a positive identification for Am-241. The ability to identify this spectrum has come from tweaking the calibration, lowering the low energy threshold and lowering the minimum energy for deconvolution. This results in a higher dead time but the price of this is insignificant in relation to positively identifying low energy dominated spectra. Note that some counts are still placed in a phantom peak, but this is much lower than observed in the 50cm V-Plank and is insignificant when compared to the intensity of the photo-peak in the spectrum. The Ba-133 spectrum shown in Figure 6.13 is similar

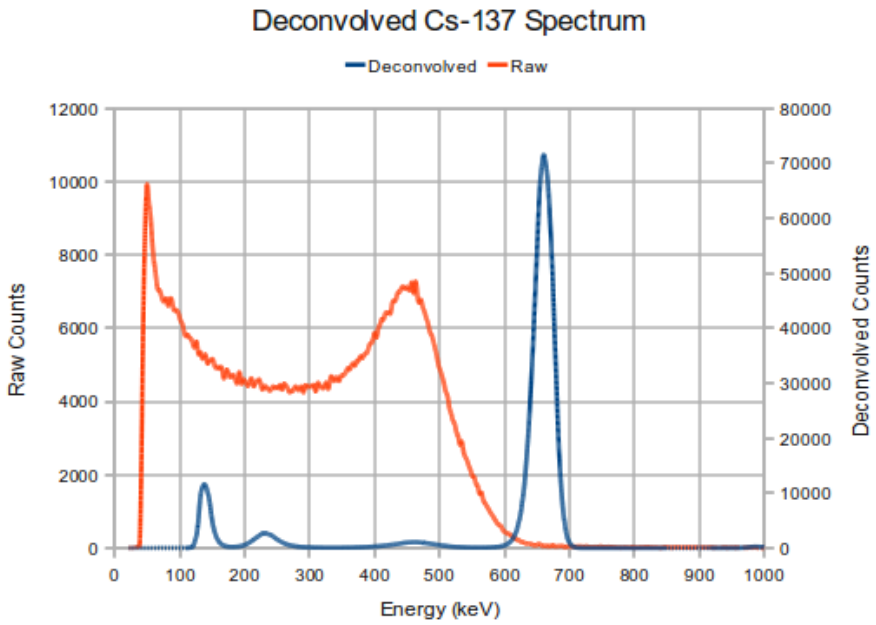

Figure 6.11: A Deconvolved Cs-137 Spectrum from the 2m X-Plank

to the 50cm V-Plank with the 356keV peak from the PVT library identifying correctly. The 31keV peak this time gets allocated to a phantom peak at around 120keV, which is more representative of the predicted confusion between a photo-peak and Compton edge. A deconvolved Co-57 spectrum is shown in Figure 6.14. This spectrum shows a good peak located at the correct energy of 120keV. The Co-60 spectrum in Figure 6.15 shows two clear deconvolved peaks both in the correct location. The clarity is slightly below that of the 50cm V-Plank, but easily good enough for a positive identification. Some back scatter from both incident energies is apparent at lower energies. The Ra-226 spectrum in Figure 6.16 shows a good match for 7 of the spectral lines, giving a positive identification. The quality is similar to that of the 50cm V-Plank. A deconvolved Eu-152 spectrum is shown in Figure 6.17. This figure is similar in quality to that of the 50cm V-Plank. Seven spectral lines are identified with the 40keV line missing due to combination with the 122keV induced Compton edge. The final spectrum shown for the 2m X-Plank is the Th-232 spectrum in Figure 6.18. The raw spectrum is of relatively low quality but eight peaks are identified in the deconvolved spectrum making a positive identification. In this spectrum the gain was not adjusted to cope for the high energy 2.6MeV line and its broad Compton edge. This accounts for the unrealistically sharp deconvolved peak found 70keV off target for this line. In subsequent spectra, the gain was reduced to allow for the full scope of the Compton

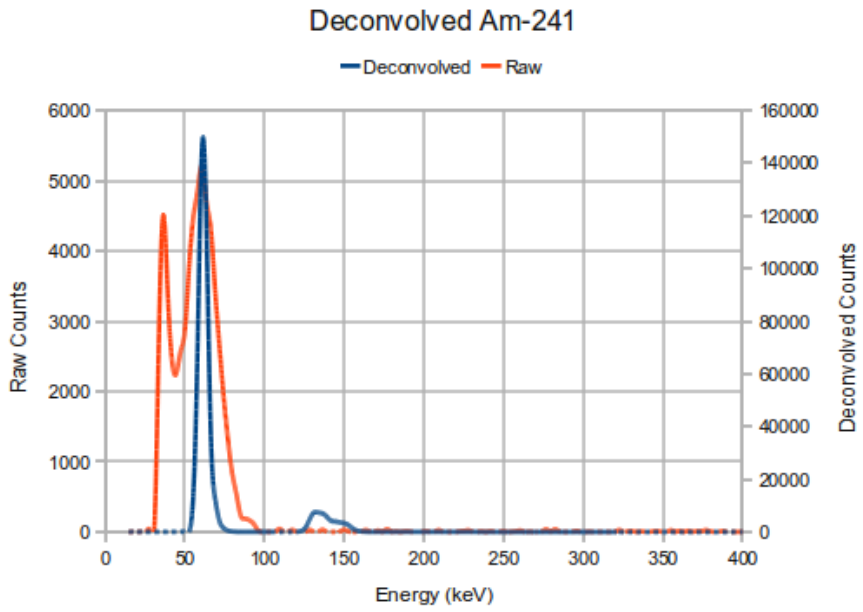

Figure 6.12: A Deconvolved Am-241 Spectrum from the 2m X-Plank

edge from this energy gamma-ray.

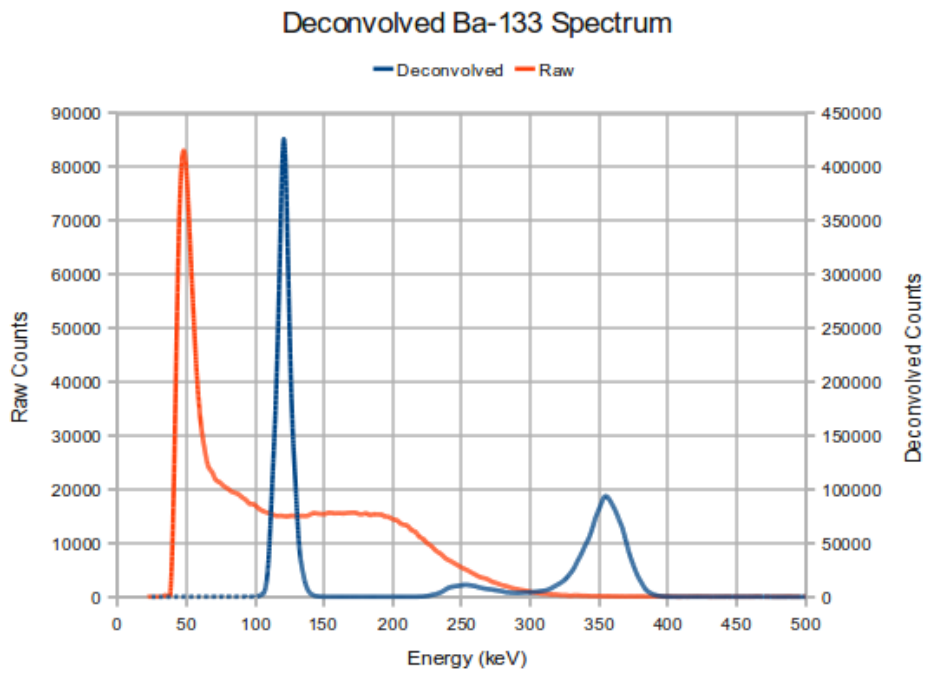

Figure 6.13: A Deconvolved Ba-133 Spectrum from the 2m X-Plank

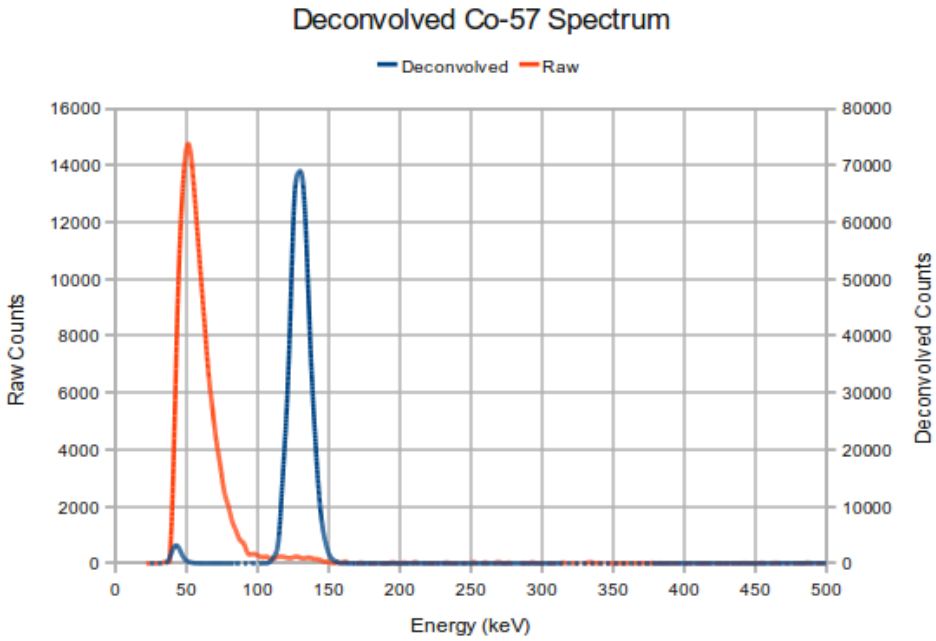

Figure 6.14: A Deconvolved Co-57 Spectrum from the 2m X-Plank

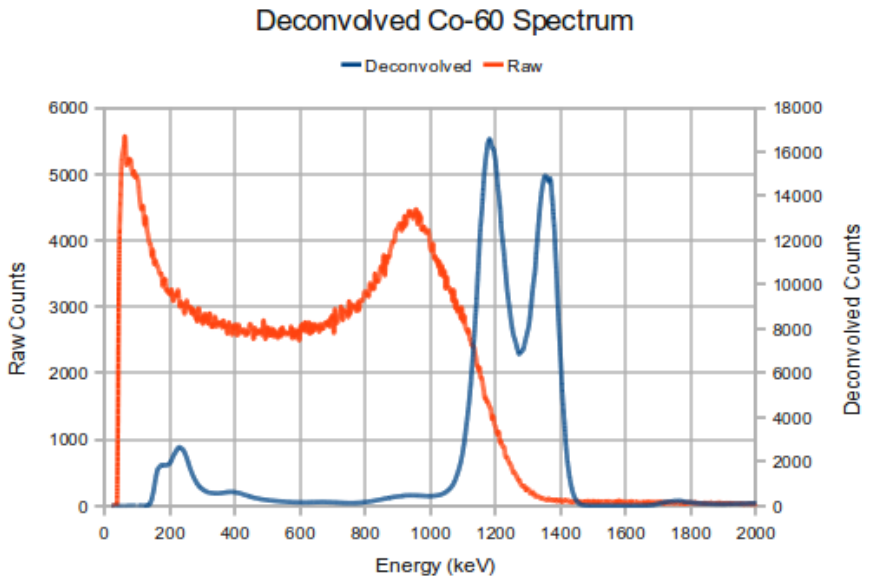

Figure 6.15: A Deconvolved Co-60 Spectrum from the 2m X-Plank

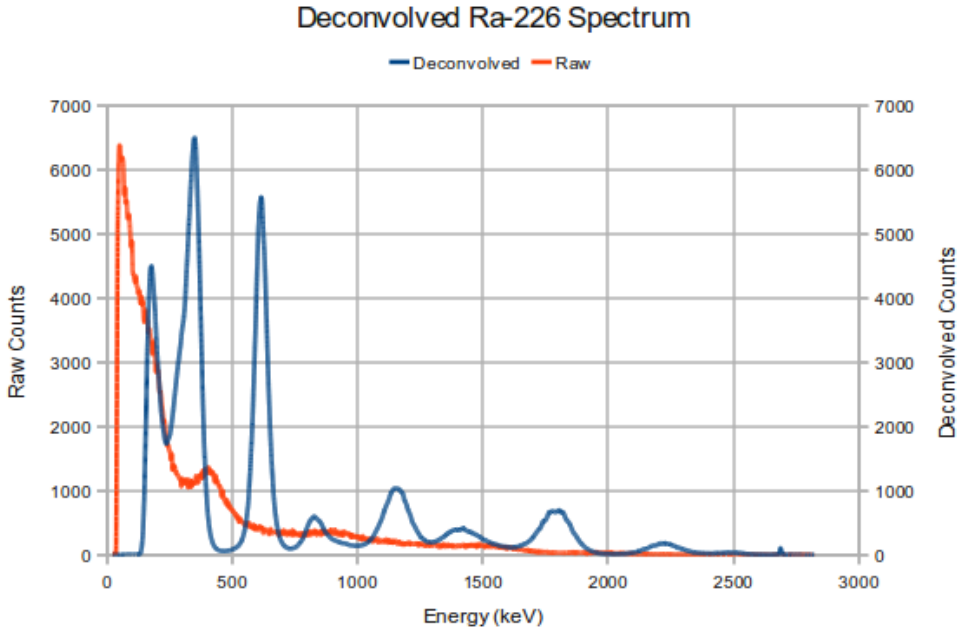

Figure 6.16: A Deconvolved Ra-226 Spectrum from the 2m X-Plank

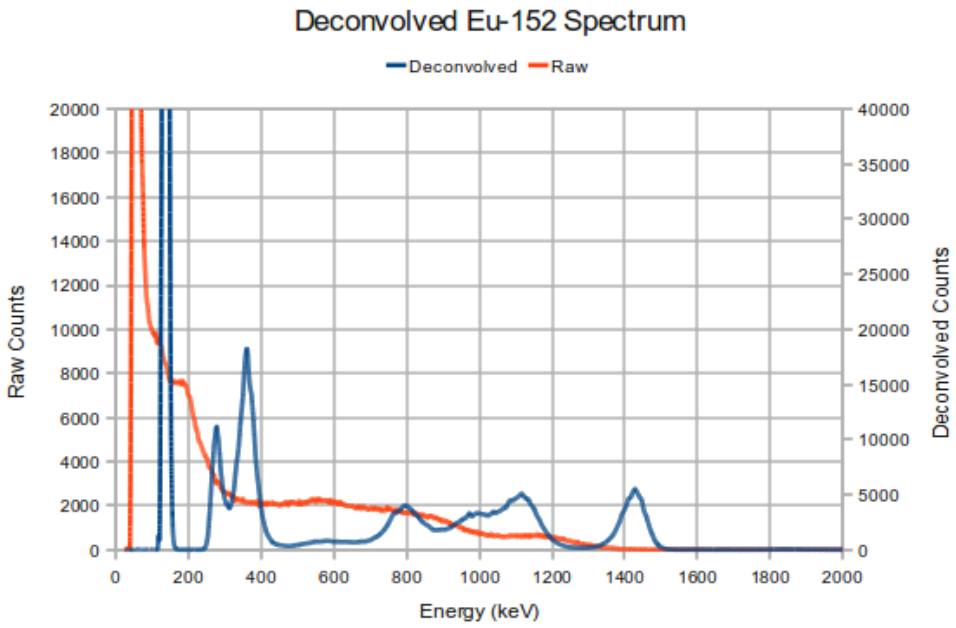

Figure 6.17: A Deconvolved Eu-152 Spectrum from the 2m X-Plank

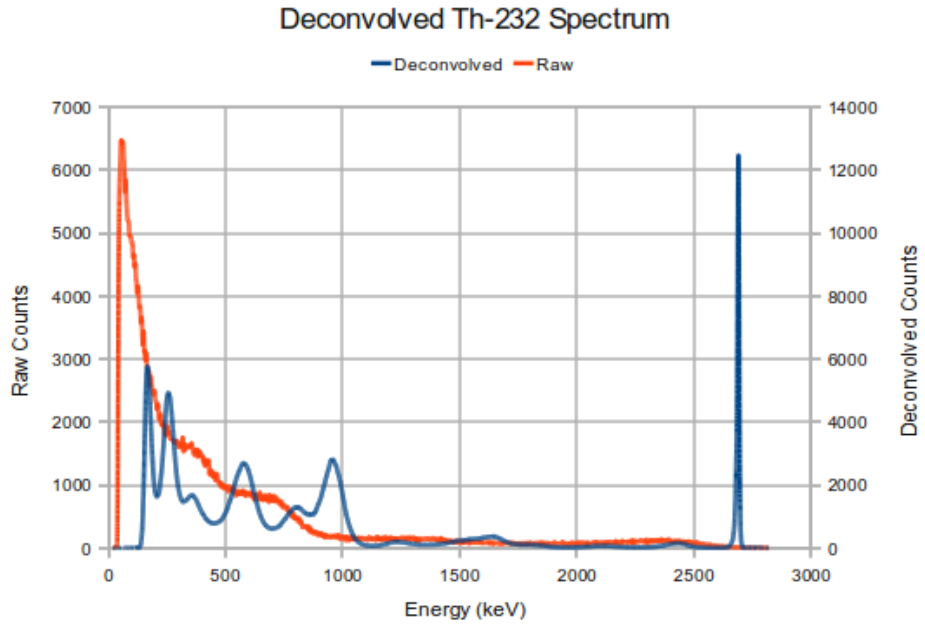

Figure 6.18: A Deconvolved Th-232 Spectrum from the 2m X-Plank

6.4.2 1m V-Plank

The 1m V-Plank produced some of the best quality spectra, partly due to its slightly better performance than the 2m X-Plank, but largely due to the software, which was further optimised when it came to testing this design. Each spectrum was produced by placing the source around 40cm above the detector. The detector was suspended horizontally around 60cm above the floor. Figure 6.19 shows the first spectrum, a deconvolved Na-22 spectrum. The figure shows excellent Compton edge clarity and therefore good deconvolved peaks at the correct locations. Some back scatter is present at low energies in this spectrum. The Cs-137 spectrum in Figure 6.20 is simi-

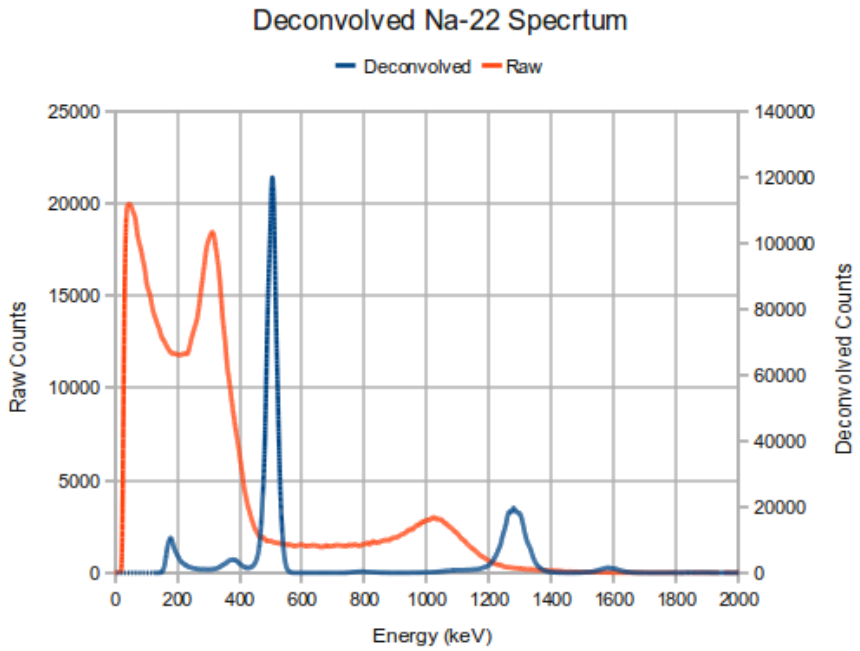

Figure 6.19: A Deconvolved Na-22 Spectrum from the 1m V-Plank

lar to the Na-22 spectrum in that it too has excellent clarity in both the raw Compton edge and deconvolved peak. The Am-241 spectrum shown in Figure 6.21 shows a well defined raw photo-peak and subsequent deconvolved peak at the correct location. This time the deconvolution process has assigned counts to a more localised region at higher energies. This energy again represents what would be a higher energy incident gamma-ray scattering to produce a Compton edge at 60keV. The Ba-133 spectrum shown in Figure 6.22 again shows trouble with the 31keV X-ray. This time the deconvolution threshold is lowered, allowing the majority of the photo-peak in the spectrum. The line is interpreted closer to a 105keV induced Compton edge at around

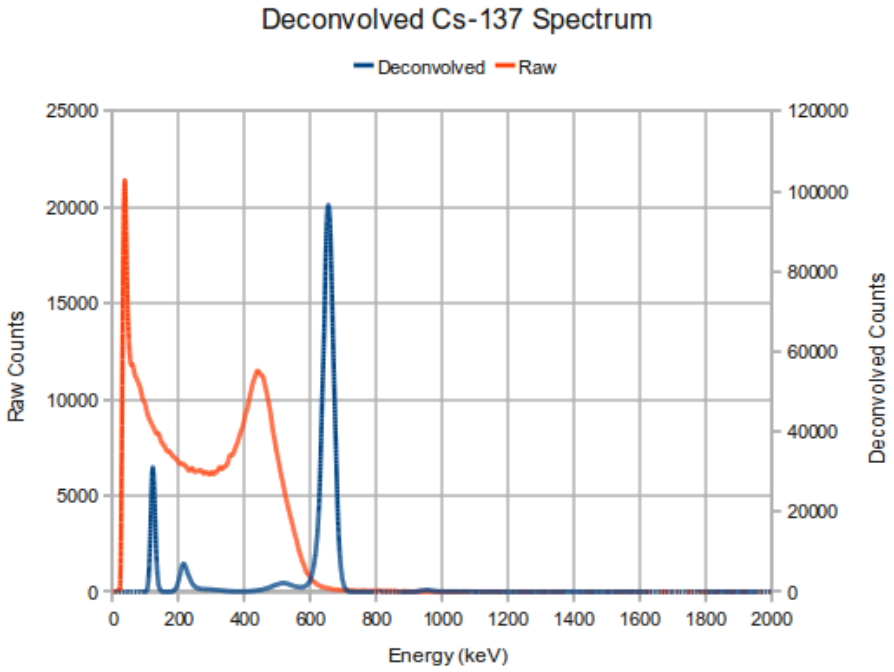

Figure 6.20: A Deconvolved Cs-137 Spectrum from the 1m V-Plank

110keV, which confirms the theory that this line is in fact a 31keV photo-peak inducing a 105keV phantom peak in the spectrum. The 356keV peak however is identified without a problem. The Co-57 spectrum shown in Figure 6.23 is similar to the other Co-57 spectra, and causes no problems in identification. Figure 6.24 shows the Co-60 spectrum, which is again lower in quality than the 50cm V-plank but still easily identifiable. Some back scatter from both gamma-rays can be seen at lower energies. Radium-226 is shown in Figure 6.25. Some of these lines are slightly out of the range of the identification algorithm's limits, meaning that only 6 of the shown peaks are registered. This is still more than enough to identify Ra-226. The Eu-152 spectrum in Figure 6.26 finally shows counts in all eight of the resolvable peaks. Some counts are placed in the 40keV energy bin from the 122keV bin. All lines are within the limits of their location variation and contribute to a positive identification. Figure 6.27 is the final spectrum showing Thorium-232. This spectrum shows a much better 2615keV peak than the 2m X-Plank as the gain is reduced to account for this energy. Seven peaks are used in total to positively identify this isotope.

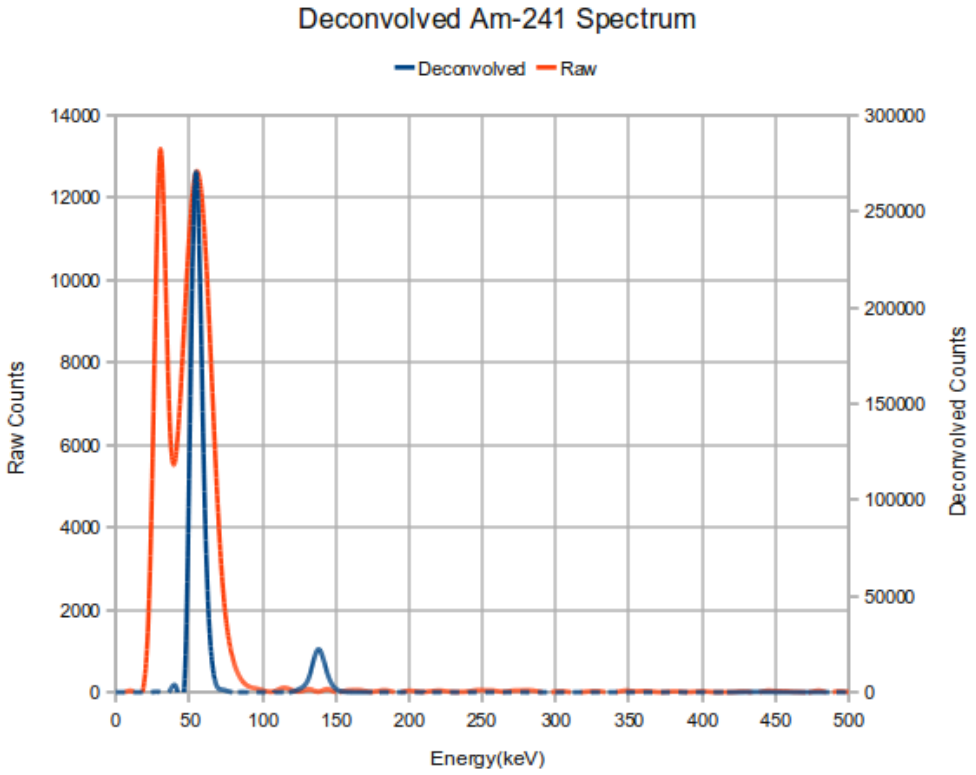

Figure 6.21: A Deconvolved Am-241 Spectrum from the 1m V-Plank

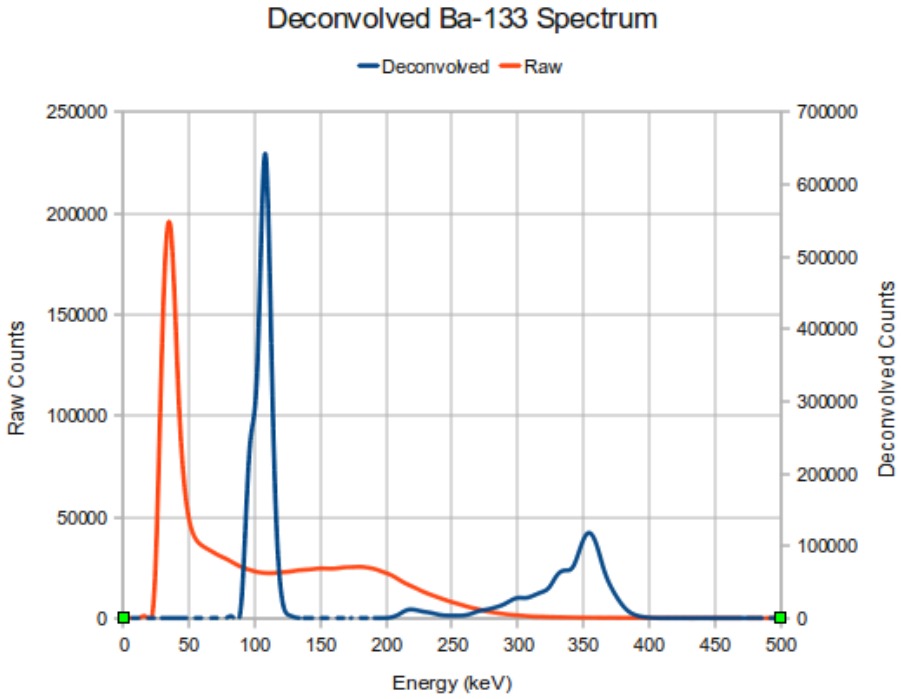

Figure 6.22: A Deconvolved Ba-133 Spectrum from the 1m V-Plank

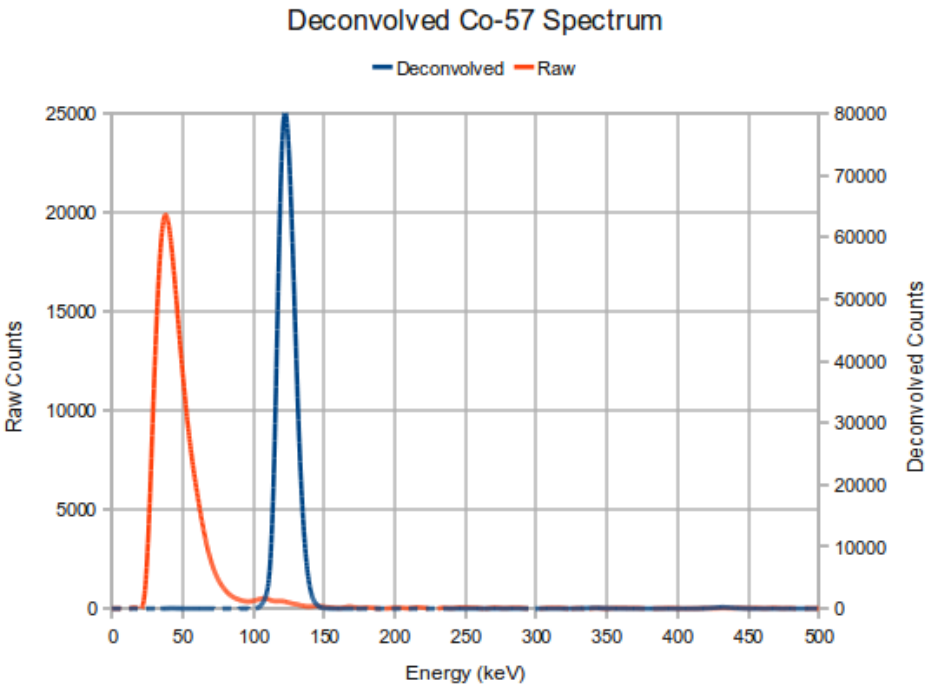

Figure 6.23: A Deconvolved Co-57 Spectrum from the 1m V-Plank

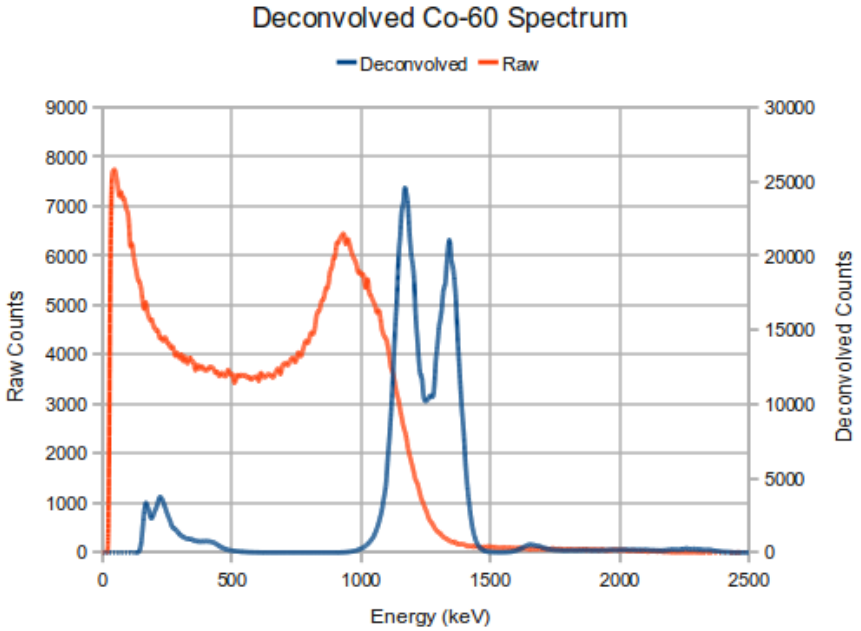

Figure 6.24: A Deconvolved Co-60 Spectrum from the 1m V-Plank

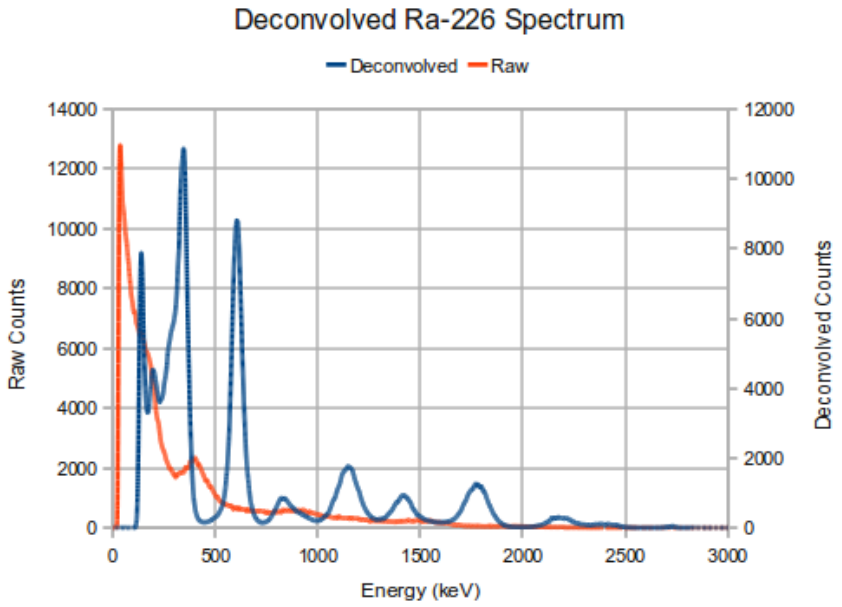

Figure 6.25: A Deconvolved Ra-226 Spectrum from the 1m V-Plank

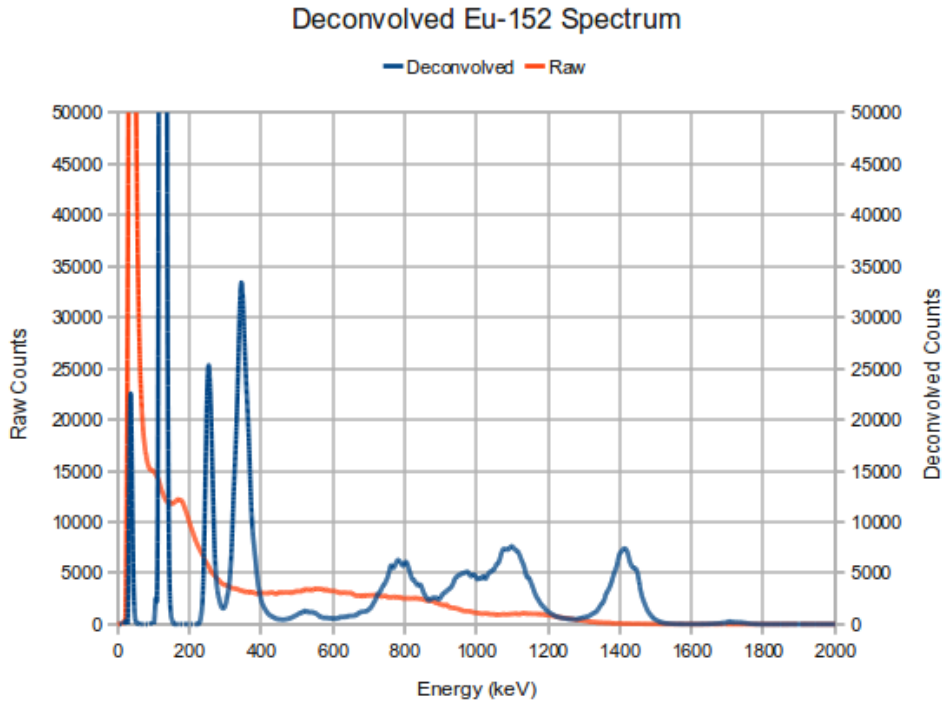

Figure 6.26: A Deconvolved Eu-152 Spectrum from the 1m V-Plank

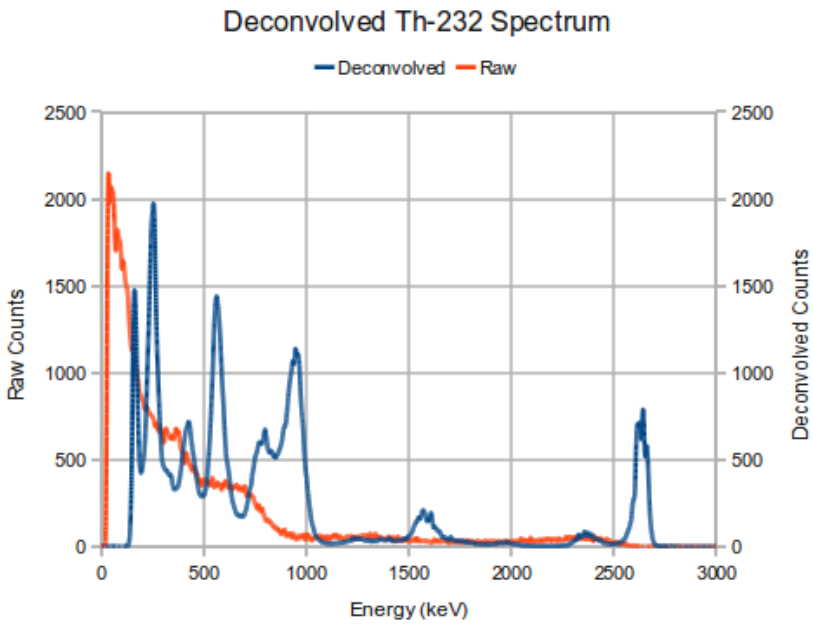

Figure 6.27: A Deconvolved Th-232 Spectrum from the 1m V-Plank

6.5 Deconvolved Resolution

To evaluate the deconvolved performance of each detector design, the deconvolved resolution of each detector was determined at the 662keV. To measure the FWHM, a Gaussian function was generated with mean value equal to that of the location of each of the 662keV deconvolved peak. The standard deviation in the mean was then altered manually until the difference between the data and the model was minimal. Figure 6.28 shows the Gaussian fitting process to a 662keV induced Compton edge from the 50cm V-Plank. Table 6.2 shows the results of all the detector designs. The

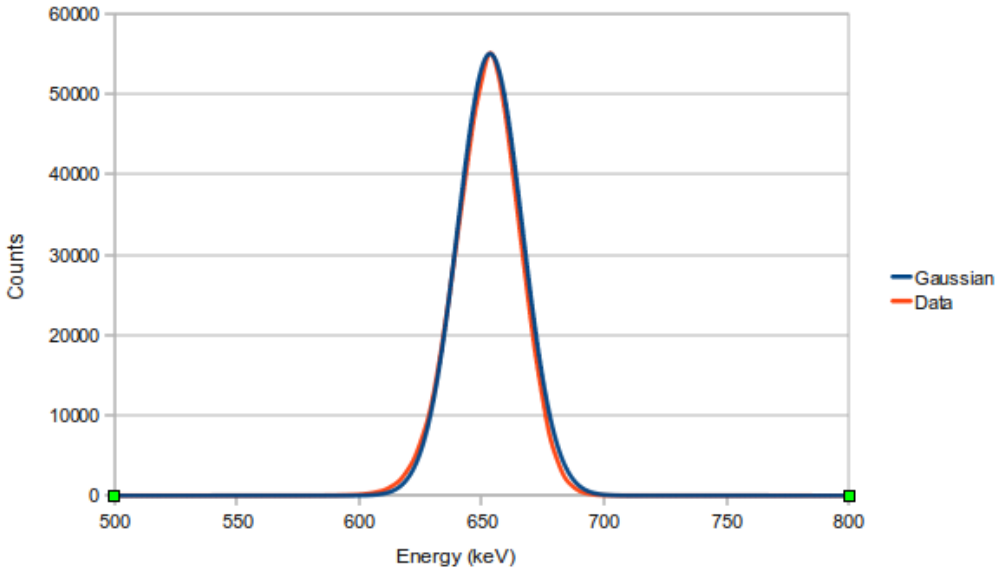

Figure 6.28: The Gaussian fitting process of a deconvolved 662keV peak from the 50cm V-Plank.

Table 6.2: Deconvolved FWHM of each detector design at 662keV

Detector	Deconvolved FWHM @ 662keV
2m X-Plank	6 +/- 0.5%
1m V-Plank	6 +/- 0.5%
50cm V-Plank	5 +/- 0.5%

50cm V-Plank shows a slight increase in resolution over the two larger PVT designs, this is expected due to its better light collection efficiency. The two larger designs show little difference in performance after deconvolution at 662keV. The 2m X-Plank was expected to be slightly worse in resolution than the other two designs due to its increased variation in the light collection.

6.6 System Testing

To investigate the quality of the spectra produced by these new PVT designs, an experiment was designed to observe how the number of counts in a spectrum affects the performance of the identification software and the quality of the acquired spectra. The 50cm V-Plank was used for this experiment as it had the best resolution of the three detectors. The investigation gives insight into the minimum number of counts required in an energy loss spectrum to correctly identify the corresponding radioactive isotope. As the radioactive decay process is a series of randomly occurring events, the spectra are subject to a statistical error equal to the square root of the total number of counts. As the number of counts per spectrum is increased, the statistical error decreases and the quality of the spectra increase.

At a low total number of counts per spectrum the Compton edge locations in the spectrum can vary significantly and the spectral quality is often poor. The Compton edges become increasingly resolved and appear more reliably in one location as the number of counts is increased. This is directly translated into the quality of the deconvolved spectra. For this reason a higher number of counts per spectrum lead to an increased chance of correct identification. The standard deviation in the deconvolved peak locations for a specific isotope can be used as an indicator of the ability of the isotope identification software to assign an appropriate incident gamma-ray energy for that isotope. The isotope identification software was designed by Symetrica to include a confidence rating for each identification, giving an indication of how certain the software is that the isotope is present. This rating was used to determine a correct identification. The confidence function can list many possible isotopes as candidates for identification, only the top of the confidence list was considered to be the correct

isotope.

The experiment composed of taking numerous sets of 25 spectra from both complex and simple isotopes. For the simple spectra, the isotope Sodium-22 with 2 clearly identifiable Compton edges was chosen. For the more complex spectra, Europium-152 was chosen. Each set of spectra had an assigned acquisition time starting from 64 seconds for Eu-152 and 32 seconds for Na-22 and halving in a binary fashion until the time reached 0.5 seconds. The location of the test source remained constant at a distance of 50cm above the centre of the detector. The number of counts in each spectrum therefore halved for each time acquisition, starting from 174,000 counts and finishing at 1400 counts per spectrum for Eu-152 and 124,000 to 2000 counts for Na-22. This gave 200 spectra for Eu-152 and 175 spectra for Na-22; each set corresponding to a number of counts per spectrum. The spectra were acquired using the 50cm V-Plank connected to an Ortec digiBASE. The digiBASE was then attached to a PC running Maestro-32 multi channel analyser emulation software. The Maestro-32 job function was used to automatically acquire spectra which were then in turn manually exported into a text format and processed with Symetrica's deconvolution software. The processed spectra were individually analysed manually to determine the locations of the resulting Compton edges.

6.6.1 Na-22 Results

350 spectral lines were analysed in total for Na-22. Figure 6.29 shows the standard deviation in the location of the spectral lines with respect to the number of counts in the spectrum. The standard deviation in both of the spectral line locations starts relatively high at 10.70 for the 1275keV line and 5.39 for the 511keV line. Both values decrease rapidly with an increase in the number counts in each spectrum. At just under 20,000 counts the decrease becomes more gradual. At 124,000 counts the standard deviation for the 511keV edge reaches zero and the standard deviation for the 1275keV line reaches 1.55. However, the mean locations for the spectral lines at this point are 499keV and 1257keV respectively. This shows that the calibration was slightly inaccurate and is an important factor in correct spectral line identification, only becoming apparent at a relatively high number of counts per spectrum. A

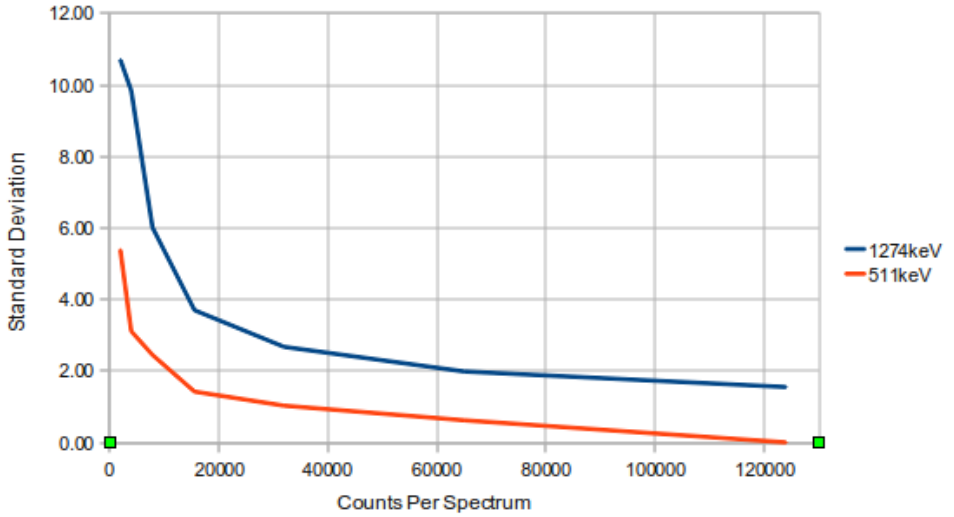

Figure 6.29: The standard deviation in the mean of the deconvolved peak locations for Na-22 as a function of the number of counts in each spectrum.

slight increase in the magnitude of the calibration equation would enable both edges to appear at their correct locations. The accuracy of the calibration equation used can be improved by using a longer calibration acquisition time.

Na-22 spectra are readily identifiable using the 50cm V-Plank, with only 4 misidentified spectral lines throughout the whole experiment. For 2000 and 4000 counts per spectrum there were 3 spectral lines identified but not assigned to Na-22 and 1 spectral line that was present but not found by the peak search algorithm due to poor resolution. Na-22 was correctly identified 96% of the time even at the lowest number of counts. At 7900 counts and above, all spectral lines were identified correctly and 100% correct isotope identification was reached for these trials. Figure 6.30 shows a graph of the percentage of correct isotope identifications as a function of the number of counts in each spectrum. The increase in the performance of the identification of Na-22 with respect to Eu-152 can be attributed to 2 main factors. The first is that the number of counts in each spectrum is allocated to only 2 Compton edges instead of 7 and therefore has a higher number of counts in each spectral line after processing. The second factor is that the two spectral lines are located at a significant distance from each other which prevents them from interfering. The quality of the spectra in terms of the standard deviation of the location of the spectral lines are good at a minimum of 7900 counts. The identification process reaches an optimal level at 7900 counts.

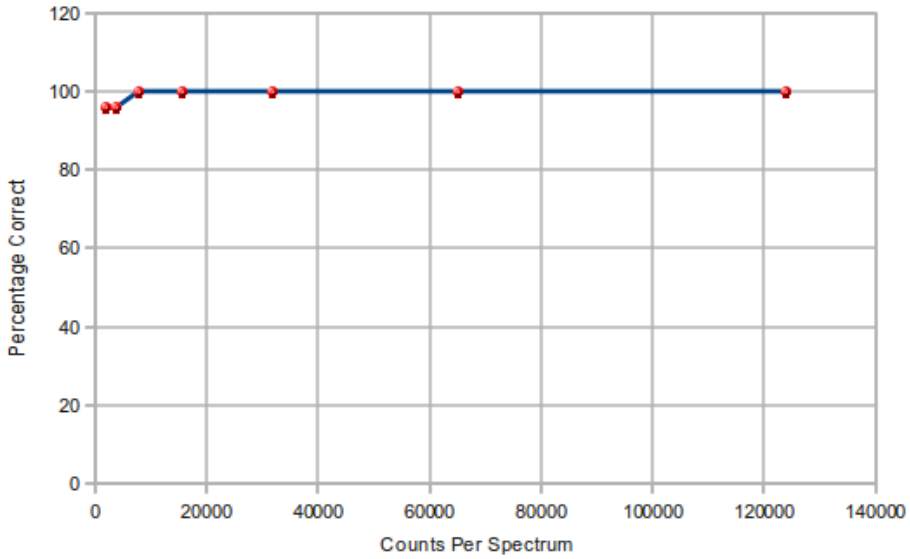

Figure 6.30: The percentage of correct isotope identifications as a function of the number of counts in each Na-22 spectrum.

6.6.2 Eu-152 Results

A maximum of 7 spectral lines are typically resolvable using the V-Plank with deconvolution software. These spectral lines are present at the following energies: 122keV; 245keV; 344keV; 779keV; 964keV; 1100keV and 1408keV. The location of each of these spectral lines was recorded and the standard deviation in their locations were calculated for each data set. For this set of data, each spectral line was placed into an identification category to establish the major causes of a subsequent isotope misidentification. These categories were as follows:

- Correctly Identified: The spectral line was resolved, detected by the peak search algorithm and correctly assigned to Eu-152
- Found but not associated with Eu-152: The spectral line was resolved and found by the peak search algorithm but not attributed to Eu-152
- Found At Wrong Energy: The spectral line was found and associated with the correct isotope but at an energy so far removed from the actual energy that they were mistaken for the next peak in the spectrum.
- Present But Not Found: The spectral line was resolved to the human eye but not found by the peak search algorithm and hence not attributed to any isotope

- Not Present: The spectral line was unresolved.

Maestro-32 software job functions were used to acquire the spectra automatically for the given acquisition times. The job function was also programmed to strip each spectrum of a pre-recorded background radiation spectrum. Once the calibration was determined, the job function was used to apply the calibration to each spectrum and export the data into text format for deconvolution. The deconvolved data was then analysed manually; the spectral line locations and their standard deviation were calculated and each spectral line was assigned an identification category. A total of 1400 spectral lines were analysed for the Eu-152 tests. The standard deviations of the spectral line locations are shown in Figure 6.31. At 1400 and 2700 counts the standard

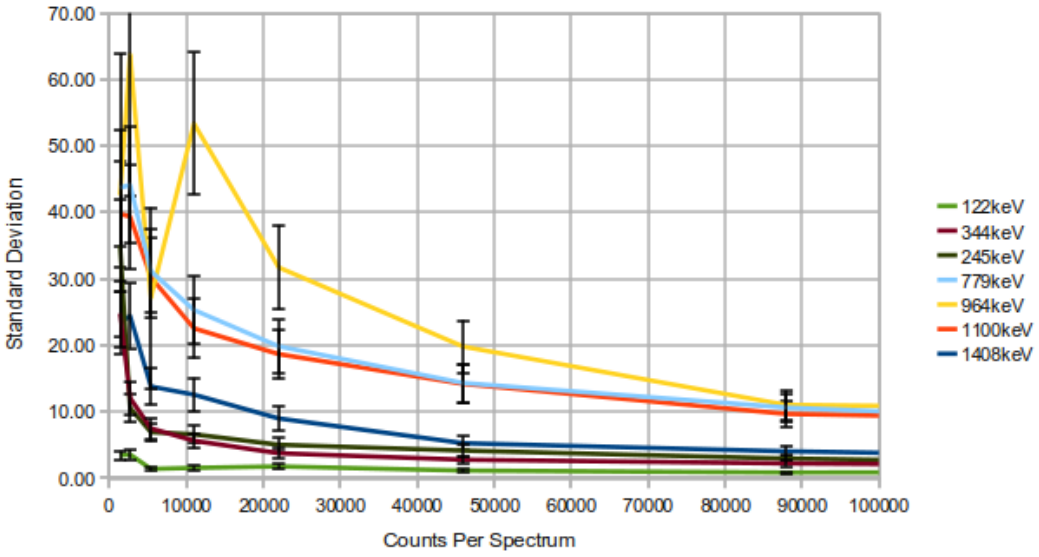

Figure 6.31: The standard deviation in the mean of the deconvolved peak locations for Eu-152 as a function of the number of counts in each of the raw spectra.

deviation is relatively high for all spectral lines in Eu-152, especially the 964keV line which had a maximum value of 63.75keV. More isolated spectral lines such as the 122keV line had a much lower standard deviation starting at a value of 3.44keV. As the number of counts increased the standard deviation dropped in all of the spectral lines and the fluctuation in the values decreased. At 20,000 counts and over, the extent of the decrease was significantly lessened. After this point the standard deviation fell very gradually as the counts increased. How the identification categories were affected with the number of counts in each spectrum is shown in Figure 6.32. The number of correct spectral line identifications increased at a similar rate as the stan-

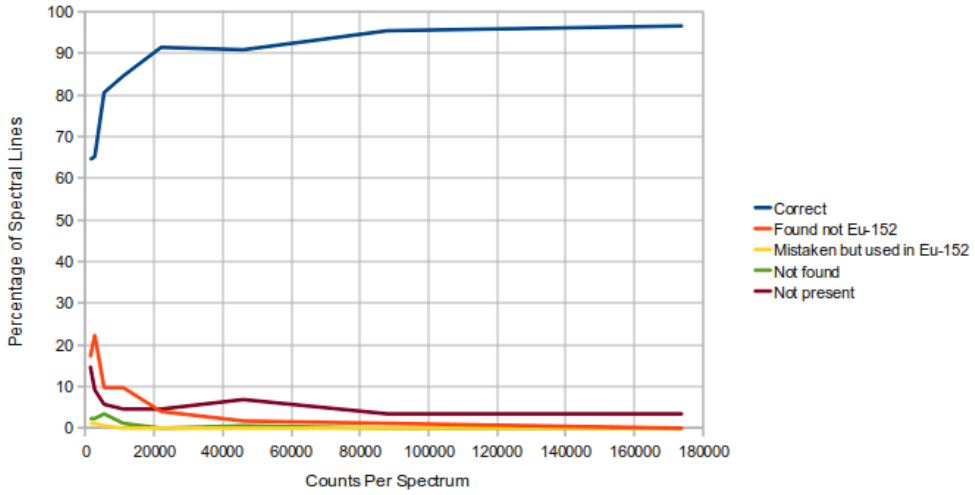

Figure 6.32: Percentage of spectral lines categorised into reasons for line misidentification as a function of the number of counts in each spectrum.

dard deviation decreased. At 1400 counts the number of correct identifications was around 65%, increasing to 91% at 20,000 counts and peaking at 96%. The number of correct line identifications never reached 100% because the 964keV line was not always resolved. The major cause of misidentification was the presence of spectral lines that were resolved and found by the peak search algorithm but not associated with Eu-152 because their locations were not within the limits defined for correct identification.

The minimum number of correct isotope identifications was 65% at 1400 counts. Correct isotope identification rose with the number of counts until 22,000 counts were reached, at this point the number of correct isotope identifications did not fall below 100% for these trials. At a low number of counts per spectrum the number of correctly identified spectra was in direct relation to the number of spectral lines correctly identified. Figure 6.33 shows a graph of the percentage of correct isotope identifications as a function of the number of counts in each spectrum. The quality of the spectra in terms of the standard deviation of the location of the spectral lines reaches an optimal level at a minimum of 22,000 counts. The quality of the identification process also reaches an optimal level at 22,000 counts, though there is possibility of improvement with adjustments to the identification software.

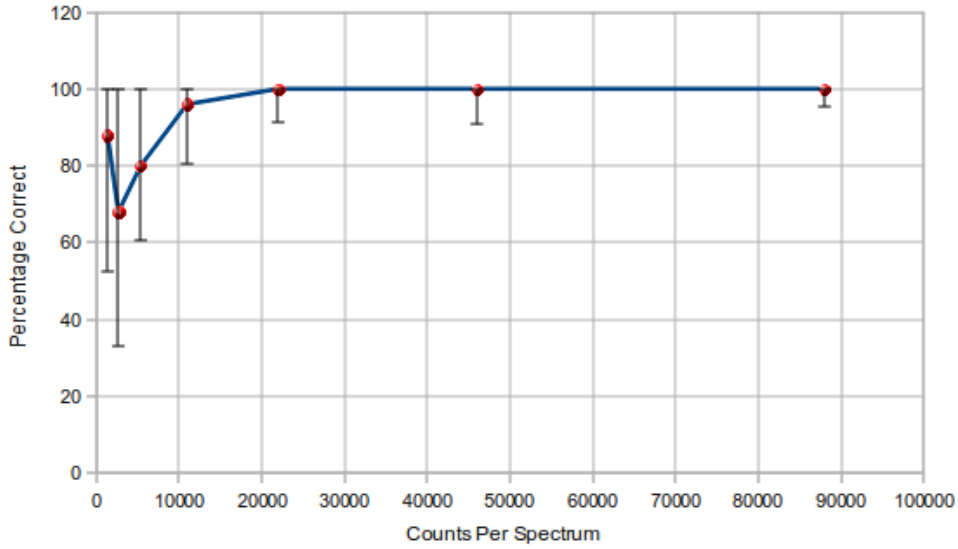

Figure 6.33: The percentage of correct isotope identifications as a function of the number of counts in each Eu-152 spectrum.

6.7 Neutron Detection

The ability to detect neutrons is extremely advantageous in the detection of radioactive isotopes such as those of plutonium and uranium, given the fissile nature of such materials. In contrast to gamma-ray radiation, a presence of neutron radiation will more likely indicate a prohibited material given that industrial and medical applications rarely have use for neutron emitting isotopes. Neutrons are also largely unaffected by the standard shielding or casing used to attenuate gamma-ray emissions, giving a second set of search criteria if the cargo being scanned is suspected as heavily shielded.

6.7.1 Physical Processes

Fast neutrons are usually detected by dedicated neutron counters such as moderated helium-3 based counters and lithium glass scintillators via the 3He(n,p) and 6Li(n,α) reactions respectively. PVT based detectors can be used as proton recoil scintillators in order to detect fast Neutrons directly [Knoll, 1989]. Fast neutrons interact with PVT by elastically scattering off the hydrogen nuclei present in the hydro-carbon composition. The elastic scattering of neutrons with hydrogen nuclei produces a free proton which in turn creates a scintillation pulse much like the resultant electron from a Compton scattered gamma-ray interaction. The energy distribution of the resulting protons range from zero to the full energy of the incident neutron, making the distri-

bution approximately rectangular in shape for a mono-energetic neutron source. This creates a problem with any potential identification of the source of incident neutrons given the lack of specific peaks in subsequent energy loss spectra. The scintillation light produced from scattered protons is also not as bright as that produced by electrons from a Compton scattered gamma-ray interaction. Chiang & Oberer [Chiang and Oberer, 2000] explain this as the increased stopping power of the proton over the electron. The protons deposit energy more densely than electrons and are therefore more susceptible to quenching. To decipher the source of neutron radiation, a dedicated neutron spectrometer would need to be employed. A PVT detector can however still be used to detect neutrons, even if the source cannot be identified, the ability to distinguish neutrons from gamma-rays without any extra equipment would be hugely beneficial. The large areas of PVT used for scanning cargo at customs and borders would give a much larger probability of detecting neutrons than the smaller, more accurate neutron spectrometers. The cross section for fast neutrons with a few MeV of energy interacting with hydrogen nuclei in PVT is roughly 1 - 4 barns [McLane et al., 1988] whereas for helium counters it ranges from approximately 1 - 7 barns [Bashkin et al., 1951] and for lithium glass the cross section is around 2 - 5 barns [Knoll, 1989]. All of these cross sections are dependent on the incident neutron energy, though often in a non-linear fashion. The cross sections for helium-3 counters and lithium glass counters are often greatly increased by the addition of a polyethylene spherical moderator to thermalise the neutrons, increasing their cross sections to around 5330 barns and 940 barns respectively [Knoll, 1989]. The cross section for detecting neutrons with PVT can also be greatly increased by adding a small amount of boron to the plastic. Concentrations of 1% - 5% natural boron are common place for neutron detection. The principle reaction for boron loaded PVT with neutrons is shown in equation (6.1).

$$^{10}B + n \rightarrow \alpha +^{7} Li \tag{6.1}$$

The boron captures a thermal neutron and converts to an alpha particle and lithium-7 particle. The energy of the reaction is kinematic and shared equally between the two resulting particles. Given that the reaction relies on the neutrons being in the thermal region of the energy spectrum, fast neutrons must be thermalised before the boron reaction can take place. Table 6.3 shows some properties of boron loaded scintillators:

The light output of boron loaded scintillators is significantly lower than that of a typi-

Table 6.3: Properties of boron loaded scintillators

Boron Load	5%	2.5%	1%
Light Output (% Anthracene)	48	56	60
Scint. Efficiency (photons/MeV)	7,500	8,600	9,200
Wavelength Max. Emission (nm)	425	425	425
Decay Time (ns)	2.2	2.2	2.2
No. C Atoms/cm^3,$\times 10^{22}$	4.44	4.55	4.62
No. H Atoms/cm^3,$\times 10^{22}$	5.18	5.17	5.16
No. ^{10}B Atoms/cm^3,$\times 10^{20}$	5.68	2.83	1.14
Density at 200C (g/cm^3)	1.026	1.023	1.021

cal PVT based scintillator of 68% Anthracene. Given that the amount of scintillation light produced is critical to the performance of the detector in identifying gamma-ray sources, loading the PVT with boron would not be a viable option. The alpha particle released as part of the boron-neutron interaction process would register in the same energy range as a 100keV electron, which would directly interfere with the gamma-ray spectrum. The only viable option in using PVT directly as a neutron detector is as an unloaded, stand alone detector, despite the relatively low neutron interaction probability.

6.7.2 Californium 252 Measurements

To evaluate the viability of using PVT as a neutron detector, an experiment was performed using a Californium-252 neutron source. Cf-252 undergoes decay by alpha emission (96.91% probability) and spontaneous fission (3.09% probability) resulting in an overall half-life of 2.645 years with a specific activity of 0.536 mCi/pg. The neutron energy spectrum has the average energy of 2.1 MeV [Martin et al., 1999].

For this experiment a 10μCi Cf-252 source was placed 10cm above the 1m V-plank, which was previous calibrated with a Na-22 source, and multiple spectra taken. The

resulting energy loss spectrum was then background subtracted. This process was then repeated with a 10cm cubic polyethylene moderator which the Cf-252 source was placed inside to measure the affect of reduced energy neutrons. Figure 6.34 shows the energy-loss spectra produced using a Cf-252 source both with a poly-ethylene moderator and without. Both spectra were background subtracted. Figure 6.34 clearly shows

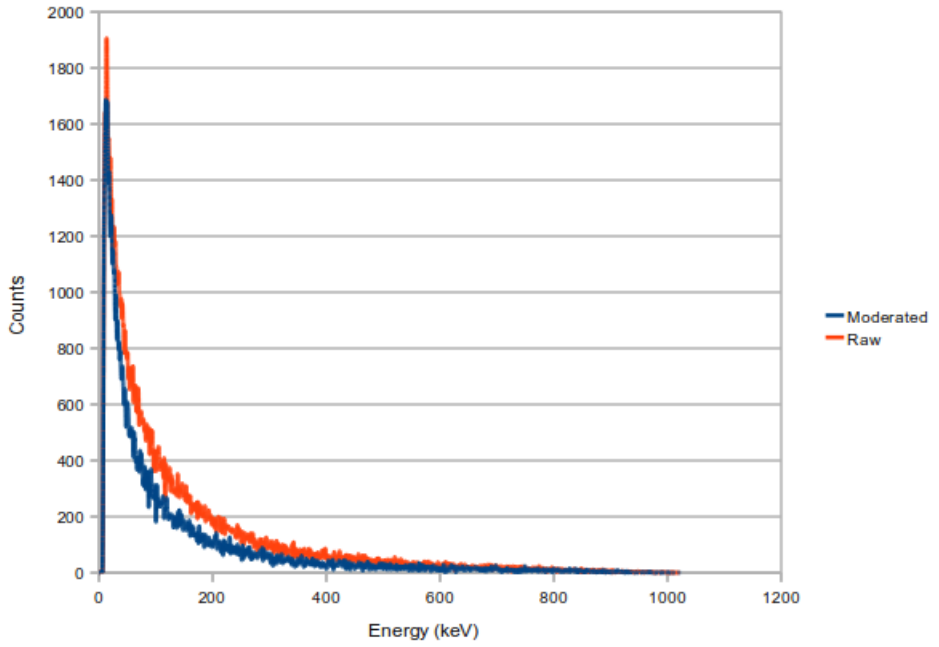

Figure 6.34: Energy loss spectra of Cf-252 neutrons with PVT scintillator both with and without a polyethylene moderator.

that no discernible energy information is present for the Cf-252 source using PVT. The polyethylene moderator serves to attenuate the neutron flux, acting as shielding would if a neutron source were being illicitly transported. The shielding does not appear to distort the shape of the spectrum, but simply reduces the number of counts in the spectrum. Similar spectra were obtained by Stromswold et al who investigated the possibility of using plastic scintillators as fast neutron detectors to detect neutrons spontaneously emitted by plutonium compounds [Stromswold et al., 2000]. The authors used time of flight techniques between two PVT detectors to produce energy loss spectra from various neutron sources. Figure 6.35 shows energy loss spectra for a Cf-252 source and a calculated energy spectrum for neutron emission from the Cf-252 source based on a Maxwellian distribution with average energy of 2.14 MeV. Figure 6.35 shows a similar shaped distribution to the Cf-252 spectra shown in Figure 6.34, though with better energy resolution from the time of flight technique used and a local

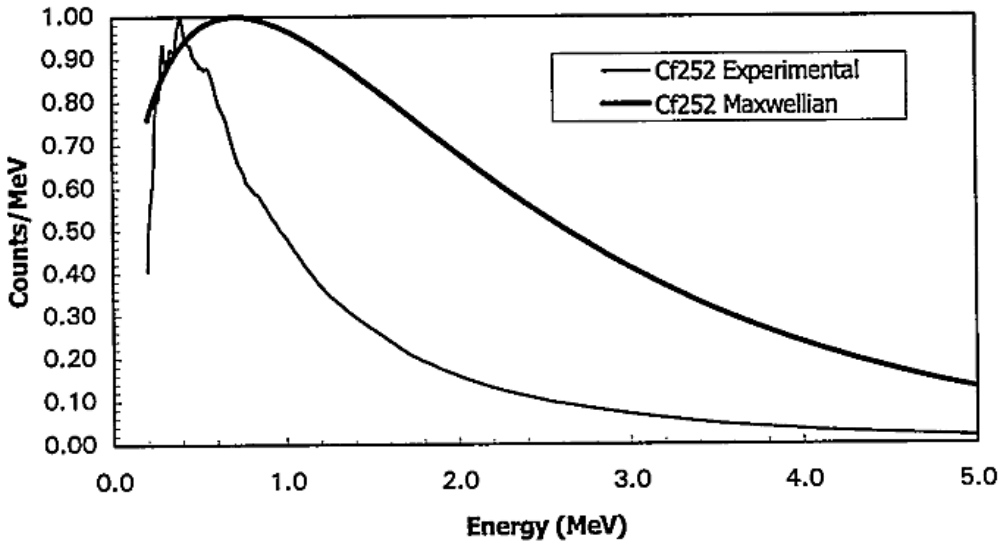

Figure 6.35: Calculated and experimental energy loss spectra of a Cf-252 source using time of flight techniques with PVT detectors. Figure from [Stromswold et al., 2000].

maximum at around 0.6MeV. Figure 6.34 shows no such maximum, presumably due to poor PVT resolution without the aid of time of flight techniques.

6.7.3 Differentiating Between Gamma-Rays and Neutrons

In their paper "Direct Fast-Neutron Detection", Stromswold et al [Stromswold et al., 2000] emphasised the importance of distinguishing gamma-ray events from neutron events and tried two different techniques to accomplish this with PVT detectors.

The first technique was using pulse shape analysis to distinguish gamma-ray events from neutron events on a pulse by pulse basis. The authors predicted that neutron events should produce longer pulses than gamma-ray events given the longer scattering times of neutrons over gamma-rays. For a neutron with an average energy of 1MeV, the speed at which it travels would be around 30cm/ns, whereas a gamma-ray travels at 1.4cm/ns. The time interval between successive scatterings of fast neutrons in a single piece of plastic is therefore about 3ns whereas the successive scattering time for gamma-rays would be around 1ns. In order to experimentally verify these predications a cylindrical 5.1cm diameter by 7.6cm long section of fast plastic scintillator was used as a detector and subjected to gamma-ray and neutron emissions from a Cf-252 source. The authors relied on multiple scattering in each event to determine

the type of radiation detected. Their results showed that even the fastest scintillator employed was not fast enough to distinguish neutron events from gamma-ray events. Although the widest neutron event was around 5.2ns versus around 4.3ns for gamma-ray events, the average pulse width was 3.5ns and 3.3ns respectively; an insignificant difference for accurate differentiation. Resolution of 1ns would be required to differentiate gamma-rays from neutrons using a single plastic scintillator.

The author's second technique was to use neutron time of flight scattering to distinguish neutrons events from gamma-ray events. Two plastic scintillators were used, separated by a distance of 30cm. The first scintillator, closest to the radiation source, was thinner than the second so that incident neutrons/gamma-rays would first scatter from the initial thin scintillator and then go on to interact with the second, thicker scintillator. The timing between the two coincident events was then the distinguishing factor between the event types. Neutrons, being much slower than gamma-rays would have coincident events in a much larger time gap than those of gamma-rays. The authors calculated that for gamma-rays the flight time was around 1ns, whereas for neutrons at the appropriate energy it was around 22ns. A filter of 10ns was applied, so that any coincident events above this threshold were considered neutron events. The technique was successful and proved useful for the sources tested, successfully differentiating between gamma-rays and neutrons and providing a broad neutron energy spectrum. Figure 6.36 shows the time of flight spectrum produced by the authors of both gamma-rays and neutrons simultaneously. Neutron time of flight scattering is a viable technique for detecting, differentiating and measuring the energy spectrum of neutrons solely using plastic scintillator. The benefits of this system would be in the cost and the sensitivity; by using the relatively cheap PVT based scintillator the need for more expensive separate detectors is eradicated, and using large areas plastic greatly increases the probability of detection. A fully PVT based system built around the range of detectors currently presented in this thesis would need to have its limitations and benefits discussed.

The first factor of such a system is that the presence of multiple gamma-ray/neutron sources might produce significantly more false coincident events, giving rise to false

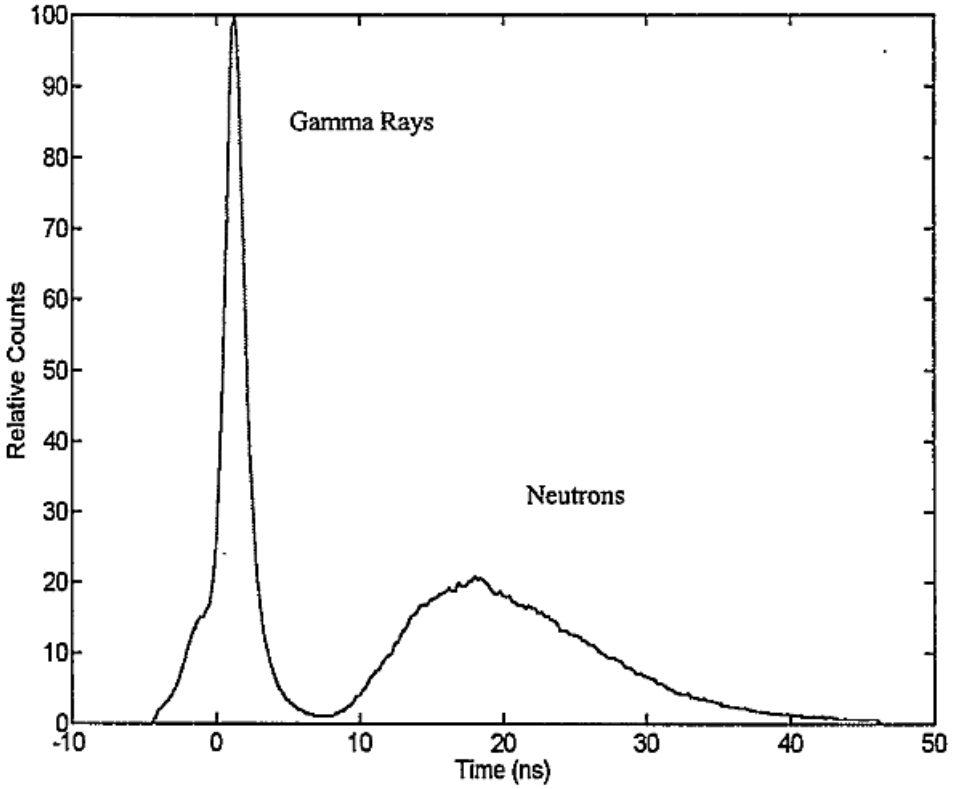

Figure 6.36: Time of flight spectrum for neutrons and gamma-rays from ^{239}PuBe using 2x PVT scintillators 30cm apart. Figure from [Stromswold et al., 2000].

positives for neutron coincidences. Though this is a minor issue given the potential to successfully measure the neutron spectrum, it would still impair the accuracy of the system. Stromswold et al do not test their system with multiple sources simultaneously, but do show that coincident events from multiple gamma-ray and neutron events from the same source can cause false neutron positives. Coincident gamma-ray events registered in both detectors would also need to be vetoed when compiling the gamma-ray spectrum from the main detector, in order to prevent logging multiple scattered events.

The second factor is the use of such as system in a portal type scenario where the source of the radiation could be at any position in relation to the detectors dimensions. This means that the path length of a neutron scattered from the first scintillator could vary a significant amount before interacting with the second scintillator depending on the source location and the scattering angle. Whilst not a concern for the absolute detection of neutrons, using two full-sized plastic scintillators would greatly reduce the

energy resolution if any energy loss spectra were compiled. The first scintillator of the pair, closest to the radiation source, would need to be the thinner scintillator, leaving the original gamma-ray spectrometer outlined in this thesis, such as the 1m V-Plank or the 2m X-Plank as the second, thicker scintillator. This thin scintillator would need to be small enough in area to be attached to a single small area photomultiplier tube to keep costs minimised. Stromswold et al use up to four fast photomultiplier tubes to get the best discrimination between gamma-rays and neutrons, though this comes as a cost to the overall neutron detection efficiency.

If spectroscopic information is desired for neutrons, the large range of potential flight paths after scattering from the first scintillator should be minimised. This could be achieved using a relatively small area thin detector to limit the region from which scattered neutrons can project from. Position sensitivity could be used in the second scintillator to determine its interaction point and therefore calculate its trajectory for an increased accuracy of the estimated energy. Larger scintillator could be used if simple neutron detection is desired rather than spectroscopy. A trade off between sensitivity and spectroscopic performance would be required.

The third and most important factor is the cost/ability of manufacturing such a system. The detector system would need to be around 30cm wider on each detection panel, incorporate more scintillator material, photomultiplier tubes, electronics and software development, all of which add to the total cost of the system. Multiple photomultiplier tubes used for larger detectors would greatly increase the cost, and the associated electronics needed to read the signals would need to be purchased. The timing resolution of the digiBASE electronics currently used is far from the nanosecond timing resolution required and the cost for high precision timing units would add significantly. All these added costs may simply outweigh the benefits of an integrated PVT based system. A separate neutron detector such as a helium proportional counter might, for example, provide the same detection capability at a similar cost, or in a more convenient format. The final problem with using plastic scintillator based neutron detectors is that of shielding. If a smuggler were incorporating dense shielding to attenuate or intentionally scatter gamma-rays from a threatening source, they may well also incor-

porate polyethylene shielding to thermalise neutrons. Given that plastics only directly detect fast neutrons, the resulting thermalised neutrons from a shielded source would be much better detected by a helium-3, or lithium based counter.

A more detailed analysis of the costs associate with incorporating a fully PVT based system would be required to fully weigh its benefits, but it would seem initially that without the ability to differentiate neutrons from gamma-rays in a single, all purpose detector, a PVT based system is simply not a cost effective solution given the range of alternative products available that have already been proven to work well.

6.8 Conclusions

In this Chapter the deconvolution of spectra from all three detector designs was presented. The full width half maximum of the 662keV peak in the deconvolved spectra for each design was calculated as 6% for the two larger PVT designs and 5% for the 50cm V-Plank. A number of other spectra were also measured and correctly identified such as Na-22, Co-60, Am-241 and Ra-226. Tests were conducted with the 50cm V-Plank to determine the minimum number of counts for both simple and complex spectra for correct spectral identification. Na-22 and Eu-152 sources were used for this purpose and gave the number of counts required as 8,000 counts per spectrum for 100% identification of Na-22 and 22,000 counts per spectrum for 100% correct identification of Eu-152 in this set of experiments. These results were accurate when tested with sets of 25 spectra, but a larger number of spectra would be required in proper field trials for a more accurate figure. A phantom peak anomaly was highlighted, caused by the presence of optimised Compton edges and photo-peaks present in the same low-energy region of the spectrum and appearing similar to one another in shape. This can cause the deconvolution process to predict the existence of higher level energy peaks which don't exist in the raw spectra. The problem can be remedied by incorporating such events into the isotope identification library. Tests were also conducted into the ability of PVT to directly detect neutrons. It was found that standard PVT detectors can detect neutrons, but not distinguish them from gamma-rays in an energy loss spectrum. Whilst differentiating neutrons from gamma-rays is possible

using time of flight techniques, extra detectors would be required increasing the cost and design requirements. These requirements reduce the viability of PVT based neutron detection given the possible incorporation of other, well-tested neutron detectors such as Helium-3 based counters.

Chapter 7

Practical Portal Considerations

7.1 Introduction

In this section practical considerations of a radiation portal monitor are considered. Environmental factors such as temperature, magnetic fields and background radiation are investigated. A number of other phenomena are also described which occurred unexpectedly during the investigation of PVT spectroscopy, such as non-linearity and dynamic range problems. Positional sensitivity in the large 2m design is also investigated as an additional attribute without the need for new hardware.

7.2 Non-linearity in the Detector system

During measurements of Na-22 spectra it was noted that the detector system was giving a non-linear response in the energy calibration. The induced Compton edges for the 511keV and 1275keV gamma-rays from a Na-22 source should be detected at 341keV and 1061keV respectively. The ratio of 1061keV to 341keV is equal to 3.11 and this value should remain constant regardless of the detector settings to ensure a linear response of the system with respect to the incident gamma-ray energy. To this end a small experiment was conducted by taking a number of Na-22 spectra with the 50cm V-Plank and varying the photomultiplier tube voltage and gain settings for each of these measurements. The ratios of the Compton edge positions were then calculated and compared to the expected value of 3.11 to determine the linearity of the system. These values were found to vary with the voltage and gain and none equalled

the expected value of 3.11. Figure 7.1 shows the results of this experiment. Figure

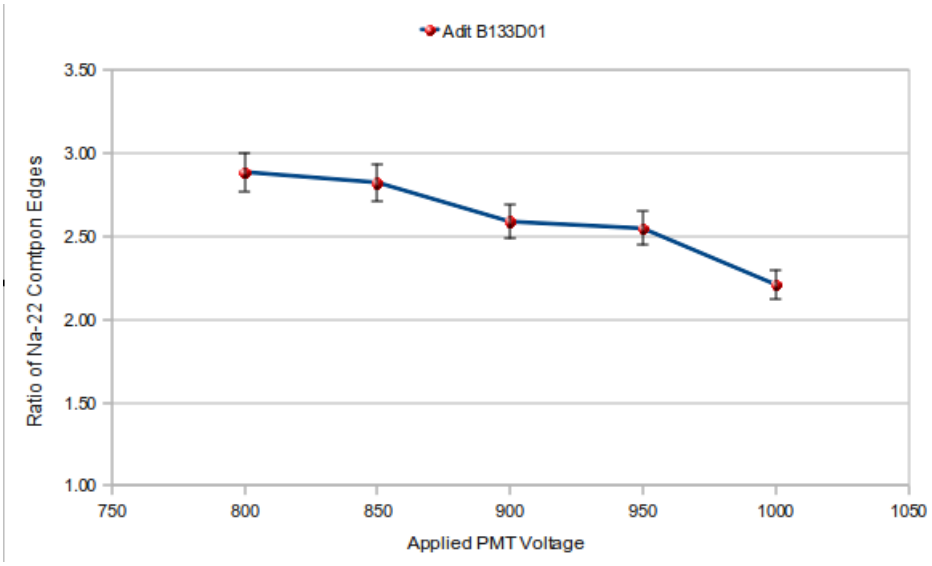

Figure 7.1: The ratio of the locations of 1275keV and 511keV induced Compton edges for a range of applied photomultiplier voltages using the 50cm V-Plank prototype.

7.1 shows that the ratio of the Compton edges decreases as the voltage is increased, with no voltage settings giving the expected value of 3.11. There are few factors that could have affected the linearity of the detector. Starting with the plastic scintillator itself and then moving to the detector hardware, each of these factors were explored to isolate the cause of the non-linearity. The factors investigated were the linearity of various multi channel analysers, photomultiplier tube base electronics, pre-amplifiers, photomultiplier tubes and the linearity of the PVT itself.

Two multi channel analysers were tested with the 50cm V-Plank; the Ortec digiBASE and the Ortec Scintipack. Both multi channel analysers showed that various voltages applied to the photomultiplier tube base gave a different Na-22 Compton edge ratio for the same detector. The electronics used in both of these units were able to cope with the fast response of plastic scintillators. Both units however showed the expected linearity with other detectors such as NaI(Tl) based systems. The multi channel analyser was therefore not the major cause of the non-linearity. As plastic scintillators have a fast response time the pre-amplifier rise time could have been too slow in the default pre-amplifiers contained in the digiBASE or Scintipack. An Ortec fast pre-amplifier was used to test this and found that using either the fast pre-amplifier or the Scintipack's built in pre-amplifier gave no difference in the resulting spectra.

The only available explanation for the non-linearity of the system was the photomultiplier tubes. Upon consultation with the manufacturer of these tubes, ADIT, the 5" B133D01 tube being used is based on a box and grid dynode design. The box and grid design in this instance shows little linearity except for when used in conjunction with a narrow voltage range which is provided by the manufacturer. Therefore whilst presenting good value for money in general photon counting experiments, these tubes are not suitable for use in spectroscopy. This information was not commonly known because 5" photomultiplier tubes are not generally used for spectroscopy, given that typically used scintillation crystals are of much smaller dimensions. These photomultiplier tubes were therefore used mostly for counting purposes on large area PVT detectors. As spectroscopy with PVT is not widely practised, there was no way of knowing this type of photomultiplier tube would not be appropriate. Given this information, a new set of photomultiplier tubes were acquired from the manufacturer Photonis. The photomultiplier tubes purchased were model number XP3540/BC which were blue optimised, 5" photomultiplier tubes and were based on a linear dynode design as opposed to the previous box and grid design. These new tubes were tested using the same method of Na-22 Compton edge location ratio with respect to applied photomultiplier tube voltage and compared to the results of the Adit B133D01 tubes. Figure 7.2 shows the results. The Photonis linear dynode design showed excellent linearity over the full range of tested voltages. All the ratios for the 1275keV to 511keV Compton edges are close to the 3.11 expected value and within the limits of the Compton edge location measurement error. These photomultiplier tubes, although around double the price of the Adit B133D01, gave an excellent linearity and were therefore implemented permanently for all detector designs.

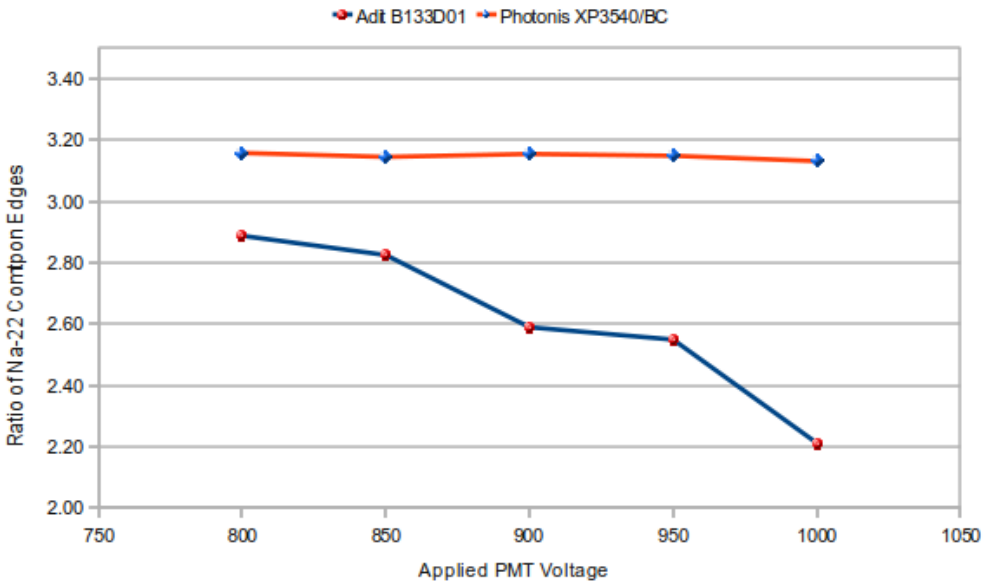

Figure 7.2: The ratio of the locations of 1275keV and 511keV Compton edges for a range of applied voltages using Photonis XP3540/BC and Adit B133D01 photomultiplier tubes.

7.3 Dynamic Range

The dynamic range of the multi channel analyser was an important factor in spectroscopy with PVT as it balances the resolution with the range of incident gamma-ray energies available and the total cost of the detector system. For gamma-ray spectroscopy in this work the required energy range is from 30keV to 3MeV. The highest energy measured is that of Th-232 in which a 2.6MeV gamma-ray produces a 2.4MeV Compton edge. In order for the identification program to operate correctly the whole of the broadened Compton edge must be included in the spectrum, which means the upper limit is around 2.8MeV for PVT. This must be balanced with the lower limit, which is currently set as the Compton edge for Co-57, which has a Compton edge at 40keV. The multi channel analyser used had 1024 channels available, but for use with NaI(Tl) based detectors, Symetrica's software transposed each spectrum into a 512 channel spectrum to match that of the 512 file q-matrix. This gave a 6keV bin width which can present problems with resolution at the lower energies. Even though the resolution of PVT is much lower than that of NaI(Tl), there are a number of coincidental features at lower energies such as the 40keV Compton edge from Co-57 and the 60keV photo-peak from Am-241, the resolution at these energies is of vital importance for distinguishing between such isotopes. The 6keV bin width supports

the ability to distinguish such isotopes, but retaining the maximum dynamic range to encompass the features of a Th-232 spectrum requires a lower gain, therefore the 512 channel configuration was just within the limits of providing both features. A slight calibration or gain error however can remove this ability, forcing the user to choose the ability to distinguish low energy isotopes or identify Th-232 spectra. To compensate for this problem in the future, a higher number of channels should be used, such as 1024 channels, whilst decreasing the bin width only fractionally, and increasing the gain so that the energy range scaled to around 4500keV for example. This would give 4.5keV bin widths and a high enough energy scale to encompass the 2.6MeV Th-232 gamma-ray.

7.4 Environmental Factors

7.4.1 Background Scattering

The immediate physical environment surrounding the detector is of vital importance when using PVT based scintillators. If any nearby material is of roughly the same density as the PVT, such as wood, it will cause degradation in the spectrum due to multiple coincident Compton scattering. This happens if two simultaneously emitted gamma-rays interact with the PVT in a given time window. If one of these gamma-rays is unhindered by the PVT, but then goes on to back scatter from an external material, the resultant scattered gamma-ray can then interact with the PVT detector in the same time window as the other, unhindered gamma-ray. This can distort specific regions of the energy loss spectrum. Figure 7.3 shows a diagram of this effect. In this example the 1275 keV gamma-ray can scatter by 180 degrees in the detector giving a Compton edge as expected, however, the 511 keV gamma-ray does not interact with the PVT as expected, but instead interacts with the external material, back scattering towards the detector. This scattered gamma-ray then interacts with the PVT within the accepted integration time of the 1275keV gamma-ray's interaction, causing the sum of the two scattered gamma-rays to be binned in the spectrum. This effect can significantly broaden the 1275 keV Compton edge, but shows little or no effect on the 511 keV Compton edge. Figure 7.4 shows the 1275keV induced Compton edge from a Na-22 spectrum, alongside a standard Na-22 spectrum removed from any interfering

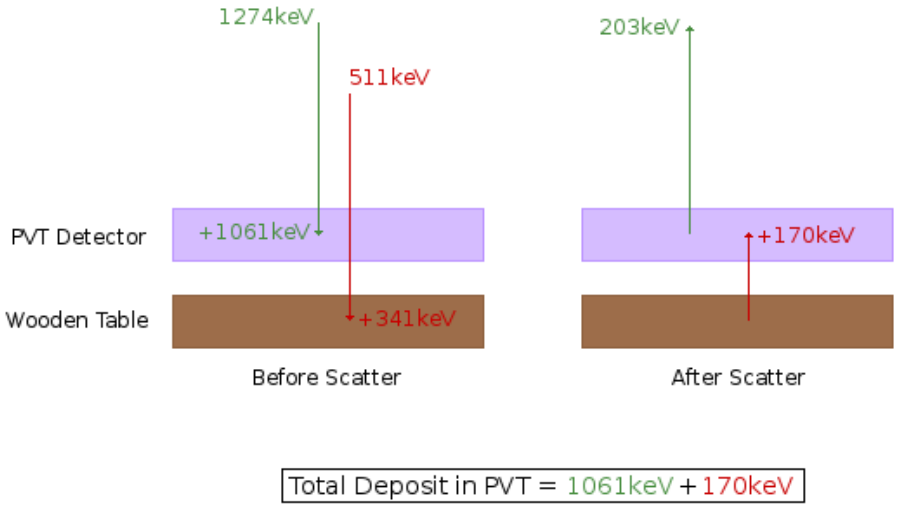

Figure 7.3: The multiple coincident Compton scatter event. Two gamma-rays interact with a detector, one of which has already been back scattered by an underlying material. The result is a broadened Compton edge.

materials. The effect was observed to some extent with any sized detector, but more so for large area detectors when the detector was placed close to anything of similar density. The effect subsides gradually as the detector is moved away from such objects, and could no longer be observed for the large area detectors when the detector was greater than 30cm from the object. The distance is reduced for the smaller 50cm V-Plank detector, which only required around 10-15cm or so for the effect to disappear. Other materials also incur this behaviour, though to a lesser extent. Thick slabs of Lead for example were shown to display a similar effect. The effect also degrades with the thickness of the objects that are close by. A prime example is using any of the detectors above a standard lab bench, where the table top is made of around 5cm thick wood. This has a large effect on a Na-22 spectrum. A similar sized office desk with a desktop just 1cm thick has a barely noticeable effect. This effect is of key importance in both the positioning of the detector, and also any material that might be used to reduce the detector's exposure to background radiation. Standard background scattering of gamma-rays from a nearby surface can also create problems for PVT detectors and must be accounted for. Gamma-rays scattering from any surface and interacting with PVT detectors is a problem because of the low energies that the scattered gamma-rays

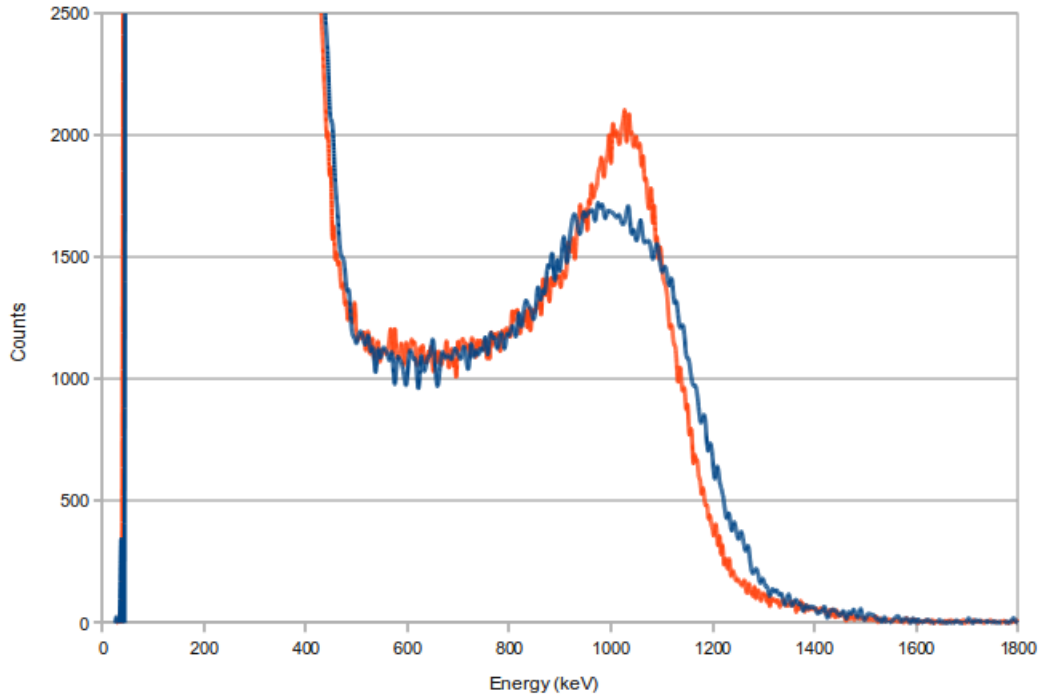

Figure 7.4: The 1275keV region of an example Na-22 spectrum showing the scattering effect caused by the detector being placed too close to a wooden bench.

have. These low energy events can hinder the clarity of energy loss spectra at low energies, the most important region for PVT detectors to distinguish many isotopes correctly.

7.4.2 Temperature Sensitivity

Each detector must be able to withstand reasonable temperatures at both the hot and cold ends of the temperature scale. The detectors may be employed in cold areas such as those found in Alaska, or hot areas such as those found in Nevada. The detectors must also be able to withstand rapid changes in temperature due to the possibility of being in a desert-like environment where temperatures are hot during the day and cold at night. To test the effects of temperature on PVT based detectors the 50cm V-Plank and corresponding equipment were placed inside a large environmental chamber where the temperature was changed gradually from one extreme to the other. The detector then took a spectrum of a Cs-137 source, also inside the chamber, to measure any changes in the location of the Compton edge from the 662keV gamma-ray with respect to temperature change. These measurements were performed from -20 degrees Celsius to +40 degrees Celsius in increments of 10 degrees Celsius. Three

temperature sensors were used to measure the chamber temperature, two in the chamber itself and one attached to the detector using thermal adhesive. The temperature sensor attached to the detector also had a large section of Styrofoam bonded over the top to ensure that the temperature being measured was that of the PVT and not that of the surrounding environment. The temperature in the chamber was initially started at -20 degrees Celsius and held there until the reading on the PVT temperature sensor agreed a -20 degrees Celsius reading. A spectrum was then acquired and a computer program was started to take the temperature of the chamber upwards by 10 degrees for the next measurement. Each temperature change was done over a period of 30 minutes with an additional 120 minutes to allow the detector to adjust to the same temperature as the environment. This experiment measured the temperature dependence of the detector as a whole, the results for which are shown in Figure 7.5. Figure

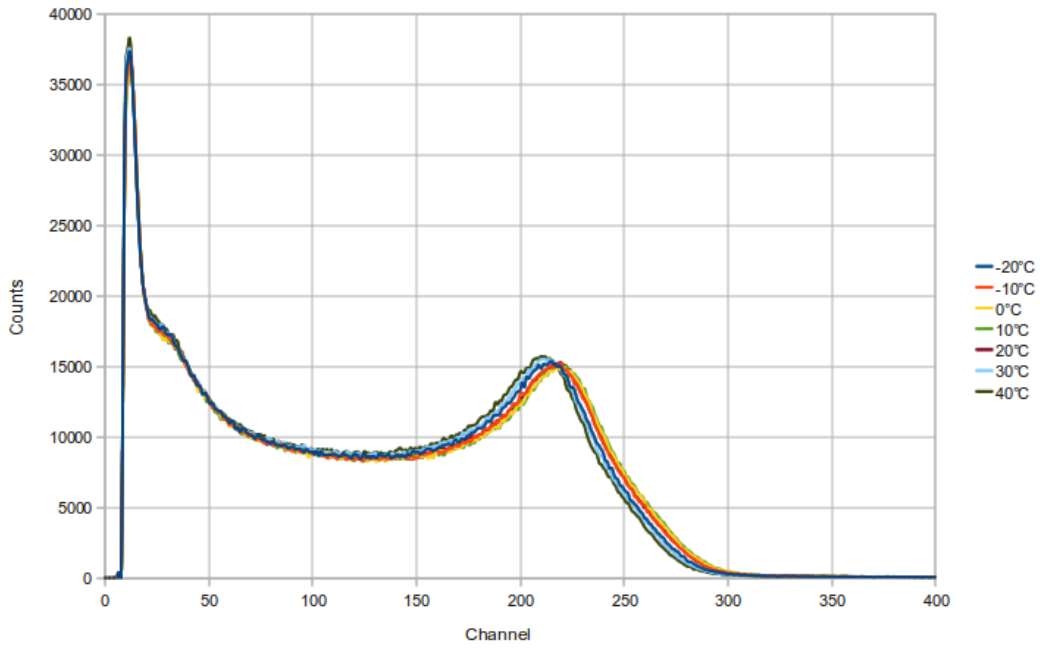

Figure 7.5: Variation in the location of a 662keV induced Compton edge with respect to temperature for the 50cm V-Plank detector.

7.5 shows that a small variance can be observed in the location of the 662keV induced Compton edge with respect to temperature change. As the temperature was increased the collection efficiency appeared to decrease, and mostly this effect was observed at greater than room temperatures. The standard deviation in the mean Compton edge channel number was 4 channels giving a total variance of 2% over the full range of the temperature change. This means that the detector would have little cause for con-

cern for minor temperature fluctuations, but would have more cause for concern in a desert like environment where temperatures are cold in the morning but reach extremely high numbers in the afternoon. Re-calibrating the detector system could solve this issue, perhaps at various known times of the day or on a trigger from an internal temperature sensor. Built in fans or air conditioner units are also an option to keep the temperature constant regardless of the environment. The temperature measurements conducted here are somewhat correlated to a statement made by Eljen concerning the temperature dependence of their EJ200 plastic scintillator. Eljen state that the light output at +60C is 95% of that at +20C with no change from -60C to +20C [Eljen Technology, 2009].

7.4.3 Magnetic Shielding

External magnetic fields have a great effect on the performance of scintillation detectors. This is due to the detectors dependence on photomultiplier tubes for photon collection, which are very sensitive to such fields [Hamamatsu, 2006]. The main concern for a portable detector is the rotation of the detector in the Earth's magnetic field, which subsequently alters the trajectory of electrons undergoing amplification inside the photomultiplier tube. For stationary detectors the Earth's magnetic field is not so much of a concern, but nearby electronics can incur a magnetic field and therefore compromise the detector's performance. As security devices, the notion that intentional disruption may also be a factor must be entertained. Anyone with even a limited knowledge of scintillation detectors may anticipate their dependence on magnetic fields and therefore employ powerful magnets in their cargo in an attempt to disrupt the identification of any illicit materials they are carrying. Fortunately the solution to this problem is relatively simple, the employment of sufficient mu-metal shielding. Such shields are typically in sheet form only a few millimetres in thickness and are placed around each photomultiplier tube inside the detector so that they cover the full length of the photomultiplier tube plus an additional few centimetres over the edge of the photomultiplier tube [Hamamatsu, 2006]. Mu metal shielding will negate the majority of magnetic interference caused by electronics but significantly large magnetic fields will still have an effect. If this is the case then a magnetic sensor such as a basic Hall probe could be incorporated into the portal monitor housing to warn against any

external magnetic fields present.

7.4.4 Degradation

Degradation of the light collection efficiency is apparent in plastic scintillators as a consequence of radiation damage, age and handling of the material [Amsler et al, 2008]. Ageing of plastic scintillator occurs where the material is exposed to factors such as temperature changes and solvent vapour causing gradual degradation over time. Handling the material without gloves also leaves grease marks on the material which over time cause cracks in the surface, diminishing the material's ability to reflect light by total internal reflection. The combination of these processes mean that the detector will gradually decrease in resolution over time and therefore the plastic will need to be replaced over a number of years as part of the detector's maintenance.

7.5 Automatic Calibration

An automated calibration routine is required in a portal monitor scenario so the detector system can be calibrated as and when it needs to be without the need for human intervention. A small number of techniques were available for this, such as using a tagged Na-22 source to provide 511keV and 1275 keV gamma-rays constantly whilst the detector is in operation. These gamma-rays would then be vetoed using a separate smaller crystal detector to detect the recoil 511keV gamma-ray. This system has the advantage that the calibration source is constantly available and requires no machinery to use, just more complex programming in the data acquisition program. The disadvantages of this system however are that only a maximum of 90% of the 1275keV gamma-rays can be successfully vetoed and an extra smaller detector must be installed inside the larger system for each PVT detector. The chosen method for calibration was therefore to use a shielded source in which a Na-22 source is placed nearby inside a lead chamber. This chamber has a mechanical shutter which enables access to the source during calibration and attenuates the source when it is not required. This solution is cheap and relatively simple to implement whilst providing a reliable calibration source. Both of these solutions require a radioactive source installed inside the detector itself which can be a cause for concern amongst the general

public. However the source required is of minimal activity and differing solutions can be used for the various applications of the detector system. A personal portal for example is more likely to be used indoors, where the temperature and other environmental factors rarely change. The system would therefore not need as many calibrations as an outdoor system and the possibility to keep an external source locked away for less frequent calibrations is an option. Hand held type detectors also benefit from this arrangement.

Having established the means by which the system is calibrated, the method of calibration was also of key importance to producing a reliable system. As outlined previously in "Dynamic Range" the system must have a specific dynamic range which reduces the work for calibration. The system has as higher gain as possible whilst still retaining the ability to identify a 2.6MeV gamma-ray. This gain setting will differ for each photomultiplier tube used in each system but the channel numbers where various Compton edges are expected will remain the same. Therefore once the optimum voltage and gain are found for the dynamic range, a Na-22 source is placed near the detector and a spectrum taken. This spectrum can then serve as a template, with the exact positions of both Compton edges recorded. Future calibrations then only need to increase the gain of the photomultiplier tubes until the positions of each Na-22 Compton edge match that of the template. To ensure better compatibility with the identification program, a Geant4 simulation of a Na-22 spectrum was simulated for each detector system and used as a template. This ensures that each experimentally measured spectrum matches the exact position predicted by Geant4 and therefore increases the probability of matching the isotope library.

7.6 Positional Sensitivity

A limited positional sensitivity was available to the large X-Plank design detector during testing. The detector was able to give a spatial localisation of a measured source based on calculations of the intensity of photons received at each photomultiplier tube on the detector. Positional sensitivity is useful for a number of reasons, for personnel portals the time required to find sources that might be concealed on the person

is greatly reduced if the operator knows exactly where to look. Warning alarms that might be caused by signatures of Iodine in thyroid related medical treatment could also be verified as coming from the throat region of the person. For external applications, a detector may be employed to scan the ground for contaminated areas, a large detector with positional resolution might be the most efficient way of achieving this goal. As positional sensitivity is an additional feature that can be employed in double ended design scintillators at almost no extra cost, the usefulness of such a feature however is negligible when compared to the ability to identify isotopes being measured. Therefore positional sensitivity is given a lower priority when evaluating how such a feature might affect the rest of the detector's intended functionality.

7.6.1 Software Considerations & Calculations

On a single detector, positional sensitivity is only available to detectors which employ photomultiplier tubes at either end of the PVT. The only design investigated in this work which meets this criterion is the 2m X-Plank design. The 1m V-Plank design uses two photomultiplier tubes but as they are attached to the same end of the PVT, positional resolution would be limited to which side of the PVT the gamma-rays were interacting with. The calculation of the position of a source relies on the attenuation of the scintillation light as it reaches either end of the PVT from its point of origin. The proportion of the light received by the photomultiplier tubes at each end of the detector is then an indicator of where the scintillation pulses originated from. To calculate the position of a measured isotope, the response of the detector must therefore be known for each end of the PVT. A simple calculation can then be performed based on the response of the detector to estimate the source's location. Figure 7.6 shows the simulated response for a 200cm$\times$12.5cm$\times$4cm plank shaped PVT detector with photomultiplier tubes at either end. This simulation shows how the signal from each photomultiplier tube varies along the length of the plank with respect to the location of single ideally collimated source placed above the detector. Given that the response of the detector follows attenuation in the form of equation (7.1):

$$I = I_0 e^{-\mu x} \tag{7.1}$$

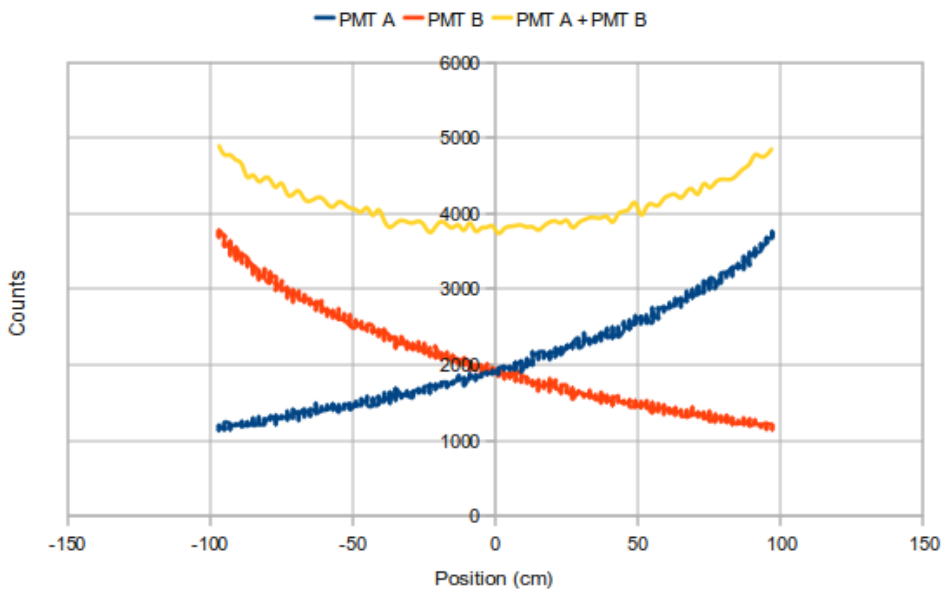

Figure 7.6: Simulated variation in the light collection efficiency of a 200cm×12.5cm×4cm plank shaped PVT detector with photomultiplier tubes at both ends.

Where I is the resultant intensity, I_0 is the initial intensity, μ is the attenuation coefficient and x amount of material traversed. The position of the source can be calculated using equation (7.2):

$$x = ln\frac{\frac{P_a}{P_b}}{2\alpha} \tag{7.2}$$

Where x is the position of the source, P_a and P_b are the pulse heights of the signal at end A and B respectively and α is the attenuation coefficient of the PVT. This is the theoretical ideal for a detector which has an exponential decrease in light received for each end as the source is moved further away. The 2m X-Plank design however is tapered and therefore does not give an accurate exponential response, which means the location of a source cannot be accurately calculated by equation 7.2. To model the 2m X-Plank, two further options are available. The first is to calculate an exact equation representing the deterioration of the scintillation pulse at each end of the PVT with respect to source location. This method is unfavourable as it is both complex and relies unrealistically on each detector's response being matched exactly to the theoretical ideal. The second technique is to use a look-up table or template for each detector individually. This template is then the reference for the ratio of the signals received by the photomultiplier tubes. This technique has the advantage of being relatively accurate as it is tailored for each detector, the disadvantage however is that each de-

tector must be experimentally characterised to produce the reference template. The second technique of using an experimental technique is chosen as the best candidate and compared to using a standard exponential equation to determine any increase in accuracy.

7.6.2 Measurements

To begin measurements the reference template must first be created. This was done by taking 10cm increments along the length of the detector and placing a collimated Cs-137 source at each interval. A spectrum was then acquired for each position to give the variation in the spectral location of a 662keV induced Compton edge with respect to the Cs-137 source location for each end of the detector. Figure 7.7 shows the experimental response of the 2m X-Plank using this technique. The gaps between each 10cm measurement were linearly interpolated to create a full template. This

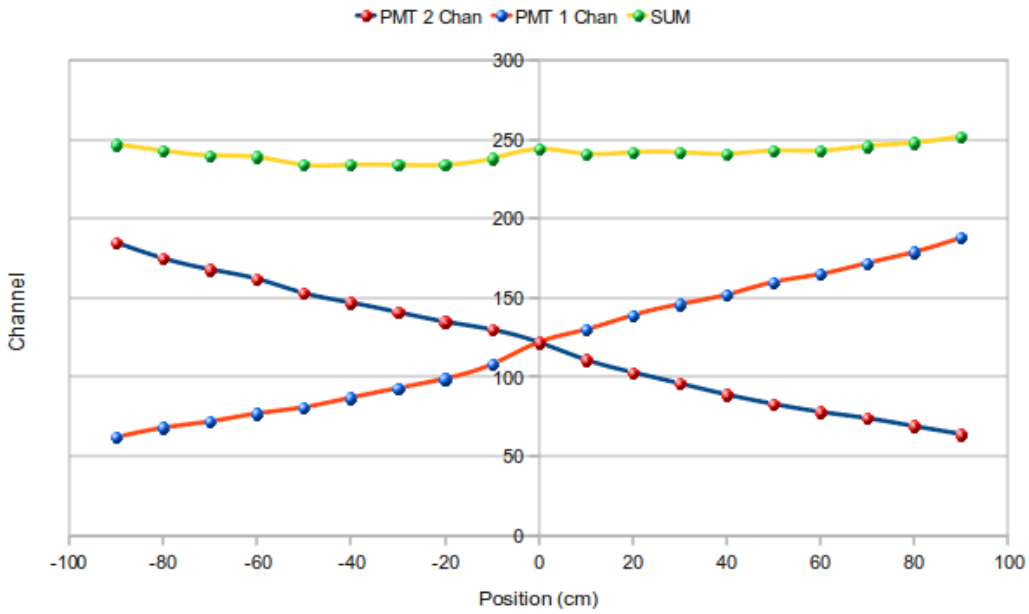

Figure 7.7: Variation in the spectral location of a 662keV induced Compton edge with respect to a Cs-137 source location using the 2m X-Plank.

model assumes that a few centimetres is enough spatial resolution for the majority of intended applications. A finer resolution than this would most likely require a dedicated positional capability beyond the abilities of a single large area detector.

7.6.2.1 Collimated Isotopes and Resolution

The estimated position of a measured isotope is shown graphically using a histogram for the location of each individual signal pulse as it arrives at the photomultiplier tubes. Each coincident pulse is recorded in the software buffer and batch processed for each acquisition interval. The pulse heights are located on the template and the corresponding location is plotted into the histogram. A Cs-137 source is initially used to test the resolution of this technique, the source being placed in the middle of the detector inside a lead collimator. The collimator was 8cm in diameter, 2.7cm thick and had a 1cm circular aperture with an instep to house radioactive sources. Geant4 Monte Carlo simulations are also conducted for the 2m X-Plank. A Cs-137 source was simulated inside a lead collimator of the same dimensions and placed above the 2m X-Plank. 10,000 gamma-ray photons were fired and the interaction position inside the PVT recorded. This simulation is presented along with the experimental positional results in Figure 7.8. The figure also includes a Gaussian distribution fitted to the experimental data to estimate the FWHM of a collimated source. The figure shows a

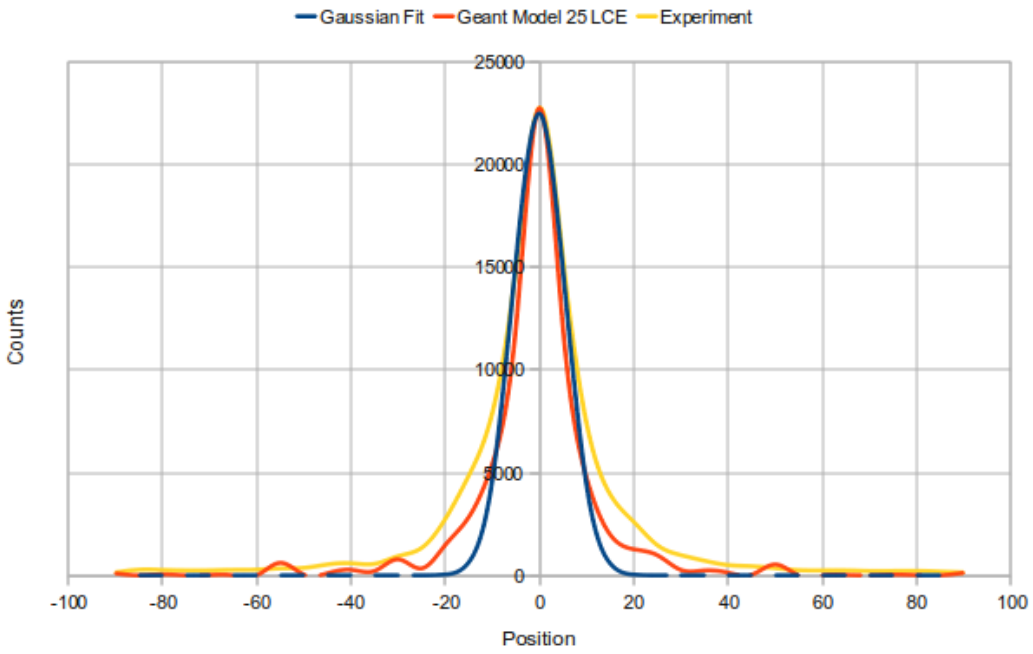

Figure 7.8: Positional histogram for a collimated Cs-137 source placed above the centre of the detector.

peak in the experimental spectrum at 0cm but a low number of counts are present to +/-40 cm of the centre. The Geant4 simulation provides a relatively good fit to the experimental data. The distribution, as measured using the Gaussian distribution, has

a full width half maximum of around 11cm. The positional resolution will depend on the spread of the collimator, which in turn is dependent on the energy of incident the gamma-rays as their ability to pass through lead unattenuated increases with energy. The Geant simulation gives similar results to the experimental data, suggesting the Collimator limits the positional resolution. The errors induced from the variation in the light collection can be ignored if the source is collimated, and also that the response of the detector is taking this error into account to predict the photons' origin. Factors affecting the energy resolution of the detector can be ignored as the total energy of each interaction is of little interest, only the proportion of that energy which reaches the photomultiplier tubes. Therefore contributions from the number of photoelectrons produced per light pulse and contributions from electronic noise constitute a minimum inherent error in the positional resolution.

The ability for the detector to estimate the location of a source is largely based on the intensity of the gamma-ray flux in a localised area of the detector, therefore an uncollimated source will generally yield a very poor positional resolution in the detector. The source must either be very close to the detector, as may be the case in a personnel portal, or the detector itself would need a large collimator placed over it to isolate the location of the source. Any uncollimated source placed further than around 10cm above the 2m X-Plank gives a near unresolvable positional distribution. Multiple isotopes can be detected and located along the length of the detector given the positional histogram employed if they are sufficiently collimated and within the detector's positional resolution limits. The main limit to the positional resolution of this detector is the fact that the source must be collimated.

7.7 Conclusions

This Chapter investigated some of the factors which must be considered when deploying a PVT based detector outside of a laboratory environment, and also unexpected factors which affected the detector's performance. The type of photomultiplier tube used was found to be an extremely important consideration. The original Adit photomultiplier tubes used were found to give a non-linear spectral response over a range

of applied voltages. Using Photonis photomultiplier tubes corrected this issue as they use a linear dynode design as opposed to a box and grid design. Background scattering was found to cause a significant degradation to various spectra, mostly Na-22 spectra in which the 1275keV induced Compton edge significantly degraded when the detector was placed close to a wooden surface. Other isotopes can also suffer from back scatter causing an increased number of counts at the lower end of the energy spectrum. The dynamic range of the multi channel analyser was also shown to be of concern, as the resolution for PVT detectors must be good enough to distinguish the many low energy Compton edges present in spectra, as well as accommodate high enough energies to identify isotopes such as Th-232. How external temperature affects the performance of the 50cm V-Plank was established, with around 2% variation in the location of a 662keV induced Compton edge over a temperature range of -20^{o}C to +40^{o}C. Positional resolution was achievable with the 2m X-Plank using the relative intensity of light received at each end of the detector. The maximum positional resolution available was a FWHM of 11cm, this was limited by the collimator used for the measurement. In order to achieve any useful positional resolution a collimator must be used.

Chapter 8

Future Portal Designs

8.1 Introduction

In this chapter the design for a detector panel for use in a personnel portal or vehicle portal detector system is outlined. This design was constructed using the results from both simulations and the quality of spectra obtained with the previous detector designs. Personnel portals are not subject to many of the problems that vehicle portal monitors experience and should therefore show a better correlation between simulated performance and industrial performance. A volume of PVT for the detector was defined for the sensitivity requirements as well as a minimum set of performance guides to ensure consistent Compton edge clarity for successful deconvolution and identification of energy loss spectra. Methods for testing such as system are given as well as the benefits and limitations that such a system can provide. Once the plastic scintillator panel is designed, a number of them can be implemented for either a personnel or vehicle portal depending on the sensitivity requirements.

8.2 Panel Designs For a Portal

The ANSI standards N42.35-2006 “American National Standard for Evaluation and Performance of Radiation Detection Portal Monitors for Use in Homeland Security” [IEEE, 2006a] define a number of portal types by their role. These are defined as:

- Pedestrian
- Package (conveyor)

- Vehicle (which includes containerised cargo)
- Rail vehicle

In this study personnel and vehicle (non-rail) portals were chosen, but such designs could be expanded into other portal types. Whilst this section can provide guidance on the best internal components and configuration for a portal, some of the engineering components are not covered. The ANSI standards N42.35-2006 provide a multitude of factors such as exterior materials, casing, ruggedisation of the portal, electrical testing and other operational requirements. These are separate topics for consideration by a company manufacturing the portal and are therefore not covered here.

8.2.1 Detector System Requirements

The minimum sensitivity required to detect isotopes with a certain activity, at a certain distance, is merely a function of detector volume. The detection of isotopes in this manner is quite crude in that it requires no refining of spectra, but simply an alarm if the gross count rate goes above a certain threshold in relation to the background count rate. For current portal monitors, standards exist for both minimum detection threshold of an isotope, and for isotope identification success rate. For PVT based portals, the detection standards and isotope identification standards will be included. Some of the factors which must be incorporated by a radiation portal monitor are shown below.

- Detector sensitivity/efficiency
- Distance between detector panels (if more than one is present in a portal)
- Height of the portal
- Source speed through the portal
- False alarm rate
- Compton edge clarity
- Isotope identification success rate

The first few items are typical of a standard PVT detector, whilst the last two are specifically for a spectrometer. A spectroscopic PVT portal monitor is more of a hybrid between the two, as it can easily fulfil the role of a passive detector but its role in spectrometry has not been previously defined. The majority of advanced spectroscopic portals being researched today incorporate NaI(Tl) detectors, it could therefore be unrealistic to expect a PVT based system to perform to exactly the same standards for identification. PVT based systems clearly can identify a range of isotopes under laboratory conditions though, and therefore to test a plastic scintillator based system the ANSI standards N42.35-2006 for identification will be used as a guideline. One factor that is essential for modern portal systems is the innocent alarm rate, which describes how often an alarm is given for radioactive materials that are not illicit in nature. Such a value must be determined by experiment and depends on a number of parameters such as the source of the radiation. This value is not covered in this work as the laboratory conditions available are not a good substitute for a real life scenario, and the number of sources available for testing fall far short of the ANSI N42.35-2006 requirements. This value is mentioned however in the future work section in Chapter 9. The ANSI standards for isotopic identification are defined in a more comprehensive list in the ANSI N42.38-2006 [IEEE, 2006b] standards for isotope identification, shown in Figure 8.1. Figure 8.1 shows values for neutron detection as well as gamma-ray detection, which can be provided by a separate Helium-3 detector inside the portal. Both Gamma-rays and neutrons must be detected with probability greater than or equal to 0.90 with a 95% confidence value. Simulations of PVT based portals meeting the above design requirements can establish whether or not a certain design will meet the sensitivity requirements in the ANSI standards N42.38-2006. As the minimum number of counts for both simple and complex spectral identification has already been established for a certain quality detector, the portal must simply meet the sensitivity requirements to provide that minimum number of counts whilst still retaining good spectral quality. Some environmental design requirements are also given, such as:

- Stabilization time
- Ambient temperature

Radionuclide	Activity (μCi) unshielded [4]	Activity (μCi) steel shielded (3 cm) [4]	Activity (μCi) poly shielded [4] [5]
^{241}Am	47	—	—
^{133}Ba(i)	9	148	—
^{133}Ba(g)	3	—	—
^{57}Co(i)	15	—	—
^{57}Co(g)	5	—	—
^{60}Co	7	25	—
^{137}Cs	16	85	—
DU [6]	4.5 kg (46 cm^2)	—	—
^{67}Ga	16	—	94
HEU[6]	237 g (6.5 cm^2)	—	—
^{131}I	10	—	23
^{192}Ir	6	61	—
^{40}K	128	—	—
^{237}Np [6]	90 mg with 1 cm Fe shielding	—	—
^{99m}Tc	16	—	127
^{201}Tl	10	—	88
^{226}Ra	8	—	—
^{232}Th	14	—	—
RGPu [6]	1.4 g with 1 cm Fe shielding	—	—
WGPu [6]	15 g with 1 cm Fe shielding	—	—
^{252}Cf [3]	2×10^4 n/s ± 20%	—	—

Figure 8.1: Test sources and activities defined for the ANSI Performance Criteria for Spectroscopy-Based Portal Monitors Used for Homeland Security [IEEE, 2006b].

- Relative humidity
- Atmospheric pressure
- Magnetic induction of external origin

The stabilisation time is set to a maximum of 15 minutes. This is easily achievable as the software in the current systems can redefine the calibration and gain stabilisation in real time with the whole process taking a less than a few minutes. Temperature dependence has already been measured but a simple set of temperature sensors both inside the portal and outside can either be used to adjust the gain and calibration of the system accordingly, or call for a new set. Humidity and pressure are not factors that were measured as part of this work, but these can be taken into account by ruggedising the portal monitor design. Magnetic field influence has also not be fully covered

for a portal as the photomultiplier tubes are the main issue here and are adequately shielded with mu metal. Any other effects should be considered in the portal structure as opposed to the instruments contained within.

8.2.2 System Design

In order to meet the detection requirements, a two sided portal was designed forming an archway for each portal type with detectors placed on both vertical sides. A distance of 1m between detector panels is the requirement for personnel portals, whilst a 5m separation between detector panels is required for vehicle portals. The previous portal simulation in Chapter 4 showed that two 1m V-Plank design detectors placed 1m apart in a portal gave 22,200 counts for a 16μCi Cs-137 source passing through at a speed of 1.2m/s in the centre of the detector, and 9,800 counts were observed at the top or bottom of the detector. These counts rates just reach the minimum limit for simple isotope identification in order to approach 100% reliability. Only the mid-section could identify a more complex spectrum, but this simulation was based on a simple isotope activity. More complex isotopes listed in the ANSI N42.38-2006 specifications do not include a Eu-152 source to represent a complex spectrum as was used previously in Chapter 6. There is however a Ra-226 source with an activity of 8μCi, half that of the Cs-137 which can be used to represent complex spectra. The system would therefore need to give at least 22,000 counts anywhere in either portal design for Ra-226 at an activity of 8μCi.

To meet these requirements, the volume and the number of the detectors were increased to allow for more counts in each of the resulting Ra-226 spectra. The length of each detector panel was therefore increased to 115cm and the widths were increased to 38cm for the wider end and 29cm for the narrow end. The number of photomultiplier tubes was also increased to three, 5-inch photomultiplier tubes per detector. This gave these detector panels a total volume of 15.4 litres each, up from 9.1 litres each from the 1m V-Plank and 2m X-Plank designs. Higher quantum efficiency photomultiplier tubes became available recently which increase the quality of energy loss spectra for a given detector, or allow the increase of the detector panel's dimensions whilst retaining a similar resulting spectral quality. The Hamamatsu R6233-100 Super

Bialkali tube is an example of this. This tube is 7.6cm in diameter and has a photocathode quantum efficiency of 34% at 400nm. The R877-100 is another example with the same specifications as the R6233-100 but 13.3cm in diameter, ideal for use in this detector panel design.

The portal consisted of a number of detector panels in order to approach 100% positive identification of complex spectra at a walk-through speed of 1.2m/s for personnel portals, and 8km/h for vehicle portals. These detector panels were stacked length-ways to cover a 2m height to start with. Along with the photomultiplier tubes and electronics, around 2.5m in height would be required to house the panels, with a varying width depending on the number of encapsulated panels.

To calibrate the system, a built in Na-22 source would be required. The most cost effective and easiest way to use the Na-22 source would be a mechanical arm to present the source to the middle of the portal, at the end of which sits the Na-22 source in a retractable lead case. The source would therefore be constantly shielded from the detector until calibration was required. Normalisation of the photomultiplier tube gains can then also take advantage of this source, triggered by and change in environmental settings. Other methods of calibration were available with Na-22 sources such as tagging the source with a small crystal scintillator and removing subsequent entries in the energy loss spectra. This method however becomes more taxing as multiple detector panels are installed in different locations with the portal.

8.2.3 Methods for Testing

To test this system, proper field trials would be ideal. This is however outside of the scope of this work and is therefore recommended in the future work section of Chapter 9. For a simple test, two isotopes from the ANSI N42.38-2006 standards for isotopic identification were chosen to represent simple and complex spectra. Cs-137 was chosen to represent simple spectra, whereas Ra-226 was chosen to represent the more complex spectra. Simulations were then carried out using a varying number of detector panels in each portal design to meet the minimum number of counts required to approach 100% identification of each isotope. The personnel portal specification

allows an exposure time of 1 second inside the portal, whilst the vehicle portal specification allows an exposure time of 5 seconds. Each portal system was tested with the simulated isotopes at both the centre of the portal, and at a height of 10cm above the ground/from the top of the detector, as the designs are symmetrical.

8.2.4 Performance and Results

The performance of the detector panel was simulated using Geant4 and gave an overall light collection efficiency of 45.4% per detector with a variation in the light collection efficiency of 5.6%. This light collection is lower than the 57% of the 50cm V-Plank used in the spectral quality trials, but the improved quantum efficiency from the new photomultiplier tubes compensate for this, providing a similar number of photo-electrons overall. The average photo-cathode quantum efficiency of the Photonis photomultiplier tubes in the previous designs was 27%, and the light collection of the 50cm V-Plank detector was 57%. The product of these two figures is 0.154, whereas the product of the 45.4% light collection from the new panel design with the 34% quantum efficiency of the recently developed Hamamatsu photomultiplier tubes also gives 0.154. Therefore the quality of the spectra should remain the same as the small V-Plank for this larger panel design. The variation in the light collection is similar to the value predicted for the original 1m V-Plank and is therefore probably also around 2% when measured experimentally, though this would need to be verified. This design might also benefit from a small spacer section of non-scintillating PVT between the detector and the photomultiplier tubes as highlighted in Chapter 3. This spacer PVT was not included in the 1m V-Plank or 2m X-Plank designs because the benefits of using it were unknown at the time of manufacturing the detectors. The spacer is not included in the new detector panel performance evaluation as although previous simulations showed a decreased variation in the light collection efficiency with its use, it has not yet been experimentally verified.

The results of the simulations for each portal design are now presented, starting with the personnel portal. For Cs-137, a mono-energetic gamma-ray source was simulated at 662keV with an activity of 16μCi. The Ra-226 source was simulated using a histogram input for all the emitted gamma-ray energies with a total activity of 8μCi.

Many portal configurations were tested, but the configuration found to meet the minimum sensitivity requirement whilst retaining as lower number of panels as possible was a three panel design. This design uses two panels stacked length-ways covering the full 2m height on one side of the portal, and one panel placed 1m away at a central height on the other side of the portal, as shown in Figure 8.2. The results for these

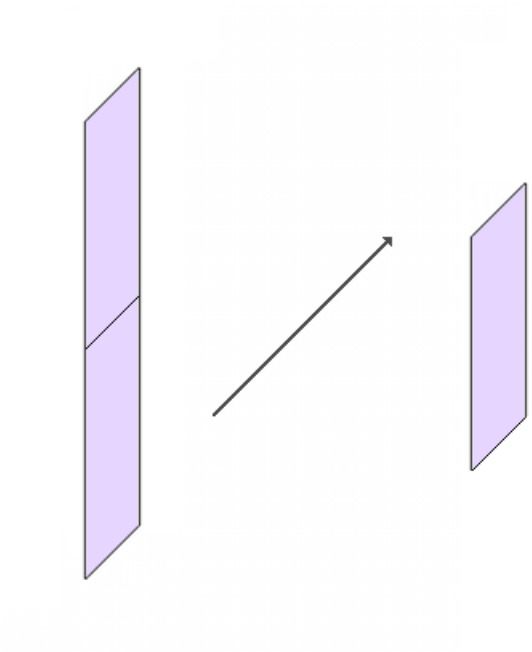

Figure 8.2: A personnel portal configuration using three detector panels.

simulations are shown in Table 8.1. These results show that the most difficult isotope

Table 8.1: Personnel portal sensitivity test with Cs-137 and Ra-226 sources at different heights

Radionuclide	Counts @ Midsection (+/- 2%)	Counts Near Floor (+/- 2%)
^{137}Cs	75,663	51,256
^{226}Ra	41,994	28,432

to identify, Ra-226, gives over 28,000 counts in the energy-loss spectrum at the highest point of the portal system. This is 27% higher than the minimum 22,000 counts needed for 100% isotope identification during the Eu-152 trials. These simulations were produced with a person walking through the portal at a speed of 1.2m/s without stopping. As this design is theoretical, real trials would need to be used to verify the

quality and sensitivity of the design, although previous analysis has shown the simulations to be a good indication of detector performance.

For the vehicle portal, a larger number of configurations were tested, culminating in a twelve panel design. This design used six panels on each side of the portal, with three stacked on top of the other three covering 2m in height. This design is shown in Figure 8.3. The results for these simulations are shown in Table 8.2. These results show that

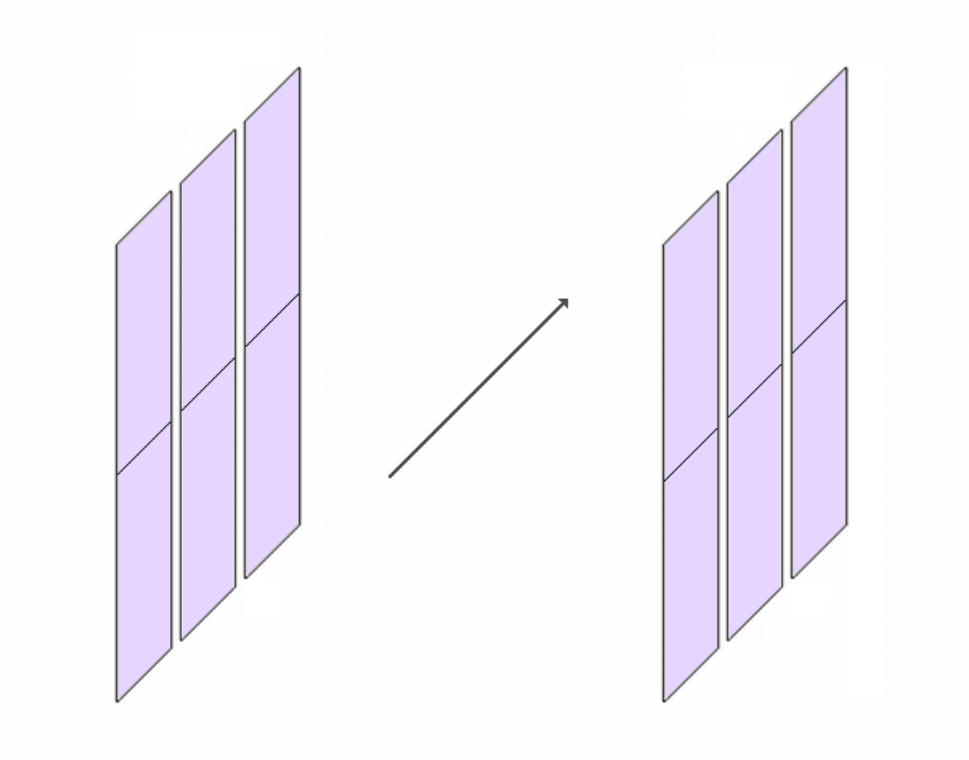

Figure 8.3: A vehicle portal configuration using twelve detector panels.

Table 8.2: Personnel portal sensitivity test with Cs-137 and Ra-226 sources at different heights

Radionuclide	Counts @ Midsection (+/- 2%)	Counts Near Floor (+/- 2%)
^{137}Cs	47,200	43,000
^{226}Ra	27,000	24,500

24,500 counts were obtained at a minimum, exceeding the 100% isotope identification specification defined in the Eu-152 trials by 11%. The vehicle portal design required

a lot of detector panels to meet the specifications of the ANSI standards N42.38-2006, requiring many photomultiplier tubes and associated electronics. This design does not consider shielding factors which are also listed as a requirement in the ANSI standards N42.38-2006, this is recommended in the future work section of Chapter 9, as a part of the proper field trials that would be required to verify the performance of this portal design.

8.2.5 Panel Design Conclusions

The personnel portal design consisted of a dual sided portal system encompassing three panels of PVT scintillator. The sides of the portal were 1m apart and the height was around 2.5m to cover the full height range. The vehicle portal required twelve panels, 5m apart, to meet the same identification requirements. Each portal had detector panels with dimensions 115cm$\times$38cm$\rightarrow$29cm$\times$4cm with three, high quantum efficiency 5-inch photomultiplier tubes attached to the large end of them. These configurations were simulated to give the same quality spectra as the 50cm V-Plank with a sensitivity to produce spectra with over 22,000 counts from the ANSI specification radioactive sources. According to the studies in Chapter 6, these systems should gain enough counts per spectrum to approach 100% positive identification of tested sources in a laboratory environment, though full field trials would be essential for verification. The calibration device suggested was a shielded Na-22 source on a mechanical arm and shutter which would extend to the mid-section of the portals to calibrate the detectors and normalise the photomultiplier tubes.

Chapter 9

Conclusions and Recommendations for Future Work

9.1 Project Aim

This thesis presents the development of several optimised plastic scintillator detector designs for use in radiation portal monitors at international borders and other areas at a higher risk of nuclear attack. The detector designs presented incorporated optical design improvements and advanced data processing in the form of spectral deconvolution. This allowed the extraction of spectral information from the Compton continua created by exposing the detectors to a range of radioactive isotopes. The design improvements along with the spectral deconvolution techniques provided the ability for plastic scintillators to detect and identify common radioactive isotopes in an attempt to distinguish illicit sources from benign sources, such as those used in the medical industry and naturally occurring radioactive sources. The ability to distinguish such sources is of great benefit to customs and borders organisations who are largely hindered by extra, more detailed, cargo inspections prompted by high false alarm rates associated with current radiation portal monitors.

9.2 Review of Spectrometry with PVT

The main aspect of plastic scintillator gamma-ray spectrometry was constructed from two parts: the optimisation of plastic scintillator detectors and the application of ad-

vanced spectral processing techniques. Optimisation of plastic scintillator detectors was investigated using both experimental techniques and Monte Carlo simulations with Geant4. Optical characteristics were the focal point of the design optimisation, with refined geometries, reflective coatings, optical bonding and applicable photomultiplier tubes all contributing to maximise the light collection efficiency of a detector and minimise its variation in light collection efficiency. This research led to the design and manufacture of three PVT detector prototypes: one small area, 2.3 litre detector and two larger-area, 9.1 litre detectors.

Spectral processing techniques were first investigated, highlighting some of the existing technologies available. Spectral deconvolution of Compton continua was later introduced to show how basic spectrometry could prove a viable means for isotopic identification. Spectral deconvolution was applied successfully to the energy loss spectra of all three detectors, identifying a range of tested isotopes. Consideration was then given to the practical aspects of incorporating these optimised detectors into a radiation portal monitor, culminating in recommended designs for a personnel portal and vehicle portal which are predicted to adhere to the ANSI standards for isotope detection and identification.

9.2.1 Optimisation of Plastic Scintillator Detectors

When optimising PVT detector designs a number of factors were identified which limit a scintillation detector's energy resolution. For PVT detectors the two most significant factors identified were the light collection efficiency and the spatial variation in the light collection efficiency. The intention was therefore to optimise these factors to produce a PVT scintillator which would give excellent clarity Compton edges in the energy loss spectra it produces. The light collection efficiency was optimised by a number of factors.

The geometry played a vital role in both the light collection and variation in the light collection. Limiting the thickness of the detector resulted in a lowered probability of multiple Compton scattering events, giving clearer Compton edges in the energy loss spectra. Around 4cm to 5cm was chosen as the optimal thickness. This relatively

low thickness produced slab or plank shaped detectors, leaving the length and width of the detector as variables for adjusting the surface area and volume of the detector. The ratio of the length to the width needed to be limited, as a long thin detector for example would give decreased light collection efficiency and increased variation in the light collection efficiency. A length to width ratio of less than 4:1 was found to be optimal. The main contributor to the light collection efficiency was the number of photomultiplier tubes attached to the detector, or more specifically, the area covered by photo-cathode. A low length to width ratio geometry with a high photo-cathode coverage area gave the best light collection, but would also increase the costs due to the number of photomultiplier tubes and associated electronics required. A trade off must always be made with the cost of equipment and the performance of the detector.

The best configuration of reflective materials applied to a detector was found to be a highly reflective specular reflector optically bonded to the edges of the detector, whilst leaving the larger faces unwrapped, or wrapped loosely with crinkled aluminium foil. Any form of light guide was found to hinder the performance of PVT detectors with the type of thickness required for gamma-ray spectrometry. Light guides in this configuration simply attenuate the light signal through increased volume of material. Direct coupling of photomultiplier tubes to the detector's edge was used throughout to avoid light loss. It was however concluded that a small section of non-scintillating PVT attached the photomultiplier tube end of the detector can reduce the variation in the light collection efficiency. This was determined by analysing the light collection of the detector as a function of scintillation pulse location; eliminating scintillation events close to the photo-cathode reduces the overall variation in the light collection efficiency.

The final refinement made was to taper the width of a detector such that the width is larger at the photo-cathode end and narrower at the opposite end of the detector. This adjustment ensured that light reflecting inside the detector was encouraged to propagate towards the attached photomultiplier tubes, resulting in increased light collection and reduced variation in the light collection efficiencies.

9.2.2 New PVT Based Detector Designs

The detector optimisations led to three detector prototypes being designed and manufactured. All of these detectors used Photonis 5" photomultiplier tubes for light detection and Ortec digiBASEs as integrated high voltage supplies, shaping amplifiers and multi channel analysers. Each of the detectors were calibrated by simulating energy loss spectra of a Na-22 source and matching the simulated spectra to experimentally measured ones. These simulations incorporated all the resolution broadening factors of each detector respectively to produce the most accurate result.

The first detector design was 50cm in length, 4cm in thickness and tapered from 12.7cm in width at the photomultiplier tube end to 10cm at the opposite end. This design was the first to be manufactured and was named the 50cm V-Plank due to its V-shaped geometry. Multiple tests and simulations were performed on this detector, giving a simulated average light collection efficiency of 57%, and a simulated variation in the light collection efficiency of 2.8%. The light collection efficiencies of these detector designs could not be accurately measured directly due to the lack of reliable photo-peaks in the energy loss spectra. However, simulations of the detector incorporating all of the resolution broadening factors produced artificial spectra which were matched to experimental spectra. The estimated light collection came out much lower than expected at around 35%. This was accounted for by taking into consideration various factors of photomultiplier tubes which reduced their overall quantum efficiency far below the manufacturer's stated figures for the photo-cathode quantum efficiency. Such factors included spatial variation in the photo-cathode efficiency and less than perfect cathode to dynode efficiencies. The variation in the light collection was measured by placing a collimated Cs-137 source at various locations of the detector and measuring the corresponding change in the location of the 662keV induced Compton edge in the energy loss spectrum. The variation in the light collection efficiency was found to be less than 2%. A number of spectra were taken with the 50cm V-Plank from various radioactive sources. Sources such as Cs-137 and Na-22 produced sharp Compton edges and were easily recognisable by eye. More complex sources such as Eu-152 and Ra-226 were a convolution of many Compton continua resulting in an indistinguishable energy loss spectrum. In order to quantify the relative quality of the

spectra produced for each detector design, a measurement similar to the full width at half maximum was taken at the 662keV induced Compton edge in each of the energy loss spectra. The equivalent FWHM for the 50cm V-Plank was 32%.

The second detector design was 1m in length and 25.4cm in width at the wide end, tapering to 20cm at the narrow end. It was also 4cm in thickness. This design was called the 1m V-Plank and was similar to the 50cm V-Plank except with 4x the area and volume. The 1m V-Plank had two 5" photomultiplier tubes at the wide end of the detector and operated in a coincidence mode. The simulated light collection efficiency for this design was 47% with a simulated variation in the light collection of 5.6%. The measured variation in the light collection was around 2%, much lower than predicted by simulation. The equivalent FWHM at 662keV induced Compton edge of this design was 33%, slightly poorer than the 50cm V-Plank, which was expected due to its poorer light collection efficiency.

The final design was the 2m X-Plank. This design was 2m in length, 4cm in thickness and a width of 12.7cm at each end, tapering to 10cm in the middle of the detector. It had two 5" photomultiplier tubes, one at each end, and resembled two V-Planks joined together end to end. The benefit of this design was to provide a similar volume and performance detector to the 1m V-Plank but to also investigate the viability of positional sensitivity as an extra feature. The simulated light collection of this design was the same as the 1m V-Plank at 47%, with a simulated variation in the light collection efficiency of 5.5%. The measured variation in the light collection was found to be slightly higher than the other designs though at around 3%. Normally such high length to width ratio designs would give much poorer performance, but the tapered width gave significant performance benefits. The equivalent FWHM at the 662keV induced Compton edge of this design was 34%, slightly poorer than the other two designs.

9.2.3 Spectral Deconvolution

The aim of current spectral processing techniques is to classify spectra according to either the general shape of the overall Compton continuum, or the relative number of

counts in certain areas of the spectrum. Typically energy windowing techniques were used with high, medium and low energy regions. This approach had some success as special nuclear materials could be distinguished from naturally occurring radioactive materials, but other sources such as industrial or medical sources could not be distinguished as their gamma-ray spectra occupy similar regions of the energy loss spectrum as naturally occurring sources. Spectral deconvolution was used due to its previous successful implementation in NaI(Tl) based detectors, increasing the energy resolution of these detectors significantly. Spectral deconvolution uses a maximum likelihood by expectation maximisation algorithm to predict the incident gamma-ray spectrum from the resulting energy loss spectrum. To do this the detectors were individually characterised and Monte Carlo simulations were produced modelling the response of the detector for the entire energy range of interest. Once the incident gamma-ray spectrum was constructed for a given isotope measurement, it was analysed with isotope identification software. As spectral deconvolution of energy loss spectra from PVT detectors has not previously been used, a new isotope identification library was devised based on transforming libraries from high purity germanium detectors. A set of rules were used to broaden and remove certain entries from the libraries until they were appropriate for PVT based spectrometry.

Spectral deconvolution and isotope identification were applied to all three of the new detector designs for a range of available isotopes. The settings for the deconvolution and isotope identification software were optimised for use with spectra from PVT and successful identification took place of all isotopes tested. These included Cs-137, Na-22, Eu-152, Am-241, Ba-133, Co-57, Co-60, Th-232 and Ra-226. The quality of the deconvolved spectra was excellent, showing clear, photo-like peaks which were readily identifiable by the isotope identification software. The full width at half maximum of the 662keV peaks present in the deconvolved spectra were measured for each of the detectors. The results were as follows:

- 50cm V-Plank: 5%
- 1m V-Plank: 6%
- 2m X-Plank: 6%

The number of counts in each of the raw spectra was found to heavily influence the quality of the resulting deconvolved spectra. This was quantified by conducting an experiment with the 50cm V-Plank. The experiment consisted of taking spectra with a varying number of counts, deconvolving them and measuring the deviation in the locations of the deconvolved peaks and the identification success rate. This was done for a Na-22 spectra and for Eu-152 spectra to represent both simple spectra with only a few, well-spaced gamma-rays and complex spectra with multiple gamma-rays which appear convolved in the raw energy loss spectrum. The results showed that successful identification was, as predicted, heavily dependent on the number of counts per spectrum. This was the case for two reasons, the quality of the peak in the spectra, and the variation in their location. The standard deviation in the location of the peaks was related to the number of counts per spectrum, resulting in figure being produced for the minimum number of counts required per spectrum to obtain a positive identification. The minimum number of counts per spectrum was therefore established for both simple and complex spectra in order to approach 100% correct identification of all 25 spectra tested per isotope. The results were as follows:

- Simple spectra (Na-22): 8,000 counts per spectrum
- Complex spectra (Eu-152): 22,000 counts per spectrum

These figures are correct for 25 trials in a laboratory environment. More rigorous testing in an industrial environment would be required to give a more accurate figure for subsequent use in radiation portal monitors.

Neutron detection using PVT based detectors was investigated by researching published techniques and by taking direct measurements of neutrons from a Cf-252 neutron source. When measuring neutrons with PVT the resulting energy loss spectra were poor, with no spectral information present. This meant that although a standard PVT detector can detect neutrons, distinguishing them from gamma-rays or obtaining any sort of energy information was not possible. The only viable method found in the available literature was to use time of flight techniques with multiple PVT detectors. This method can successfully distinguish neutrons from gamma-rays as neutrons are much slower in speed. Spectral information obtained using this information was limited however and implementing the required equipment would take twice the number

of PVT detectors and associated electronics in one portal. It was therefore concluded that a standalone helium 3 counter might be of more practical benefit for detecting neutrons.

9.2.4 Practical Requirements and a Possible Future Portal Design

A number of considerations and problems were resolved when investigating the implementation of the new PVT designs into a radiation portal monitor. The first problem encountered was non-linearity of the detector system. The cause for this was found to be the type of photomultiplier tube being used. Adit 5" tubes were initially used, which were based on a box and grid dynode design. They were only suitable for counting purposes and gave poor energy linearity when the applied voltage varied. Photonis 5" tubes were used to replace these and performed very well with excellent linearity, these tubes used a linear dynode design. The second issue was the dynamic range of the multi channel analyser and the energy resolution of the q-files used in the Monte Carlo simulations. The range used consisted of 512 channels, each separated into 6keV bins. This presented a problem at lower energies as some of the features were becoming indistinguishable when accommodating the 2.6MeV gamma-ray of Th-232 into the energy scale. To solve this problem, a larger number of q-files would be required, decreasing the bin width and allowing an increase in the gain of the system whilst also allowing for the 2.6MeV gamma-ray.

Environmental factors such as temperature, magnetic fields and surrounding materials could all affect the detector performance. Experiments with temperature dependence showed that the location of a 662keV induced Compton edge varied by around 2% with temperature changes from -20C to +40C. Magnetic shielding must be used to cover photomultiplier tubes or external magnetic fields can distort the electron flow and corrupt the resulting spectral data. Materials in close proximity to the detector of a similar density affected spectra by adding low energy, back scattered gamma-rays to the Compton continua and also broadened some high energy Compton edges due to multiple coincident scattering events. This can be avoided by simply moving the detector far enough away from such surfaces as to not have any significant effect.

Positional resolution of the 2m X-Plank was investigated as an extra feature to the PVT detector series. This feature would allow personnel portal operators to quickly identify where a smuggled source might be hidden. Optimal positional resolution of +/- 11cm FWHM was achieved using the ratio of the two photomultiplier tube signals to calculate the position of a collimated Cs-137 along the detector. This resolution was however dependent on the collimator and therefore in industrial applications a large collimator would need to be applied to the detector, which may subsequently degrade energy resolution and detector efficiency.

Outlines for future portals were given in the final Chapter. Personnel portals are not subject to many of the problems that arise with vehicle portal monitors and therefore the results obtained for this design are more likely to correspond to real world trials. Personnel portals are used by airport security and security at large events, such as the Olympics, to detect the same threats that radiation portal monitors do at international borders. Both portal designs incorporated all of the previously stated detector optimisations along with some newer technology that has since become available. Recent photomultiplier tube research has led to an increase in photo-cathode quantum efficiency available. Hamamatsu now provides 5" photomultiplier tubes with an average photo-cathode quantum efficiency of 34%. This means that detectors can be made larger whilst retaining the same quality spectra. A portal design consisting of three large area PVT detectors with a total volume of 46.2 litres was produced for a personnel portal, whilst twelve such detectors where required for the vehicle portal, totalling 184.8 litres. Simulations of each system gave the number of counts per spectrum of a person or vehicle carrying an 8μCi Ra-226 source through the portal. A minimum of 28,000 counts were measured for the personnel portal, whilst 24,500 were measured for the vehicle portal. These were above the minimum number of 22,000 counts required for complex sources to identify accurately during laboratory tests on detectors of the same quality. Simple sources such as a 16μCi Cs-137 were also simulated, far exceeding the minimum number of counts for accurate identification. A minimum of 51,000 counts were measured for the personnel portal and 47,000 counts for the vehicle portal. A fully working prototype would need constructing in each scenario and testing in an industrial environment to fully evaluate the portals' performance.

9.3 Recommendations for Future Work

There are a number of sections recommended for future work on PVT based spectrometry. The following is a selection of possible work to provide a more complete evaluation of an industrial portal system based on PVT spectroscopy with spectral deconvolution.

Due to the nature of this work a large number of materials have been unavailable for testing. Special nuclear materials are the main example of this, with access severely restricted to those in security cleared establishments. Tests to catalogue special nuclear materials of interest are key to using this system to identify them and therefore studies must be completed with such sources available. A full catalogue of the most common NORM sources is also required to identify them. Though the presence of NORM can be inferred using the process of elimination, positively identifying NORM is of great importance. An updated version of the PVT identification library could be created with both special nuclear materials and common NORM sources included. Such test and trials are readily accessible to many establishments already conducting their own research into plastic scintillators. In early 2009 plans were established by Symetrica to test a 1m V-Plank PVT based prototype at PNNL, but unfortunately the detector was damaged beyond use from improper handling during shipment.

Industrial trials can also provide data to determine a number of figures which were not included in this study such as the determination of a minimum gross count rate that triggers the detector's alarm. Determining the minimum count rate to produce and alarm is not an arbitrary process in vehicle portal monitors as vehicle shadowing largely affects the background count rate. As large containers are driven through a portal system the vehicle itself blocks some of the background radiation, lowering the count rate baseline. The minimum gross count rate must take this into consideration to avoid false alarms. Gaps between vehicle trailers can then momentarily increase the count rate causing further confusion to the system. These factors must be fully investigated and accounted for before a full portal system can be implemented. An accurate reliability index must also be established for these detector designs, such as the false alarm rate for a portal monitor based on detector designs presented here. These

figures can only be accurately established with proper field trials.

Vehicle portal monitors are largely susceptible to shielding from the containers that any radioactive material might be encased in. The steel casing of a shipping container may be just the minimum shielding involved, other lead casing could be used if materials were being intentionally smuggled. At present there is no detector system which can completely negate the affects of large amounts of shielding, however, the system should be able to distinguish lightly shielded sources. Most types of shielding will not only attenuate radiation but also cause Compton scattering of gamma-rays, which could result in poor quality energy loss spectra with respect to spectrometry. The PVT isotope library must be updated to include sources with various degrees of shielding. Neutron detection can play an important role in this scenario as lead and other dense materials have little effect on the neutron flux from a source, though even this can be suppressed with the use of appropriate materials.

Further work into multi channel analysers which accept many signals would also be beneficial. Currently the use of Ortec digiBASEs for each photomultiplier tube is an expensive option and the LIST mode used for producing spectra from coincident counts on larger detectors is complex and limited in its functionality for more than a few digiBASEs. At least 1024 channels in the multi channel analyser would allow better separation of low energy content in the energy loss spectrum, reducing the volatility of the system at these energies.

Bibliography

C. Amsler et al. Review of particle physics. *Physics Letters B667*, 1:10, 2008. http://www-pdg.lbl.gov/2008/pardetrpp.pdf.

E. Argonne National Laboratory. Radiological dispersal device (RDD). *Human Health Fact Sheet*, 2005.

G. D. Badhwar, C. L. Deney, B. R. Dennis, and M. F. Kaplon. The nonlinear response of the plastic scintillator NE102. *Nuclear Instruments and Methods*, 57:116–120, 1967.

S. Bashkin, F. P. Mooring, and B. Petree. Total cross section of helium for fast neutrons. *Physical Review*, 82:378 – 380, 1951.

E. Brannen and G. L. Olde. The response of organic scintillators to electron energy deposited in them. *Radiation Research*, 16:1–6, 1962.

C. Burt and D. Ramsden. The development of large-area plastic gamma-ray spectrometers. *Nuclear Science Symposium Conference Record, IEEE*, pages 1186–1190, 2008.

G. W. Bush. The department of homeland security, June 2002. http://www.dhs.gov/xlibrary/assets/book.pdf.

I. H. Campbell and B. K. Crone. Efficient plastic scintillators utilizing phosphorescent dopants. *Physical Review*, 90:012117, 2007.

L. G. Chiang and R. B. Oberer. Method to correlate CFD discriminator level and energy deposition by neutrons and photons in a fast plastic scintillating detector. *ORNL Oak Ridge National Laboratory (US), Technical report*, 2000.

Eljen Technology. EJ200 data sheet, 2009. http://www.eljentechnology.com/datasheets/EJ200%20data%20sheet.pdf.

J. Ely, R. Kouzes, J. Schweppe, E. Siciliano, D. Strachan, and D. Weier. The use of energy windowing to discriminate SNM from NORM in radiation portal monitors. *Nuclear Instruments and Methods in Physics Research A*, 560:373–387, 2006.

J. H. Ely, E. R. Siciliano, and R. T. Kouzes. Comparison of NaI(Tl) scintillators and high purity germanium for vehicle portal monitor applications. *IEEE Nuclear Science Symposium Conference Record*, 3:1584–1587, 2004.

J. H. Ely, K. Anderson, D. Bates, R. Kouzes, C. L. Presti, R. Runkle, E. Siciliano, and D. Weier. The use of energy information in plastic scintillator material. *Journal of Radioanalytical and Nuclear Chemistry*, 276:743–748, 2008.

R. Firestone1 and L. Ekstrm. LBNL isotopes project - LUNDS universitet - WWW table of radioactive isotopes, 2004. http://ie.lbl.gov/toi/.

Government Accountability Office. DHS improved testing of advanced radiation detection portal monitors, but preliminary results show limits of the new technology. *COMBATING NUCLEAR SMUGGLING*, Report to Congressional Requesters: GAO–09–655, 2009.

Hamamatsu. *Photomultiplier Tubes Basics and Applications*. Hamamatsu Photonics K.K., third edition, 2006. http://www.sales.hamamatsu.com/assets/applications/ETD/.

IEEE. American national standard for evaluation and performance of radiation detection portal monitors for use in homeland security. ANSI N42.35-2006, 2006a. http://standards.ieee.org/getN42/download/N42.35-2006.pdf.

IEEE. American national standard performance criteria for spectroscopy-based portal monitors used for homeland security. ANSI N42.38-2006, 2006b. http://standards.ieee.org/getN42/download/N42.38-2006.pdf.

International Atomic Energy Agency. The IAEA illicit trafficking database (ITDB). 2007.

D. V. Jordan, B. D. Geelhood, P. L. Reeder, D. L. S. Jr, R. C. Craig, and J. I. McIntyre. Progress report on the advanced large area plastic scintillators (ALPS) project. *Pacific Northwest National Laboratory*, PNNL-14283, 2003.

D. V. Jordan, P. L. Reeder, L. C. Todd, G. A. Warren, K. R. McCormick, D. L. S. Jr, B. D. Geelhood, J. M. Alzheimer, S. L. Crowell, and W. A. Sliger. Advanced large area plastic scintillator project (ALPS): Final report. *Pacific Northwest National Laboratory*, PNNL-17305, 2007.

L. J. Kangas, P. E. Kellera, E. R. Sicilianoa, R. T. Kouzes, and J. H. Ely. The use of artificial neural networks in PVT-based radiation portal monitors. *Nuclear Instruments and Methods in Physics Research A*, 587:398–412, 2008.

G. F. Knoll. *Radiation Detection and Measurement*. John Wiley and Sons Inc, second edition, 1989. ISBN 0471815047.

G. F. Knoll. *Radiation Detection and Measurement*. John Wiley and Sons Inc, third edition, 2000. ISBN 978-0-471-07338-3.

N. Kudomi. Energy calibration of plastic scintillators for low energy electrons by using compton scatterings of gamma rays. *Nuclear Instruments and Methods in Physics Research A*, 430:96–99, 1999.

E. Lipton. U.S. to spend billion more to alter security systems. *The New York Times*, 8th May 2005.

J. O. Lubenau and J. G. Yusko. Radioactive materials in recycled metals. 68:440–451, 1995.

J. O. Lubenau and J. G. Yusko. Radioactive materials in recycled metals - an update. *Health Physics*, 74:293–299, 1998.

R. C. Martin, J. B. Knauer, and P. A. Balo. Production, distribution, and applications of californium-252 neutron sources. *Applied Radiation and Isotopes*, 53:785–792, 1999.

V. McLane, C. L. Dunford, and P. F. Rose. *Neutron cross sections: Volume 2, Neutron cross section curves*. Academic Press, 1988.

L. J. Meng and D. Ramsden. An inter-comparison of three spectral-deconvolution algorithms for gamma-ray spectroscopy. *IEEE TRANSACTIONS ON NUCLEAR SCIENCE*, 47:1329–1336, 2000.

L. J. Meng, D. Ramsden, V. M. Chirkin, V. N. Potapov, O. P. Ivanov, and S. M. Ignatov. Scintisphere the shape of things to come in gamma-ray spectroscopy. *IEEE TRANSACTIONS ON NUCLEAR SCIENCE*, 49(4):1681–1686, 2002.

L. J. MENG, D. RAMSDEN, V. M. CHIRKIN, V. N. POTAPOV, O. P. IVANOV, and S. M. IGNATOV. The design and performance of a large-volume spherical CsI(T1) scintillation counter for gamma-ray spectroscopy. 485:468–476, 2002.

National Commission on Terrorist Attacks Upon the United States. Final report of the national commission on terrorist attacks upon the united states, July 2004. `www.9-11commission.gov/report/911Report.pdf`.

NATO. Statement by the north atlantic council, September 2001. `http://www.nato.int/docu/pr/2001/p01-124e.htm`.

Pacific Northwest National Laboratory. Radiation detection and nuclear sciences - projects, April 2009. `http://rdnsgroup.pnl.gov/projects.stm`.

D. Ramsden and C. Burt. Spectrometer with plastic scintillator provided with a specular reflector, February 2009. `http://www.freepatentsonline.com/EP2019974A1.html`.

Saint Gobain. Light guides and waveshifter bars, 2009a. `http://www.detectors.saint-gobain.com/Data/Element/Product/product.asp?ele$\_$ch$\_$id=P00000000000000001908$`.

Saint Gobain. Crystals and scintillators: Plastic scintillators, 2009b. `http://www.detectors.saint-gobain.com/Data/Element/Node/Category/Category$\_$edit.asp?ele$\_$ch$\_$id=C00000000000000001855\&Lang=US`.

S. Scheu, H. Kaspar, P. R. A. Van Der Schaaf, and P. Truöl. Studies on wrapping materials and light collection geometries in plastic scintillators. *Nuclear Instruments and Methods in Physics Research A*, 567:345–349, 2006.

D. Scraggs. Klein-nishina distribution. 2009. http://en.wikipedia.org/wiki/File:Klein-Nishina$_$distribution.png.

E. R. Siciliano, J. H. Ely, R. T. Kouzes, B. D. Milbrath, J. E. Schweppe, and D. C. Stromswold. Comparison of PVT and NaI(Tl) scintillators for vehicle portal monitor applications. *Nuclear Instruments and Methods in Physics Research A*, 550: 647–674, 2005.

D. C. Stromswold, A. J. Peurrung, R. R. Hansen, and P. L. Reeder. Direct fast-neutron detection. *Pacific Northwest National Laboratory*, PNNL-13068, 2000.

J. F. Williamson, J. F. Dempsey, A. S. Kirov, J. I. Monroe, W. R. Binns, and H. Hedtjärn. Plastic scintillator response to low-energy photons. *Physics in medicine and biology*, 44:857–871, 1999.

T. S. Winkowski. Hearing before the senate homeland security and government affairs committee. *Senate Committee on Homeland Security and Governmental Affairs*, 2008.